03890

DNPL/R31

DARESBURY LECTURE NOTE SERIES No. 12

PARTONS AND QUARKS

by

F. E. Close

Science Research Council

DARESBURY NUCLEAR PHYSICS LABORATORY

Daresbury, Nr. Warrington, Lancashire

MASTER

DISTRIBUTION OF THIS DOCUMENT IS UNLIMITED

DISCLAIMER

Portions of this document may be illegible in electronic image products. Images are produced from the best available original document.

© SCIENCE RESEARCH COUNCIL 1973

Enquiries about copyright and reproduction should be addressed to:– The Librarian, Daresbury Nuclear Physics Laboratory, Daresbury, Nr. Warrington, Lancashire.

IMPORTANT

The SRC does not accept any responsibility for loss or damage arising from the use of information contained in any of its reports or in any communication about its tests or investigations.

Printed by McCorquodale Printers Ltd., Newton-le-Willows, Lancashire.

DARESBURY LECTURE NOTE SERIES No. 12

PARTONS AND QUARKS

by

F .E. Close

Daresbury Nuclear Physics Laboratory

Notes on a series of lectures given
at Daresbury Laboratory 2-12 April,
1973

Science Research Council

DARESBURY NUCLEAR PHYSICS LABORATORY

1973

MASTER

DISTRIBUTION OF THIS DOCUMENT IS UNLIMITED

THIS PAGE

WAS INTENTIONALLY

LEFT BLANK

FOREWORD

One of the most exciting developments of recent years has been the discovery of scale invariance in the structure function νW_2 measured in the deep inelastic electron scattering experiments at SLAC. Motivated by this discovery theoretical developments rapidly flourished along many avenues, one of the first being the parton model which postulated that the data could be showing evidence of pointlike substructure in the proton (quarks?).

The purpose of these lectures was to show the reasons why parton models describe the data, show what other phenomena can be understood and what predictions can be made within the parton hypothesis. The audience consisted mainly of experimentalists and some graduate students, so technicalities were either avoided or, where needed, described in some detail. The first half of the course was a detailed introduction to the parton ideas. The second half made use of this background in reviewing various topics in the field.

I would like to thank Mr. I. Mohammad for reading the original manuscript and for making various valuable suggestions many of which were incorporated in the final version.

F. E. CLOSE

THIS PAGE

WAS INTENTIONALLY

LEFT BLANK

CONTENTS

		Page
Foreword		(iii)
1.	ELASTIC ELECTRON SCATTERING	1
	1.1 Elastic Electron-Muon Scattering	1
	1.2 Elastic Electron-Proton Scattering	6
2.	INELASTIC ELECTRON SCATTERING	10
3.	DEEP INELASTIC SCATTERING AND PARTONS	16
4.	STRUCTURE FUNCTIONS AND SUM RULES IN THE QUARK PARTON MODEL	25
5.	INELASTIC NEUTRINO SCATTERING	31
6.	FORWARD COMPTON SCATTERING	42
	6.1 Kinematics and Amplitudes	42
	6.2 Dispersion Relations and the Drell-Hearn Sum Rule	46
7.	COMPTON SCATTERING IN SIMPLE MODELS	49
	7.1 Compton Scattering from an Elementary 'Pion'	49
	7.2 Compton Scattering from a 'Physical' Pion	50
	7.3 Compton Scattering from a Nucleus	52
	7.4 From Nuclei to Nucleons	53
8.	A J = 0 FIXED POLE IN COMPTON SCATTERING?	54
	8.1 Dispersion Approach	55
	8.2 Finite Energy Sum Rule (FESR) Approach	58
	8.3 Critique of Errors and Assumptions	60
	8.4 A J = 0 Fixed Pole in Off-Shell Compton Scattering?	61
9.	THE NON-PERTURBATIVE PARTON MODEL WITHOUT TEARS	68
10.	THE PARTON MODEL AND VECTOR-MESON DOMINANCE - RIVALS OR PARTNERS?	74
11.	DO RESONANCES SCALE?	81
12.	RESONANCES, SU(6) AND THE QUARK PARTON MODEL.	93

Page

13. TOWARDS A DYNAMICAL PARTON MODEL 97

14 POSTSCRIPT 108

Bibliography and References 108

1 ELASTIC ELECTRON SCATTERING

1.1 Elastic Electron-Muon Scattering

Let us begin by calculating the cross section for electron-muon scattering. This is useful as an exercise in quantum electrodynamics and will be a central theme in our later work when we look at electron-proton scattering. The main difference between electron-proton and electron-muon scattering is that whereas the muon and electron interact by exchanging a photon (fig. 1) in a known and calculable fashion (the electron-photon and muon-photon couplings are believed to be known exactly viz "pointlike coupling") the proton is a more complicated object containing an unknown structure. The purpose of electron-proton scattering experiments is to explore that structure. In order to see the way in which the proton's structure manifests itself in the cross section it will be useful to compare the form of the electron-proton cross section with the form of the analogous cross section with a muon target. Apart from the fact that the muon and proton have different masses the only differences in the cross sections will come from the corrections to the "pointlike coupling" which arise due to the proton's structure (e.g. its anomalous magnetic moment).

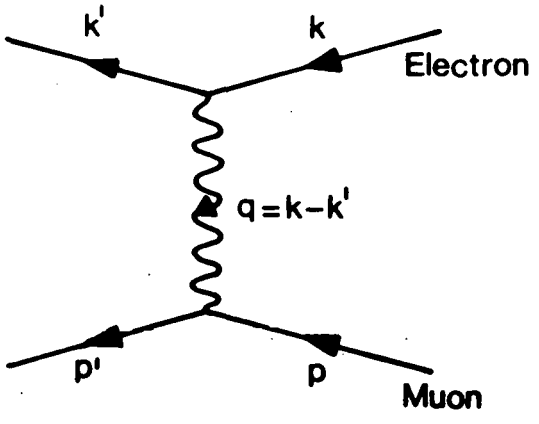

Fig. 1 Electron-muon scattering in one photon exchange.

The amplitude for electron-muon scattering due to exchange of a single photon may be formally written[1]

$$M \sim j_{\mu}^{(e)} \frac{g_{\mu\rho}}{q^2} j^{\rho(\mu)}$$

where $j_\mu^{(e)} \sim \bar{u}(k')\ \gamma_\mu\ u(k)$ is the electron's electromagnetic current, u and $\bar{u}$ the spinors for the initial and final electron, with four momenta k and k' respectively. The electromagnetic current of the muon is similarly defined. The propagator of the exchanged photon yields the $1/q^2$ and, because the photon is a vector particle represented by polarisation vector ε_μ; summing over the spin states of the exchanged photon yields* the $g_{\mu\rho}$. The amplitude for electron-muon scattering may then be written

$$M \sim \bar{u}(k')\ \gamma_\mu\ u(k)\ \frac{1}{q^2}\ \bar{u}(p')\ \gamma^\mu\ u(p) \qquad (1.1)$$

which is shown schematically in fig. 2.

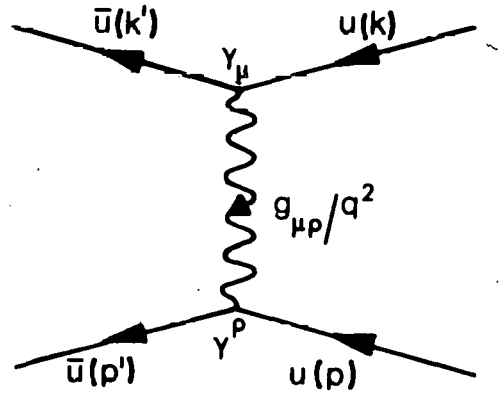

Fig. 2 Schematic representation of electron-muon scattering amplitude.

The differential cross section for the electron to emerge into solid angle dΩ with energy in range dE' is given by the square of the matrix element multiplied by suitable kinematic flux and phase space factors and may be written

$$\frac{d^2\sigma}{d\Omega dE'} = 1/2\ \frac{4\alpha^2 m^2}{q^4}\ \frac{E'}{E}\ \delta(\Sigma E_f - \Sigma E_i)\ L_{\mu\nu}\ W^{\mu\nu} \qquad (1.2)$$

*Because of gauge invariance the photon "propagator" $g_{\mu\nu}/q^2$ may be replaced by $\left(g_{\mu\nu} - \lambda\ \frac{q_\mu q_\nu}{q^2}\right) \Big/ q^2$ without changing any observable quantity. For more details see Gasiorowicz, op. cit.

where we have summed over the final spins and averaged (hence the I/2) over the initial spins $e^2 = 4\pi\alpha$ and

$$L_{\mu\nu} = \frac{1}{4m^2} \text{Trace } (\not{k}' + m)\gamma_\mu (\not{k} + m)\gamma_\nu \rightarrow \frac{1}{m^2} \left[k_\mu k'_\nu + k'_\mu k_\nu - g_{\mu\nu} (k.k' - m^2) \right] \tag{1.3}$$

$$W^{\mu\nu} = \frac{1}{4M^2} \text{Trace } (\not{p}' + M)\gamma^\mu (\not{p} + M)\gamma^\nu \rightarrow \frac{1}{M^2} \left[p^\mu p^{\nu\prime} + p^{\mu\prime} p^\nu - g^{\mu\nu} (p.p' - M^2) \right] \tag{1.4}$$

with $L_{\mu\nu}$ the tensor arising from summing over the final spins at the electron ("lepton") vertex while $W^{\mu\nu}$ is the analogous tensor for the muon vertex and m, M are the masses of the electron and muon respectively. The origin of this tensor structure upon squaring the amplitude is shown in fig. 3.

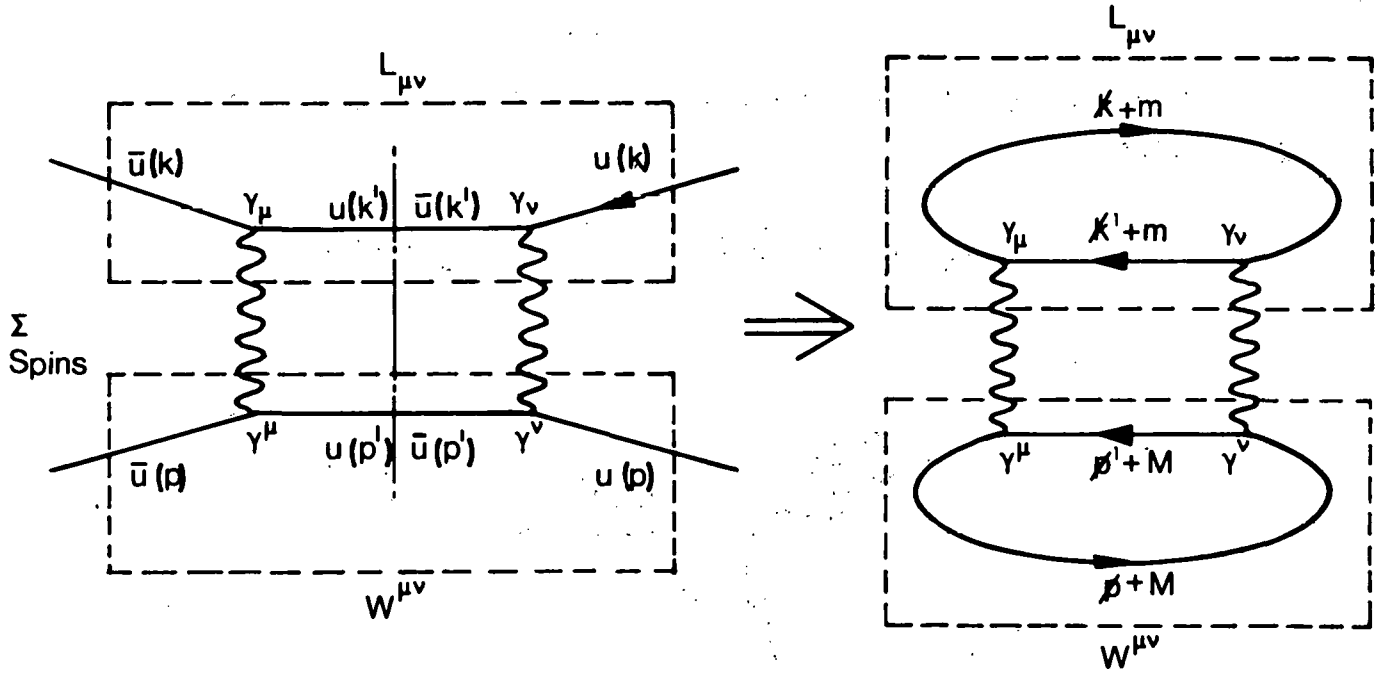

Fig. 3 Tensor structure of electron-muon cross section.

Upon contracting together the tensors $L_{\mu\nu}$ and $W^{\mu\nu}$ in eqns.(1.3) and (1.4) we immediately obtain

$$L_{\mu\nu} W^{\mu\nu} \rightarrow \frac{1}{m^2M^2} \left[p'.k' \, p.k + p'.k \, p.k' - m^2 \, p.p' - M^2 \, k.k' + 2M^2m^2 \right] \tag{1.5}$$

In the laboratory frame where the muon is initially at rest

$$p = (M, \underset{\sim}{0}), \quad k = (E, \underset{\sim}{k}), \quad k' = (E', \underset{\sim}{k}'), \quad q^2 = (k - k')^2$$

and if we neglect terms proportional to m^2 and M^2 then we see that $q^2 = -2k.k' = -2p.p'$, and hence

$$L_{\mu\nu} W^{\mu\nu} \rightarrow \frac{1}{m^2 M^2} \left[2M^2 EE' + \frac{q^2}{2} M(E' - E) + \frac{M^2 q^2}{2} \right]. \qquad (1.6)$$

Using

$$q^2 = -4EE' \sin^2 \frac{\theta}{2}$$

$$E' - E = -\nu = q^2/2M$$

$$M(E' - E) = EE' (\cos\theta - 1)$$

(see fig. 4 for the definition of these quantities), and substituting into $L_{\mu\nu} W^{\mu\nu}$, yields

$$L_{\mu\nu} W^{\mu\nu} = \frac{2}{m^2} EE' \left\{ \cos^2 \frac{\theta}{2} - \frac{q^2}{2M^2} \sin^2 \frac{\theta}{2} \right\} \qquad (1.7)$$

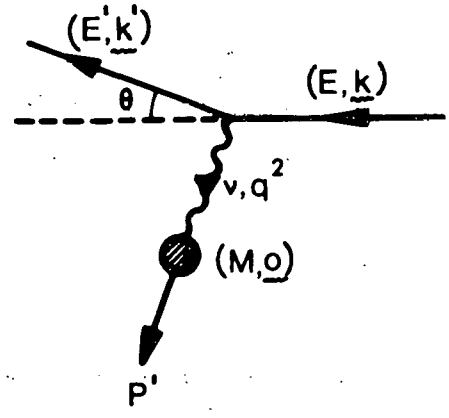

Fig. 4 Electron-muon kinematics in the laboratory frame (muon at rest).

Inserting this into eqn. (1.2) we finally obtain for the cross section

$$\frac{d^2\sigma}{d\Omega dE'} = \frac{4\alpha^2 E'^2}{q^4} \delta(\Sigma E_f - \Sigma E_i) \left[\cos^2\frac{\theta}{2} - \frac{q^2}{2M^2}\sin^2\frac{\theta}{2}\right] \qquad (1.8)$$

or in the form which will be most useful later on ($Q^2 = -q^2$)

$$\frac{d^2\sigma}{d\Omega dE'} = \frac{\alpha^2}{4E^2 \sin^4\frac{\theta}{2}} \delta\left(\frac{Q^2}{2M} - \nu\right) \left[\cos^2\frac{\theta}{2} + \frac{Q^2}{2M^2}\sin^2\frac{\theta}{2}\right] \qquad (1.9)$$

To obtain $\frac{d\sigma}{d\Omega}$ we integrate over dE' and obtain

$$\frac{d\sigma}{d\Omega} = \frac{\alpha^2}{4E^2 \sin^4\frac{\theta}{2}} \frac{1}{\left[1 + \frac{2E}{M}\sin^2\frac{\theta}{2}\right]} \left[\cos^2\frac{\theta}{2} + \frac{Q^2}{2M^2}\sin^2\frac{\theta}{2}\right] \qquad (1.10)$$

Exercise: Prove this. Hint:

$$\int dx\, \delta(f(x)) = \left[\frac{df(x)}{dx}\right]^{-1}$$

This cross section is often written in the form

$$\frac{d\sigma}{d\Omega} = \left(\frac{d\sigma}{d\Omega}\right)_{MOTT} \left\{1 + \frac{Q^2}{2M^2}\tan^2\frac{\theta}{2}\right\} \qquad (1.11)$$

where

$$\left(\frac{d\sigma}{d\Omega}\right)_{MOTT} \equiv \frac{\alpha^2 \cos^2\frac{\theta}{2}}{4E^2 \sin^4\frac{\theta}{2}\left[1 + \frac{2E}{M}\sin^2\frac{\theta}{2}\right]} \qquad (1.12)$$

is the cross section for scattering a spin I/2 particle in the Coulomb field of a target with mass M. Hence the quantity $1 + \frac{Q^2}{2M^2} \tan^2 \frac{\theta}{2}$ is the correction to the Mott (Coulomb) cross section arising from the magnetic interaction between the electron and the muon.

1.2 Elastic Electron-Proton Scattering

Electron-proton scattering[2] takes place by photon exchange just like the previous example but now the photon-proton coupling is not known (contrast the γ_ρ coupling for the muon). If account is taken of the fact that the proton spinors $\bar{u}(p')$ and $u(p)$ obey the Dirac equation then the most general form of the proton's electromagnetic current $J_\rho \sim \bar{u}(p') \Gamma_\rho u(p)$ can only involve γ_ρ, q_ρ and $i \sigma_{\rho\alpha} q^\alpha$ multiplied by general functions of p^2 ($\equiv M^2$), p'^2 ($\equiv M^2$) and q^2 standing between the spinors, viz

$$J_\rho \sim \bar{u}(p') \left\{ \Gamma_1(q^2)\gamma_\rho + \Gamma_2(q^2)\, i\, \sigma_{\rho\alpha}\, q^\alpha + \Gamma_3(q^2)\, q_\rho \right\} u(p) \quad (1.13)$$

where $\sigma_{\rho\alpha} = \frac{i}{2} [\gamma_\rho, \gamma_\alpha]$. Current conservation, $q^\rho J_\rho = 0$, forces $\Gamma_3(q^2) \equiv 0$ since the terms multiplying $\Gamma_{1,2}$ vanish identically and hence we have

$$J_\rho \sim \bar{u}(p') \left\{ \Gamma_1(q^2)\gamma_\rho + \kappa \frac{F_2(q^2)}{2M}\, i\, \sigma_{\rho\alpha}\, q^\alpha \right\} u(p) \quad (1.14)$$

where $F_1(0) = 1$ (proton charge) and $F_2(0) = 1$. The quantity κ is the anomalous magnetic moment of the proton ($\equiv 1.79$ Bohr magnetons). By making use of the Gordon identity, viz

$$\bar{u}(p')\, i\, \sigma_{\rho\alpha}\, q^\alpha\, u(p) = \bar{u}(p') \left\{ 2M\, \gamma_\rho - (p + p')_\rho \right\} u(p) \quad (1.15)$$

we can re-write J_ρ in the alternative form

$$J_\rho \sim \bar{u}(p') \left\{ \gamma_\rho \left[F_1(q^2) + \kappa F_2(q^2) \right] - \frac{(p+p')_\rho}{2M} \kappa F_2(q^2) \right\} u(p) \quad (1.16)$$

This may be written

$$J_\rho \sim \bar{u}(p') \left\{ \gamma_\rho \, G_M(q^2) + \frac{(p+p')_\rho}{2M} \, \frac{G_E(q^2) - G_M(q^2)}{1 - q^2/4M^2} \right\} u(p) \qquad (1.17)$$

with

$$\begin{aligned} G_M &= F_1 + F_2 \kappa \\ G_E &= F_1 + \frac{\kappa q^2}{4M^2} \, F_2 \end{aligned} \qquad (1.18)$$

$G_{E,M}$ are referred to as the electric and magnetic form factors of the proton[3] since $G_E(0) = 1$, $G_M(0) = \mu = 1 + \kappa$, contrast the Pauli and Dirac form factors $F_{1,2}$.

Exercise: Prove eqn.(1.15). Hint: start with $\bar{u}(p')\gamma_\mu \, u(p) = \bar{u}(p')\gamma_\mu \, \frac{\not{p} + m}{2m} \, u(p)$ and feed the $\not{p}$ through until it acts on the $\bar{u}(p')$ where $p' = p + q$.

With the form (1.14) for the proton's electromagnetic current written in terms of $F_{1,2}$ we can calculate the cross section for electron-proton scattering in direct analogy to the electron-muon case discussed above. The only essential difference is in the form of the tensor $W^{\mu\nu}$ which now reads

$$W^{\mu\nu} = \frac{1}{4M^2} \, \text{Trace} \, (\not{p}' + M) \, \Gamma^\mu \, (\not{p} + M) \, \Gamma^\nu \qquad (1.19)$$

with $\Gamma^\mu \equiv \gamma^\mu \, F_1(q^2) + \frac{\kappa \, F_2(q^2)}{2M} \, i\sigma_{\mu\alpha} \, q^\alpha$ in contrast to the muon target where this was simply γ^μ. The calculation of the cross section now proceeds as in the previous example and one finds ($Q^2 \equiv -q^2$)

$$\frac{d\sigma}{d\Omega} = \left(\frac{d\sigma}{d\Omega} \right)_{MOTT} \left[\left(F_1^2 + \frac{\kappa^2 Q^2}{4M^2} \, F_2^2 \right) + \frac{Q^2}{2M^2} \, (F_1 + \kappa F_2)^2 \, \tan^2 \frac{\theta}{2} \right] \qquad (1.20)$$

where the $F_{1,2}$ are functions of the photons mass squared q^2. We can perform a partial check on the correctness of our calculation by setting $F_1 = 1$, and $F_2 = 0$ whereupon we obtain the form of the electron-muon cross section (1.11) (the muon current was $\bar{u}(\gamma_\mu + 0\ \sigma_{\mu\alpha}\ q^\alpha)\ u$ which corresponds to $F_1 = 1$, $F_2 = 0$).

Exercise: By following the steps in the calculation of electron-muon scattering, derive the form of the cross section (1.20) for the proton target starting from the tensor $W^{\mu\nu}$ given at (1.19). The rules for taking traces of gamma matrices are given in Bjorken and Drell, p.104.

The cross section can be alternatively written in terms of the $G_{E,M}$ as defined in (1.18) and reads

$$\frac{d\sigma}{d\Omega} = \left(\frac{d\sigma}{d\Omega}\right)_{MOTT} \left\{ \frac{G_E^2 + \frac{Q^2}{4M^2} G_M^2}{1 + \frac{Q^2}{4M^2}} + \frac{Q^2}{2M^2} G_M^2 \tan^2 \frac{\theta}{2} \right\} \qquad (1.21)$$

which is known as the Rosenbluth formula. Note that in direct analogy with eqn.(1.9) for the muon target, the double differential cross section for a proton target reads

$$\frac{d^2\sigma}{d\Omega dE'} = \frac{\alpha^2}{4E^2 \sin^4 \frac{\theta}{2}} \delta\left(\frac{Q^2}{2M} - \nu\right) \left\{ \cos^2 \frac{\theta}{2} \left(\frac{G_E^2 + \frac{Q^2}{4M^2} G_M^2}{1 + Q^2/4M^2} \right) + \frac{Q^2 G_M^2}{2M^2} \sin^2 \frac{\theta}{2} \right\} \qquad (1.22)$$

By comparing the cross section formulae for the proton target with the analogous formulae for the muon target it is clear that the quantities in parentheses in (1.21 and 1.22) arise due to the proton's intrinsic structure. In particular we note that the general form of the cross sections for both the muon and proton targets (1.11 and 1.21) is

$$\left(\frac{d\sigma}{d\Omega}\right) \Big/ \left(\frac{d\sigma}{d\Omega}\right)_{MOTT} = A + B \tan^2 \frac{\theta}{2} \qquad (1.23)$$

where for the proton target

$$A \equiv \frac{G_E^2 + \frac{Q^2}{4M^2} G_M^2}{1 + Q^2/4M^2}$$

$$B \equiv \frac{Q^2 G_M^2}{2M^2} \qquad (1.24)$$

and hence A and B are functions of q^2 in general (since $G_{E,M}$ are functions of q^2). Holding q^2 fixed and constraining the final state to have the mass of the proton (i.e. elastic scattering) the experimentalist can measure $\frac{d\sigma}{d\Omega}$ at various scattering angles θ and hence separate A and B and therefore $G_{E,M}$ at that q^2 value (fig. 5). Experimentally the observation of a linear dependence in $\tan^2 \frac{\theta}{2}$ supports our assumption that the one photon exchange mechanism is a relevant approximation.

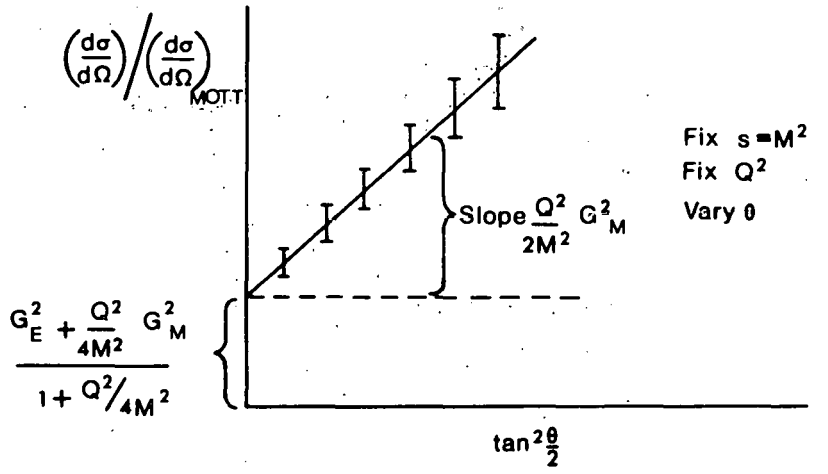

Fig. 5 Separation of $G_{E,M}$ and test of one-photon exchange for which $d\sigma/(d\sigma)_{MOTT} = A + B \tan^2 \theta/2$.

Problem: What other tests of the one photon exchange assumption can you devise?

Hint: In what way does e^-p look like/differ from e^+p in one as against two photon exchange?

---

2 INELASTIC ELECTRON SCATTERING

We come now to the focal point of the lectures, namely the process e + p → e + hadrons where the energy of the final electron and its angle of scatter are all that one measures[4]. A spectrometer sits at some angle θ to the incident electron beam and records the energies of the scattered electrons and counts events. We assume that the one photon exchange mechanism is dominant (though there is little or no evidence to support or refute this other than experience with the elastic scattering - which may or may not be a good guide).

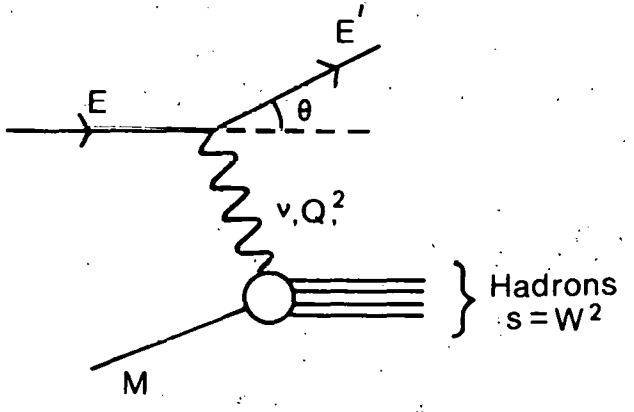

Fig. 6 Inelastic electron-proton scattering via one photon exchange.

Diagrammatically the amplitude looks like fig. 6 and, as always, the cross section has the form

$$\frac{d^2\sigma}{d\Omega dE'} = 1/2\ \frac{4\alpha^2 m^2}{q^4}\ \frac{E'}{E}\ \delta(\Sigma E_f - \Sigma E_i)\ L_{\mu\nu}\ W^{\mu\nu} \qquad (2.1)$$

which we can draw as in fig. 7 (compare fig. 3 for elastic scattering). The lepton tensor $L_{\mu\nu}$ is clearly the same as before,

$$L_{\mu\nu} = \frac{1}{4m^2}\ \text{Trace}\ (\not{k}' + m)\gamma_\mu\ (\not{k} + m)\gamma_\nu \rightarrow \frac{1}{m^2}\ \left[k_\mu k'_\nu + k'_\mu k_\nu - g_{\mu\nu}\ (k.k' - m^2)\right] \qquad (2.2)$$

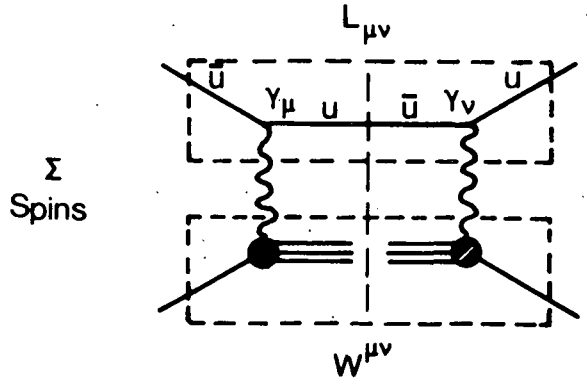

Fig. 7 Tensor structure of electron-proton inelastic cross section.

but now we do not have an explicit form for the hadronic vertex in fig. 6 since the final hadronic system is not observed and so, among other things, its spin is unknown (contrast 1.4 and 1.19 for elastic scattering). To proceed any further with our calculation we must therefore write down the most general form that the tensor $W^{\mu\nu}$ can have.

If we do not polarise the initial proton, then the most general form for $W^{\mu\nu}$ which is symmetric in $\mu\nu$ ($L_{\mu\nu}$ is symmetric in $\mu\nu$ and hence only $W^{\mu\nu(sym)}$ contributes to the unpolarised cross section) may be written[5]

$$W^{\mu\nu} = A g^{\mu\nu} + B q^\mu q^\nu + C(p^\mu q^\nu + q^\mu p^\nu) + D p^\mu p^\nu \qquad (2.3)$$

Gauge invariance constrains[6] $q_\mu W^{\mu\nu} = 0$ and on applying this to the above we find

$$\begin{aligned} &(i) && C q^2 + D p.q = 0 \\ &(ii) && C p.q + B q^2 + A = 0 \end{aligned} \qquad (2.4)$$

From (i) we have $C = \frac{-D p.q}{q^2}$ and substituting into (ii) we have that $B = \frac{D(p.q)^2}{q^4} - \frac{A}{q^2}$. Then, substituting for B, C in $W^{\mu\nu}$ we obtain (2.5)

$$W^{\mu\nu} = A(g^{\mu\nu} - \frac{q^\mu q^\nu}{q^2}) + D\left(\frac{(p.q)^2}{q^4} q^\mu q^\nu - \frac{p.q}{q^2}(p^\mu q^\nu + q^\mu p^\nu) + p^\mu p^\nu \right)$$

which, with $A = -W_1$, $D = W_2/M^2$, takes on the familiar form[7]

$$W^{\mu\nu} = W_1(\nu, q^2)\left(-g^{\mu\nu} + \frac{q^\mu q^\nu}{q^2}\right) + \frac{W_2(\nu, q^2)}{M^2}\left[(p^\mu - \frac{p.q}{q^2}q^\mu)(p^\nu - \frac{p.q}{q^2}q^\nu)\right] \tag{2.6}$$

We are now ready to calculate the cross section (2.1) by first computing $L_{\mu\nu} W^{\mu\nu}$ (2.2) with (2.6). We find

$$L_{\mu\nu} W^{\mu\nu} = 2W_1\, k.k' + \frac{W_2}{M^2}\left\{2p.k\; p.k' - k.k'\, M^2\right\} \tag{2.7}$$

and using $q = k - k'$ then $q^2 = -2k.k'$ (neglecting lepton masses) while in the laboratory with $p.k = ME$, $p.k' = ME'$ we finally obtain

$$L_{\mu\nu} W^{\mu\nu} = 2EE'\left\{2\sin^2\frac{\theta}{2} W_1 + \cos^2\frac{\theta}{2} W_2\right\} \tag{2.8}$$

and hence the cross section becomes

$$\frac{d^2\sigma}{d\Omega dE'} = \frac{4\alpha^2 E'^2}{q^4}\left(\cos^2\frac{\theta}{2} W_2 + 2W_1 \sin^2\frac{\theta}{2}\right) \tag{2.9}$$

or with $q^4 = 16\, E^2\, E'^2 \sin^4\frac{\theta}{2}$ we can write

$$\frac{d^2\sigma}{d\Omega dE'} = \frac{\alpha^2}{4E^2 \sin^4\frac{\theta}{2}}\left(\cos^2\frac{\theta}{2} W_2 + 2W_1 \sin^2\frac{\theta}{2}\right) \tag{2.10}$$

By comparison with (1.22) we can see the form that $W_{1,2}$ take for elastic scattering ($Q^2 \equiv -q^2$)

$$W_1^{el}(\nu, Q^2) = \frac{Q^2}{4M^2} G_M^2(Q^2)\, \delta(\frac{Q^2}{2M} - \nu) \tag{2.11}$$

$$W_2^{el}(\nu, Q^2) = \frac{G_E^2(Q^2) + \frac{Q^2}{4M^2} G_M^2(Q^2)}{1 + Q^2/4M^2} \delta(\frac{Q^2}{2M} - \nu) \qquad (2.12)$$

while for elastic scattering from a spin 1/2 particle with "pointlike" coupling (e - μ scattering eqn.(1.9))

$$W_1^{pt}(\nu, Q^2) = \frac{Q^2}{4M^2} \delta(\frac{Q^2}{2M} - \nu); \qquad W_2^{pt}(\nu, Q^2) = \delta(\frac{Q^2}{2M} - \nu) \qquad (2.13)$$

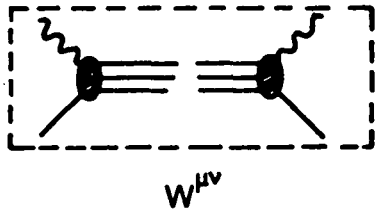

Fig. 8 Virtual photoabsorption contribution to inelastic electron-proton scattering (compare fig. 7).

Before we study the data on $\frac{d^2\sigma}{d\Omega dE'}$ we can gain some feeling for the physical significance of $W_{1,2}$ and why the cross section involves just two such structure functions. The $W_{1,2}$ enter in $W^{\mu\nu}$ which, in fig. 7, is the contribution from the hadronic vertex (fig. 8). Therefore $W^{\mu\nu}$ is the tensor for (the imaginary part of) the forward Compton scattering amplitude for off-mass shell photons. Thus, by the optical theorem, $W_{1,2}$ are related to the photoabsorption total cross sections for off-shell transverse (helicity ± 1) and scalar (helicity 0) photons. To actually compute the relation between $W_{1,2}$ and the cross sections we write the amplitude for fig. 8 as $\varepsilon_\mu W^{\mu\nu} \varepsilon_\nu$ with $\varepsilon_{\mu,\nu}$ the polarisation vectors for the photons. All we need to know is the form of ε_μ for photons with helicity ±1 or 0 and then the calculation is straightforward. Let us therefore construct the ε_μ for a photon moving along the z direction with energy ν, mass squared q^2. Gauge invariance demands that[6] $q.\varepsilon = 0$. We may then choose $\varepsilon(\pm 1) = \mp \frac{1}{\sqrt{2}} (0; 1, \pm i, 0)$ and $\varepsilon(0) = \frac{1}{\sqrt{Q^2}} (\sqrt{Q^2 + \nu^2}; 0, 0, \nu)$

all of which satisfy $q.\varepsilon = 0$. If the incident photon flux is K, then defining

$$\sigma_{\pm 1,0} = \frac{4\pi^2\alpha}{K} \varepsilon^{\mu}_{\pm 1,0} W_{\mu\nu} \varepsilon^{\nu}_{\pm 1,0} \tag{2.14}$$

we quickly find that

$$\frac{K}{4\pi^2\alpha} 1/2 (\sigma_+ + \sigma_-) \equiv \frac{K}{4\pi^2\alpha} \sigma_T = W_1 \tag{2.15}$$

and

$$\frac{K}{4\pi^2\alpha} \sigma_S = W_2 (1 + \nu^2/Q^2) - W_1 \equiv "W_L" \tag{2.16}$$

with the result that

$$W_2 = \frac{K}{4\pi^2\alpha} (\sigma_T + \sigma_S) \frac{Q^2}{Q^2 + \nu^2} \tag{2.17}$$

Thus we note that there are two photoabsorption cross sections for unpolarised targets (by parity $\sigma_+ = \sigma_-$) viz σ_T and σ_S and therefore two independent structure functions W, viz W_1 and W_2 or W_1 and W_L. Another useful quantity is

$$R \equiv \frac{\sigma_S}{\sigma_T} = \frac{W_2}{W_1} (1 + \frac{\nu^2}{Q^2}) - 1 . \tag{2.18}$$

A word about the flux factor K for virtual photons. When $q^2 = 0$ the photon flux $K = \nu$. When $q^2 \neq 0$ there is some arbitrariness about the definition. Gilman's convention[8] is to choose $K = |\underset{\sim}{q}| = \sqrt{\nu^2 + Q^2} \simeq \nu + \frac{Q^2}{2\nu}$. Hand[9], however, takes K to be the "equivalent photon energy"; namely that energy which would produce a final hadron state of the same mass as would have been created by a real photon with energy ν. Hence, since the final state mass M^* satisfies $M^{*2} = M^2 + 2M\nu - Q^2$ then $K^{Hand} = \nu - Q^2/2M$. The structure functions $W_{1,2}$ are well defined in terms of the experimentally measured $d^2\sigma/d\Omega dE'$ (eqn.(2.9)). The photoabsorption cross sections are then defined modulo this arbitrary flux factor K.

TABLE 1

A summary of useful formulae for polarised and unpolarised electron scattering

ELASTIC: e - μ :

$$\frac{d^2\sigma}{d\Omega dE'} = \frac{\alpha^2}{4E^2 \sin^4\frac{\theta}{2}} \delta\left(\frac{Q^2}{2M} - \nu\right) \left[\cos^2\frac{\theta}{2} + \frac{Q^2}{2M^2}\sin^2\frac{\theta}{2}\right]$$

or

$$\frac{d\sigma}{d\Omega} = \left(\frac{d\sigma}{d\Omega}\right)_{MOTT} \left\{1 + \frac{Q^2}{2M^2}\tan^2\frac{\theta}{2}\right\}$$

$$\left(\frac{d\sigma}{d\Omega}\right)_{MOTT} = \frac{\alpha^2 \cos^2\frac{\theta}{2}}{4E^2 \sin^4\frac{\theta}{2}\left[1 + \frac{2E}{M}\sin^2\frac{\theta}{2}\right]}$$

e - p :

$$\frac{d\sigma}{d\Omega} = \left(\frac{d\sigma}{d\Omega}\right)_{MOTT} \left[(F_1^2 + \frac{\kappa^2 Q^2}{4M^2}F_2^2) + \frac{Q^2}{2M^2}(F_1 + \kappa F_2)^2 \tan^2\frac{\theta}{2}\right]$$

$$G_M = F_1 + \kappa F_2; \qquad G_E = F_1 - \frac{\kappa Q^2}{4M^2} F_2$$

$$\frac{d\sigma}{d\Omega} = \left(\frac{d\sigma}{d\Omega}\right)_{MOTT} \left[\frac{G_E^2 + \frac{Q^2}{4M^2}G_M^2}{1 + Q^2/4M^2} + \frac{Q^2}{2M^2}G_M^2 \tan^2\frac{\theta}{2}\right]$$

INELASTIC:

$$W_{\mu\nu} = W_1\left(-g_{\mu\nu} + \frac{q_\mu q_\nu}{q^2}\right) + \frac{W_2}{M^2}\left(p_\mu - \frac{p.q}{q^2}q_\mu\right)\left(p_\nu - \frac{p.q}{q^2}q_\nu\right)$$

$$\frac{d^2\sigma}{d\Omega dE'} = \frac{\alpha^2}{4E^2 \sin^4\frac{\theta}{2}} \left[\cos^2\frac{\theta}{2} W_2(\nu, Q^2) + 2\sin^2\frac{\theta}{2} W_1(\nu, Q^2)\right.$$

$$W_1^{el}(\nu, Q^2) = \frac{Q^2}{4M^2} G_M^2(Q^2)\, \delta(Q^2/2M - \nu) \xrightarrow{\text{muon}} \frac{Q^2}{4M^2}\delta\left(\frac{Q^2}{2M} - \nu\right)$$

$$W_2^{el}(\nu, Q^2) = \frac{G_E^2(Q^2) + \frac{Q^2}{4M^2}G_M(Q^2)}{1 + Q^2/4M^2}\, \delta\left(\frac{Q^2}{2M} - \nu\right) \xrightarrow{\text{muon}} \delta\left(\frac{Q^2}{2M} - \nu\right)$$

CROSS SECTIONS:

$$W_1 = \frac{K}{4\pi^2\alpha}\sigma_T; \qquad W_2 = \frac{K}{4\pi^2\alpha}(\sigma_T + \sigma_S)\frac{Q^2}{Q^2 + \nu^2};$$

$$W_L = W_2(1 + \nu^2/Q^2) - W_1$$

$$R = \frac{\sigma_S}{\sigma_T} = \frac{W_2}{W_1}(1 + \nu^2/Q^2) - 1$$

$$K^{Hand} = \nu - \frac{Q^2}{2M}, \qquad K^{Gilman} = |\underline{q}|$$

$$\frac{d^2\sigma}{d\Omega dE'} = \Gamma(\sigma_T + \varepsilon\sigma_S), \qquad \varepsilon = \left[1 + 2\frac{Q^2 + \nu^2}{Q^2}\tan^2\frac{\theta}{2}\right]^{-1}$$

$$\Gamma = \frac{K\alpha}{2\pi^2 Q^2}\frac{E'}{E}\frac{1}{1 - \varepsilon}$$

Knowing the form for $d^2\sigma/d\Omega dE'$ in terms of $W_{1,2}$ and also our definitions of $W_{1,2}$ in terms of $\sigma_{T,S}$, we can substitute these latter in and obtain $d^2\sigma/d\Omega dE'$ in terms of the photoabsorption cross sections. This form is widely met in the literature and completes our kinematic study. The reader is invited to perform the algebra as an exercise and convince her/himself that

$$\frac{d^2\sigma}{d\Omega dE'} = \Gamma\,(\sigma_T + \varepsilon\,\sigma_S) \tag{2.19}$$

where

$$\varepsilon = \left[\,1 + 2\,\frac{Q^2 + \nu^2}{Q^2}\,\tan^2\frac{\theta}{2}\,\right]^{-1}$$

$$\Gamma = \frac{K\alpha}{2\pi^2 Q^2}\,\frac{E'}{E}\,\frac{1}{1-\varepsilon}\,.$$

3 DEEP INELASTIC SCATTERING AND PARTONS

A target of mass M sits in the laboratory and an electron of energy E emerges from the accelerator. The target sees the electron by receiving from it one photon whose energy ν and mass squared q^2 are given by

$$\nu = E - E', \qquad q^2 = -4EE'\sin^2\frac{\theta}{2} \equiv -Q^2$$

where E' is the energy of the final electron with θ the angle through which it has been scattered in the laboratory. We have seen that the cross section for observing the electron in an element of solid angle $d\Omega$ and dE' of energy may be written

$$\frac{d^2\sigma}{d\Omega dE'} = \frac{4\alpha^2\,E'^2\cos^2\frac{\theta}{2}}{Q^4}\left\{\,W_2(\nu,\,Q^2) + W_1(\nu,\,Q^2)\;2\tan^2\frac{\theta}{2}\,\right\} \tag{3.1}$$

where $W_{1,2}$ are structure functions which summarise our lack of knowledge of the dynamics in the vertex $\gamma_V p \to$ anything in fig. 6. These structure functions are dependent on both the photon energy and also q^2 which can be independently varied. The mass squared of the unobserved hadron system W^2 is

$$W^2 = (p + q)^2 = M^2 + 2p.q + q^2 \tag{3.2}$$

which in the laboratory frame reads

$$W^2 = M^2 + 2M\nu - Q^2 \tag{3.3}$$

Given a dynamical theory of the nucleon we could calculate $W_{1,2}$ and hence the cross section. For example, in electron-muon scattering we know that the final state is a muon and that the muon photon vertex is γ_μ: we calculated

$$W_1 = \frac{Q^2}{4m^2}\ \delta\left(\frac{Q^2}{2m} - \nu\right), \qquad W_2 = \delta\left(\frac{Q^2}{2m} - \nu\right) \tag{3.4}$$

and hence determined the cross section (1.9). In the case of the proton we do not have such a dynamical theory and so we do the reverse: viz, we measure the cross section at various θ and hence we extract $W_{1,2}\ (\nu, Q^2)$. Knowledge of these structure functions then tells us something about the substructure of the proton, the only problem is to decipher the meaning of the data once you have them. One can show data for W_1 and W_2, or W_1 and R or W_2 and R or any other combination of the two independent quantities. We show in figs. 9 the data for W_1 and νW_2 for $Q^2 > 1\ (\text{GeV})^2$ and for $W^2 > 4\ (\text{GeV})^2$, i.e. beyond the region of the prominent resonances. You will notice that both W_1 and νW_2, which a priori one would expect to be functions of both ν and q^2, seem to be independent of q^2 when plotted against $\frac{2M\nu}{Q^2}$ (this ratio is called ω and this phenomenon is known as scale invariance[4]) i.e. for large Q^2 and W^2, W_1 and $\nu W_2(\nu, Q^2) \to W_1, \nu W_2(\omega)$. This is seen in fig. 10 where at fixed $\omega = 4$ we find $\nu W_2(\nu, Q^2)$ is independent of Q^2 for $Q^2 > 1\ (\text{GeV})^2$. Bjorken had conjectured[10] that such a phenomenon would be observed and its observation caused great excitement. This a dramatic effect and surely is telling us something about the proton's substructure; but what exactly?

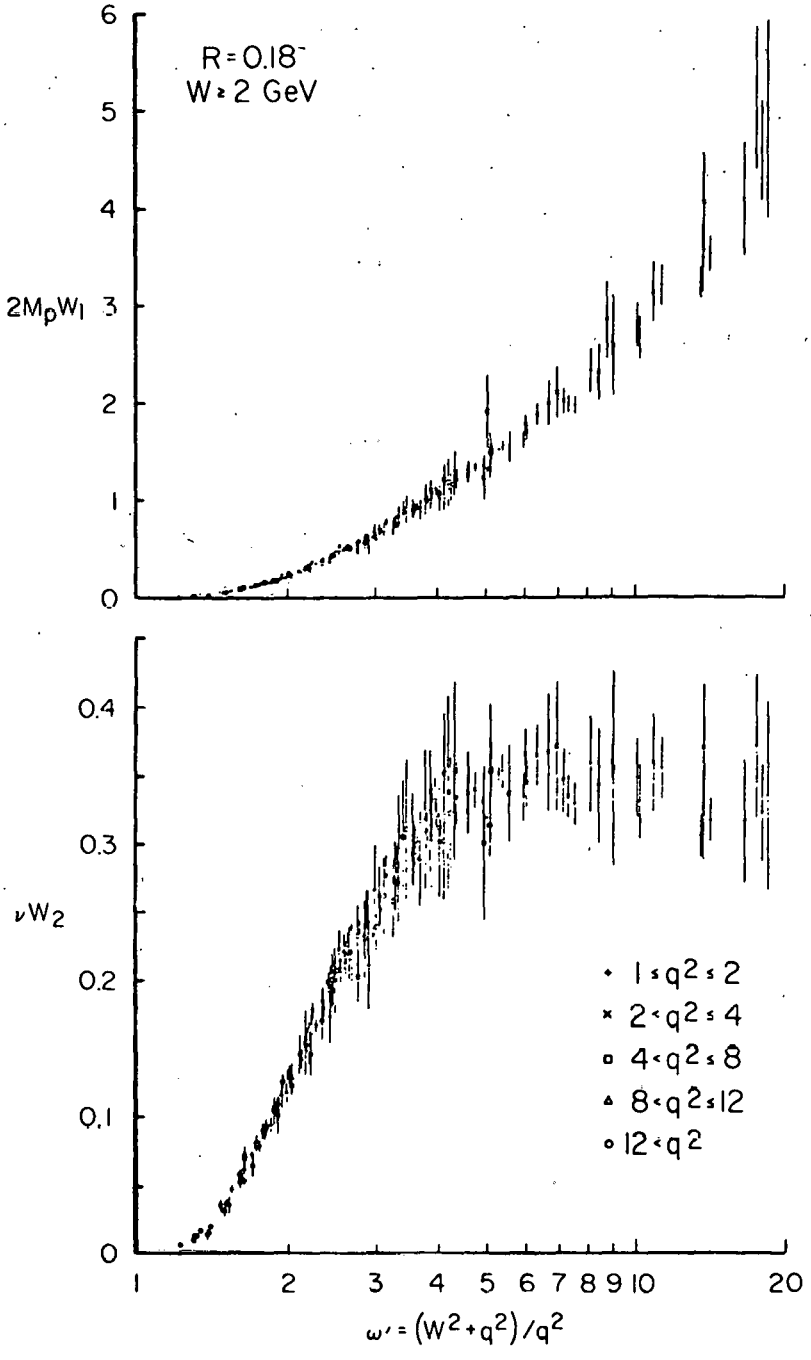

Fig. 9 Data for W_1, νW_2 (ν, q^2) plotted against $\omega' \simeq \omega$.

This phenomenon has been interpreted by many as suggesting that the nucleon is built from "partons" which interact with the electromagnetic field in a "pointlike" manner[11,12] (i.e. like a muon as discussed in the first chapter). The hypothesis is that the inelastic scattering is the incoherent sum

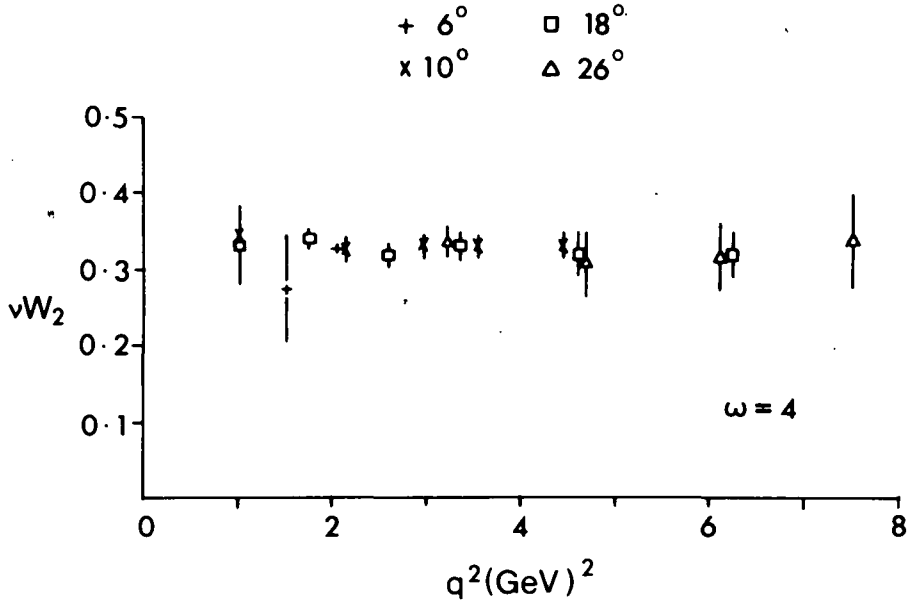

Fig. 10 Constancy of νW_2 at fixed ω.

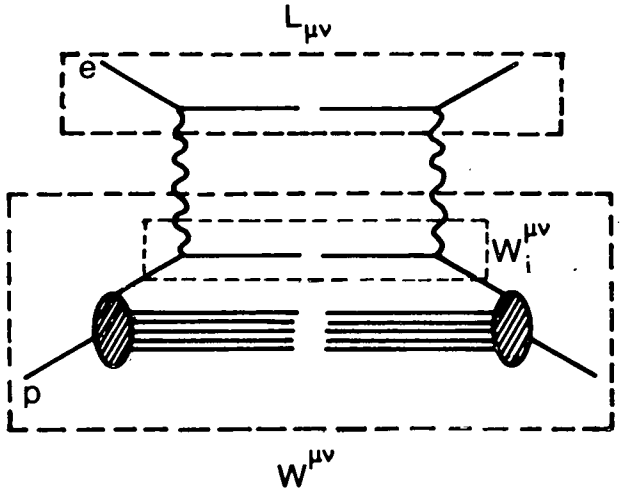

Fig. 11 Inelastic electron-proton scattering in the parton model. The proton breaks up into constituent partons from which the electron scatters elastically (contributing $W_i^{\mu\nu}$ for the ith parton).

of the elastic scattering from the constituent partons (fig. 11). Thus the inelastic cross section is the sum of the cross sections for elastic scattering from the constituent partons and hence

$$W_{1,2} = \sum_i W_{1,2}^{\text{elastic}(i)} \tag{3.5}$$

where the sum is over the partons i. Electron-parton scattering is postulated to look just like electron-muon scattering and from eqns.(1.9), (2.9) and (2.13) we know that

$$W_1^{\text{el}(i)} = \frac{Q^2}{4m^2}\,\delta\left(\frac{Q^2}{2m} - \nu\right) e_i^2\,, \qquad W_2^{\text{el}(i)} = \delta\left(\frac{Q^2}{2m} - \nu\right) e_i^2 \tag{3.6}$$

where m is the parton mass and e_i^2 is the ratio of the charge squared of the parton to that of the muon. Let the parton mass m be some fraction x of the proton mass and let $f(x)dx$ be the probability that a parton mass between xM and $(x + dx)M$ exists in the proton. Then

$$W_1(\nu, Q^2) = \sum_i W_1^{\text{el}(i)}(\nu, Q^2) = \sum_i \int_0^1 dx\, f(x)\, e_i^2\, \frac{Q^2}{4x^2M^2}\, \delta\left(\frac{Q^2}{2xM} - \nu\right) \tag{3.7}$$

and

$$W_2(\nu, Q^2) = \sum_i W_2^{\text{el}(i)}(\nu, Q^2) = \sum_i \int_0^1 dx\, f(x)\, e_i^2\, \delta\left(\frac{Q^2}{2xM} - \nu\right) \tag{3.8}$$

Rewriting $\delta\left(\frac{Q^2}{2xM} - \nu\right)$ as $\frac{x}{\nu}\,\delta\left(\frac{1}{\omega} - x\right)$ then

$$W_1(\nu, Q^2) \to \sum_i \int_0^1 dx\, f(x)\, e_i^2\, \frac{1}{2M}\, \delta\left(x - \frac{1}{\omega}\right) \to W_1(\omega) \tag{3.9}$$

$$\nu W_2(\nu, Q^2) \to \sum_i \int_0^1 dx\, x\, f(x)\, e_i^2\, \delta\left(x - \frac{1}{\omega}\right) \to \nu W_2(\omega) \tag{3.10}$$

i.e. the structure functions W_1 and νW_2 are functions of ω in this model. Furthermore we see that

$$\nu W_2(\omega) = \frac{2M}{\omega} W_1(\omega) = \frac{Q^2}{\nu} W_1(\omega) \tag{3.11}$$

and hence that

$$R \equiv \frac{\sigma_S}{\sigma_T} = \frac{W_2}{W_1}\left(1 + \frac{\nu^2}{Q^2}\right) - 1 \to \frac{Q^2}{\nu^2} \equiv \frac{4M^2}{Q^2\omega^2} \tag{3.12}$$

Note that $R \to 0$ in the limits (i) $Q^2 \to \infty$, ω fixed; and (ii) $\nu \to \infty$, Q^2 fixed. This is seen to be consistent with the data shown in fig. 12 where R is seen to be small. This suggests that the partons probably have spin 1/2 (spin 0 partons would predict that $\sigma_T = 0$ and hence $R = \infty$ in manifest disagreement with the data[13]).

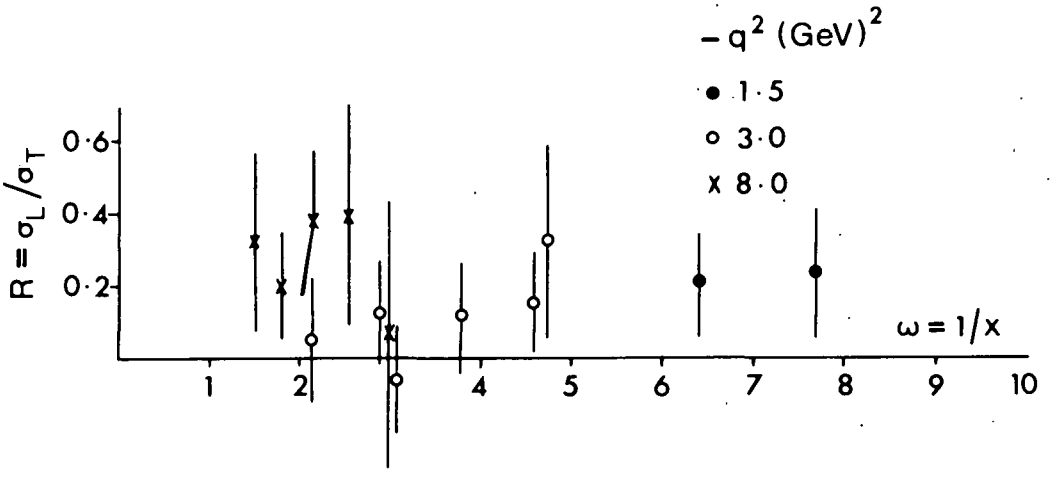

Fig. 12 $R = \sigma_L/\sigma_T$ data.

The conclusion that if there are partons in the nucleon then they have spin 1/2 suggests that the partons might be the quarks of Gell-Mann and Zweig[14]. In addition to spin 1/2 these quarks have the quantum numbers shown in Table 2. In the next section, by assuming that the partons have the quantum numbers of quarks, we will derive testable relations between weak and electromagnetic structure functions. Before doing that we will first allay a doubt which may have entered the reader's mind, namely, if the partons are

TABLE 2

The quarks' quantum numbers

	Charge	Isospin (I_3)	Strangeness	Baryon Number
p	2/3	1/2	0	1/3
n	- 1/3	- 1/2	0	1/3
λ	- 1/3	0	- 1	1/3
$\bar{p}$	- 2/3	- 1/2	0	- 1/3
$\bar{n}$	1/3	1/2	0	- 1/3
$\bar{\lambda}$	1/3	0	1	- 1/3

quarks with some fixed mass m then x is fixed = m/M and so we seem to be predicting that $\nu W_2(\omega)$ is a delta function viz fig. 13 whereas the data (fig. 9) do not exhibit such a perverse behaviour.

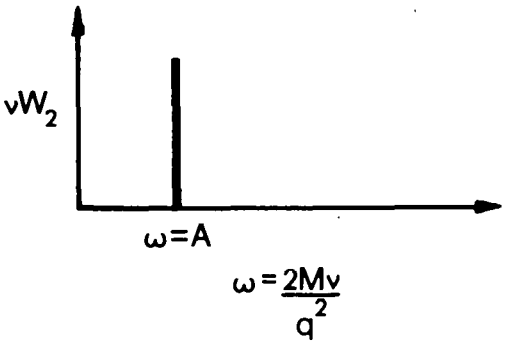

Fig. 13 νW_2 for scattering from target mass M composed of A stationary constituents.

The explanation is most easily seen by drawing analogy with nuclear physics[12] (the nucleus is built from partons - viz, the neutrons and protons!) For a nucleus of A nucleons then the above theory predicts a delta function at $\omega = A$ (with $\omega \equiv \frac{2M\nu^{\text{nucleus}}}{Q^2}$). This would indeed obtain empirically <u>if</u> the nucleons were at rest inside the nucleus (note that we have always used the lab. frame throughout for both the target and the partons). However, the

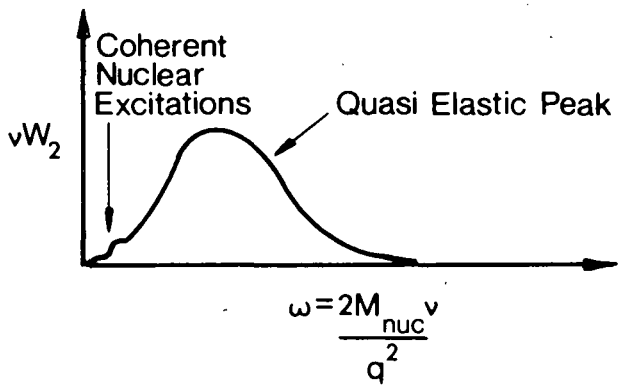

Fig. 14 Effect upon νW_2 (fig. 13) of Fermi momentum of the A constituents. The delta function has been smeared into a quasi elastic peak.

nucleons are shaking due to Fermi motion and hence have a Fermi momentum. The effect of this Fermi motion is to smear out the delta function into a "quasi elastic peak" (fig. 14) because the photon with energy ν in the lab. is seen with energy $\nu' \sim \nu + \nu_F$ by a parton with Fermi momentum ν_F. The higher the Fermi momenta present, the wider the quasi elastic peak. The position of the peak's maximum tells us how many scattering centres (nucleons) there are in the nucleus and a sum rule familiar to nuclear physics relates the area under the peak to the charges squared of the constituents[12, 15]

$$\int \frac{d\nu}{\nu} \; \nu W_2^{(\text{nucleus})} = \sum_i e_i^2 \; (\equiv \int \frac{d\omega}{\omega} \; \nu W_2) \qquad (3.13)$$

this sum rule obtaining from (3.6) or (3.8).

In direct analogy we therefore expect to see a quasi elastic peak in $\nu W_2^{(\text{proton})}$ and an analogous sum rule to hold. Due to diffraction which causes $\nu W_2 \neq 0$ as $\nu \to \infty$ at fixed q^2, the integral diverges for a proton or neutron target and in the quark picture suggests that an infinite sea of quarks and antiquarks is present and related somehow to diffraction scattering. In a model[16] where the nucleon is made up of three "valence quarks" (which can be excited to form the resonance states observed in nature and listed in the particle data tables) and a unitary singlet sea of $q\bar{q}$ pairs (which yield the diffraction scattering and do not contribute to N^* excitation) then on looking at the difference of $\nu W_2^P - \nu W_2^N$, for which the diffractive contributions cancel out, then we might hope to see the residual effect of the three valence quarks.

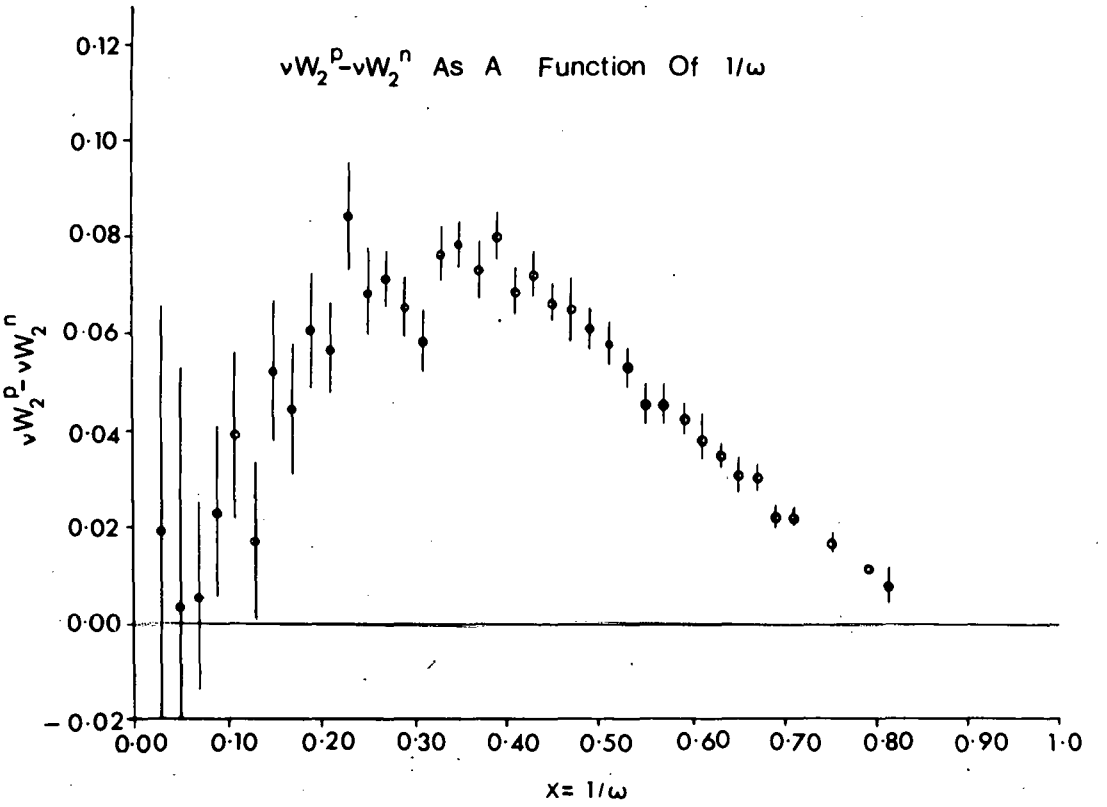

Fig. 15 Data for $\nu W_2^n - \nu W_2^p$ (compare fig. 9) for $q^2 > 1$ $(GeV/c)^2$.

Since the valence quarks in the proton are ppn with $\sum e_i^2 = 1$ and for a neutron are nnp with $\sum e_i^2 = 2/3$, then we would expect that

$$\int \frac{d\omega}{\omega} \left(\nu W_2^P(\omega) - \nu W_2^N(\omega)\right) = \sum e_i^{2(P)} - \sum e_i^{2(N)} = 1/3 \qquad (3.14)$$

Empirically this sum rule seems to have the value 0.28 ± 0.06 where we took the low ω data (fig. 15) and assumed a Regge type behaviour at high ω[13,17]. Therefore this sum rule appears to be (nearly) satisfied - (if this theory is good to 90% then I would be impressed and would conclude that this is a first approximation to something deeper). Whether or not there is any significance in the fact that $\nu W_2^P - \nu W_2^N$ looks like a smeared delta function peaking around $\omega \sim 3$ is a matter of taste!

4 STRUCTURE FUNCTIONS AND SUM RULES IN THE QUARK PARTON MODEL

We saw in eqn.(3.10) that

$$F_2(\omega) \ (\equiv \nu W_2(\omega)) \ = \ \sum_i \int_0^1 dx \, x \, f_i(x) \, e_i^2 \, \delta(x - \frac{1}{\omega})$$

or

$$F_2(x) \ = \ \sum_i e_i^2 \, x \, f_i(x)$$

where the sum is over the partons and the e_i are the charges of the partons. If we now hypothesise that the partons have the quantum numbers of the quarks of Gell-Mann and Zweig (listed in Table 2) then the structure functions become[13] (writing $u_i(x) \equiv x \, f_i(x)$)

$$F_2^{\gamma P}(x) \ = \ 4/9(u_p^P(x) + u_{\bar{p}}^P(x)) + 1/9(u_n^P(x) + u_{\bar{n}}^P(x)) + 1/9(u_\lambda^P(x) + u_{\bar{\lambda}}^P(x)) \tag{4.1}$$

$$F_2^{\gamma N}(x) \ = \ 4/9(u_p^N(x) + u_{\bar{p}}^N(x)) + 1/9(u_n^N(x) + u_{\bar{n}}^N(x)) + 1/9(u_\lambda^N(x) + u_{\bar{\lambda}}^N(x)) \tag{4.2}$$

where $u_i^{N,P}$ refers to parton (quark) i in neutron (N) or proton (P). An isospin reflection relates the amplitudes for finding a p quark in the proton with that for finding an n quark in the neutron; the complete set of such relations is

$$\begin{aligned} u_p^P &= u_n^N \\ u_n^P &= u_p^N \\ u_\lambda^P &= u_\lambda^N \end{aligned} \tag{4.3}$$

and similarly for the antiquarks. From now on we shall write our expressions referred to a proton target and drop the superscript, i.e. u_n^N for instance will

always be written as u_p. Then the structure functions eqn.(4.1, 2) become

$$F^{\gamma p}(x) = 4/9(u_p(x) + u_{\bar{p}}(x)) + 1/9(u_n(x) + u_{\bar{n}}(x)) + 1/9(u_\lambda(x) + u_{\bar{\lambda}}(x)) \tag{4.4}$$

$$F^{\gamma N}(x) = 4/9(u_n(x) + u_{\bar{n}}(x)) + 1/9(u_p(x) + u_{\bar{p}}(x)) + 1/9(u_\lambda(x) + u_{\bar{\lambda}}(x)) \tag{4.5}$$

and we immediately have the constraint

$$1/4 \leq \frac{F^{\gamma N}(x)}{F^{\gamma p}(x)} \leq 4 \tag{4.6}$$

which appears to be satisfied by the data (fig. 16).

The original motivation of the quark model was in its application to SU(3) and resonance excitation. If one believes that the resonance spectrum is generated by excitations of three quarks in the nucleon (in particular ppn for the proton and nnp for the neutron) then remarkable agreement between the predicted and the observed resonance multiplets is obtained - see R.H. Dalitz op. cit. In the spirit of two component duality the resonance excitation at low energies is believed dual to the non-diffractive or Regge contribution at high energies (see, e.g. J.K. Storrow op. cit) and a reasonable description of high energy non-diffractive phenomena is obtained in the framework of duality diagrams (where the neutron and proton are built of three quarks as above). Thus we shall proceed by assuming that these three "valence quarks" are responsible for the non-diffractive contributions to the structure functions. There is also a background over and above the resonance contributions to meson-baryon scattering and in two component duality this is hypothesised to be dual to the diffractive behaviour at high energies. We shall assume therefore that there is an isoscalar sea of quark-antiquark pairs in the nucleon which are responsible for the non-diffractive behaviour. This formulation of the quark-parton model, which originated[16] with Kuti-Weisskopf and Landshoff and Polkinghorne, may be summarised as (see also Harari, ref. 18)

$$\begin{array}{ccc} \text{3 "valence quarks"} & + & \text{"sea of } q\bar{q}\text{"} \\ \updownarrow & & \updownarrow \\ \text{Resonances} & + & \text{Background} \\ \updownarrow & & \updownarrow \\ \text{Non-diffractive} & + & \text{Diffractive} \end{array} \tag{4.7}$$

Therefore we see that for the non-diffractive component $u_p = 2u_n$; $u_\lambda = 0 = u_{\bar{n},\bar{p},\bar{\lambda}}$ with the result that upon substituting into eqns.(4.4, 4.5) we have

$$(F^{\gamma N}/F^{\gamma P})_{\text{Non-Diff}} = 2/3 \tag{4.8}$$

For the diffractive component the sea alone contributes and since this is by hypothesis an isoscalar then

$$(F^{\gamma N}/F^{\gamma P})_{\text{Diff}} = 1 \tag{4.9}$$

Finally in order to attain the lower limit of 1/4 for this ratio the current must couple to the "active quark" i.e. the quark with the isospin quantum numbers of the target viz p in the proton and n in the neutron

$$(F^{\gamma N}/F^{\gamma P})_{\text{active}} = 1/4 \tag{4.10}$$

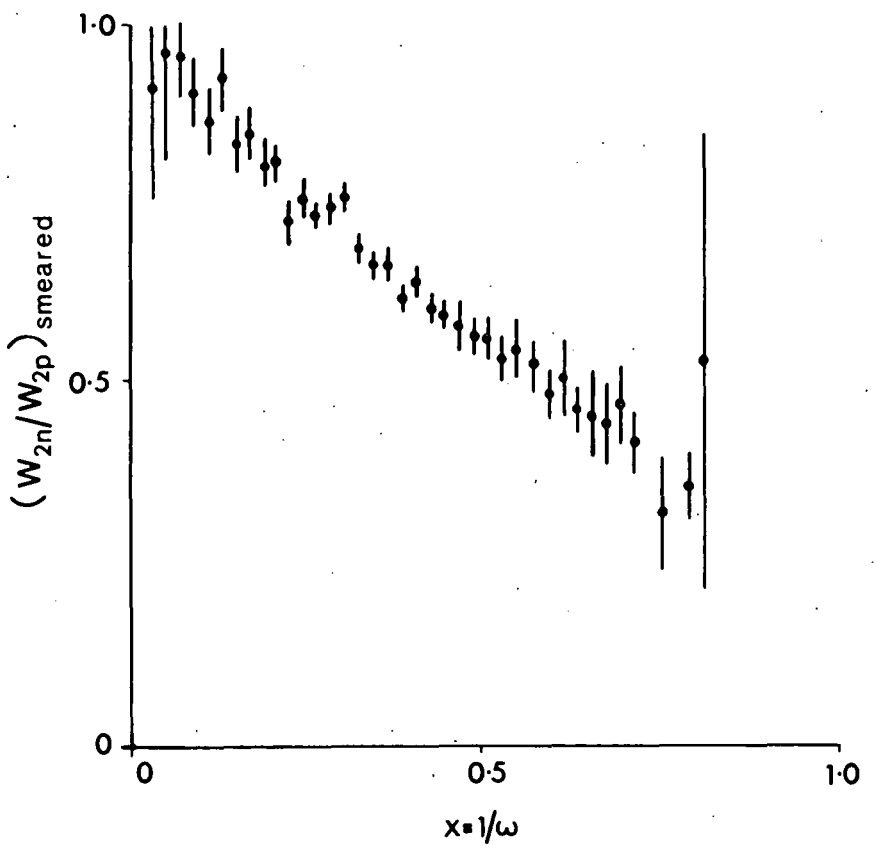

Fig. 16 Data for $\nu W_2^n/\nu W_2^p$ plotted against $x = 1/\omega$.

From the data for this ratio (fig. 16) it seems that the diffractive behaviour is important as $x \to 0$ ($\omega \to \infty$) which is intuitively reasonable[19] since this corresponds to high energies when q^2 is large (i.e. q^2 greater than about 1 GeV^2 in order that the scaling obtains). The smaller the value of ω the more important the non-diffractive contribution becomes and around ω of 3 to 5 the "canonical" 2/3 obtains. For small ω the ratio appears to fall suggesting that for some reason the "active" quark is the only quark that couples in this limit. We do not know why this should be the case though Feynman has argued[20] that if the ratio falls below 1 then it falls to 1/4 as $\omega \to 1$. A possible relation with SU(6) breaking and resonance excitation form factors is discussed in chapter 13. Therefore it seems that we have a semi-quantitative feeling for what is happening in the data using the quark-parton model as our guide. We can test the model further by looking at its predictions for the behaviour of weak interaction structure functions.

The neutrino couples to the isospin of the target or scattering centre thus

$$F_2^{\nu P} = F_2^{\bar{\nu} N}, \qquad F_2^{\bar{\nu} P} = F_2^{\nu N} \tag{4.11}$$

and for the quarks

$$\nu n \to p, \quad \nu p = 0, \quad \nu \lambda = 0, \quad \nu \bar{p} = \bar{n}, \quad \nu \bar{n} = 0, \quad \nu \lambda = 0 \tag{4.12}$$

(we deal only the VV contribution to the structure functions in this section. Inclusion of AA should double all weak structure functions in magnitude). In deriving (4.12) recall that $\nu i \to \mu^- f$ and so the charge of f is one unit higher than i. We are working in the approximation that the Cabibbo angle is zero, i.e. we are ignoring strangeness changing weak currents[13]. The relations (4.12) immediately yield

$$F_2^{\nu P}(x) = u_n(x) + u_{\bar{p}}(x) \tag{4.13}$$

$$F_2^{\nu N}(x) = u_p(x) + u_{\bar{n}}(x) \tag{4.14}$$

Guided by the electromagnetic case we expect that as $\omega \to 1$, $(x \to 1)$ the neutrino couples to the "active" quark hence

$$\frac{F^{\nu P}}{F^{\nu N}} (x \to 1) \to 0 \tag{4.15}$$

Around $\omega \sim 3$ $(x \sim 1/3)$ the three valence quarks contribute and since P = ppn then $u_p = 2u_n$ and so

$$\frac{F^{\nu P}}{F^{\nu N}} (x \sim 1/3) = 1/2 \tag{4.16}$$

Finally as $\omega \to \infty$ $(x \to 0)$ we expect that

$$\frac{F^{\nu P}}{F^{\nu N}} \xrightarrow{(x \to 0)} 1 \tag{4.17}$$

Data are not yet good enough to test these relations. We can however form relations which are amenable to test at the present time.

First we collect together our predictions for the weak and electromagnetic structure functions with neutron or proton targets.

$$\begin{aligned} F^{\nu N} &= u_p + u_{\bar{n}} \; ; \qquad F^{\nu P} = u_n + u_{\bar{p}} \\ F^{\gamma N} &= 4/9(u_n + u_{\bar{n}}) + 1/9(u_p + u_{\bar{p}}) + 1/9(u_\lambda + u_{\bar{\lambda}}) \\ F^{\gamma P} &= 1/9(u_n + u_{\bar{n}}) + 4/9(u_p + u_{\bar{p}}) + 1/9(u_\lambda + u_{\bar{\lambda}}) \end{aligned} \tag{4.18}$$

The difference of $F^{\gamma P}$ and $F^{\gamma N}$ is given by $1/3(u_p + u_{\bar{p}} - u_n - u_{\bar{n}})$ and if the sea is isoscalar then $u_{\bar{p}} = u_{\bar{n}}$ and so

$$F^{\gamma P} - F^{\gamma N} = 1/3(F^{\nu N} - F^{\nu P}) \tag{4.19}$$

For the sum we have

$$F^{\gamma P} + F^{\gamma N} = 5/9(u_n + u_{\bar{n}} + u_p + u_{\bar{p}}) + 2/9(u_\lambda + u_{\bar{\lambda}}) \tag{4.20}$$

Compare this with the sum of the neutrino structure functions

$$F^{\nu P} + F^{\nu N} = u_n + u_{\bar{n}} + u_p + u_{\bar{p}} \tag{4.21}$$

An inequality may therefore be written down which reads

$$F^{\gamma P} + F^{\gamma N} \geq 5/9(F^{\nu P} + F^{\nu N}) \tag{4.22}$$

The relation would be an equality if the electromagnetic current did not couple to the strange quarks. Since we saw from the data on $F^{\gamma N}/F^{\gamma P}$ (see fig. 16) that it appears that the strange quarks are not important contributors for $\omega \lesssim 5$ then we would expect that at small ω we will find

$$F^{\gamma P} + F^{\gamma N} \quad \underline{\underline{(\omega < 5)}} \quad 5/9\ (F^{\nu P} + F^{\nu N}) \tag{4.23}$$

This is easily testable with present neutrino data since it involves the sum of neutron and proton target data and therefore is measurable with nuclear targets. Note that if the partons were not quarks but instead were objects with the same isospin as the quarks but with different charges (e.g. integral charges say) then the weak structure functions would be unaltered while the electromagnetic would increase. In the next section we shall see that the data support the relation (4.23) which in turn suggests that the partons are indeed fractionally charged and probably the quarks of Gell-Mann and Zweig[13,21].

Finally we also note that integrals over certain combinations of the $u_i(x)$ are determined by the proton's conserved quantum numbers[13]

$$\text{Strangeness} = 0 = \int (u_\lambda(x) - u_{\bar{\lambda}}(x))\, dx \tag{4.24}$$

$$\text{Charge} = 1 = \int dx \left[2/3(u_p(x) - u_{\bar{p}}(x)) - 1/3(u_n(x) - u_{\bar{n}}(x)) \right] \tag{4.25}$$

(where we have removed the strange quark contribution by using (4.24)) and

$$\text{Baryon Number} = 1 = \int dx\ 1/3(u_p(x) + u_n(x) - u_{\bar{p}}(x) - u_{\bar{n}}(x)) \tag{4.26}$$

having again used eqn.(4.24).

Written in terms of ω these relations, together with (4.18) give sum rules: first,

$$\int_1^\infty \frac{d\omega}{\omega} \left(F_2^{\nu n}(\omega) - F_2^{\nu p}(\omega)\right) = 1 \qquad (4.27)$$

which is the Adler sum rule[22]. Note that the relation (4.19) substituted into (4.27) yields

$$\int_1^\infty \frac{d\omega}{\omega} \left(F_2^{\gamma p}(\omega) - F_2^{\gamma N}(\omega)\right) = 1/3 \qquad (4.28)$$

which was discussed in section 3. The fact that this is (nearly) satisfied suggests in turn that the Adler sum rule may also be satisfied (for contrary opinions and discussion see refs. 23). Finally one can obtain the sum rule for the vector axial interference term

$$\int_1^\infty \left(F_3^{\nu p}(\omega) + F_3^{\nu N}(\omega)\right) \frac{d\omega}{\omega^2} = -6 \qquad (4.29)$$

which is the Gross-Llewellyn Smith sum rule. This is not yet tested by data.

5 INELASTIC NEUTRINO SCATTERING

We speculated that the partons might be quarks, since they appeared to have spin 1/2, and made predictions for the magnitude of the neutrino structure functions on the basis of this speculation. The essential ingredient was noting that the photon coupled to the charges of the partons whereas the weak current coupled to their isospins. Knowing the charges and isospin quantum numbers of the partons, having assumed that they were quarks, the predictions for the ratio of weak to electromagnetic structure functions followed. We shall now examine the neutrino inelastic scattering data to see how well these relations are satisfied in nature. We shall first study the kinematics of inelastic neutrino scattering[13].

In the following discussion of neutrino scattering kinematics we shall endeavour to make comparisons with the electromagnetic case examined in section 2. The electron interaction took place by exchange of a single photon and we

shall assume that the weak interaction involves exchange of a W boson of mass M_W. The double differential cross section may be written in the familiar form*

$$\frac{d^2\sigma}{d\Omega dE'} = \frac{G^2}{(2\pi)^2}\left(\frac{m_W^2}{m_W^2 + Q^2}\right)^2 \frac{E'}{E} L_{\mu\nu} W^{\mu\nu} \delta(\sum E_f - \sum E_i) \qquad (5.1)$$

which may be compared with the electromagnetic case (eqn.(1.2))*

$$\frac{d^2\sigma}{d\Omega dE'} = 1/2 \frac{1}{(2\pi)^2}\left(\frac{e^2}{Q^2}\right)^2 \frac{E'}{E} L_{\mu\nu} W^{\mu\nu} \delta(\sum E_f - \sum E_i)$$

the extra $1/2$ arising from the averaging over the two spin states of the initial electron (left and right handed) whereas the incident neutrino is just left handed. If we send $M_W \to \infty$ then the cross section reduces to the familiar four point current-current interaction[13].

The lepton tensor is now*

$$L_{\mu\nu} = k_\mu k'_\nu + k'_\mu k_\nu - k.k' g_{\mu\nu} \pm i \varepsilon_{\mu\nu\lambda\sigma} k^\lambda k'^\sigma \qquad (5.2)$$

with the upper and lower signs for the (left handed) neutrino or (right handed) anti-neutrino beam. In the unpolarised electron beam we had a mixture of right and left handed electrons with the result that the $\varepsilon_{\mu\nu\lambda\sigma}$ term cancelled in the averaging over initial spin states[25].

The hadronic tensor may be written (for unpolarised initial nucleon) (c.f. eqn.(2.5) of ref. 13 and also the footnote in that reference)

$$W^{\mu\nu} = -g^{\mu\nu} W_1 + p^\mu p^\nu \frac{W_2}{M^2} - \frac{i \varepsilon^{\mu\nu\alpha\beta} W_3}{2M^2} + \frac{q^\mu q^\nu W_4}{M^2} + \frac{(p^\mu q^\nu + q^\mu p^\nu)}{2M^2} W_5 + \frac{i (p_\mu q_\nu - p_\nu q_\mu)}{2M^2} W_6 \qquad (5.3)$$

*We have removed m^2 from the definition of the cross section, contrast 1.2, and hence also from $L_{\mu\nu}$, contrast 1.3. This is so that we can avoid having terms involving the (zero) neutrino mass appearing explicitly in our equations.

the W_4 and W_5 terms were constrained by gauge invariance in the electromagnetic case and W_6 was not present since it multiplies a tensor anti-symmetric in $\mu\nu$; here they contribute in principle but we shall neglect them as they yield contributions to the cross section only to order of the lepton mass, and, in the absence of heavy leptons, can be dropped henceforth. The term W_3 was absent in the electromagnetic case since its contribution to the cross section violates parity (as can be seen later eqn.(5.6)).

Contracting $L_{\mu\nu}\, W^{\mu\nu}$ we obtain

$$2EE' \left\{ 2\sin^2\frac{\theta}{2}\, W_1 + \cos^2\frac{\theta}{2}\, W_2 \mp W_3 \frac{(E+E')}{M} \sin^2\frac{\theta}{2} \right\} \qquad (5.4)$$

(compare eqn.(2.8) in the electron case) the upper (lower) sign coming from ν ($\bar{\nu}$) interactions. Hence

$$\frac{d^2\sigma(\nu,\bar{\nu})}{d\Omega dE'} = \frac{G^2E'^2}{2\pi^2}\left(\frac{m_W^2}{m_W^2+Q^2}\right)^2 \left\{ 2W_1 \sin^2\frac{\theta}{2} + W_2\cos^2\frac{\theta}{2} \mp W_3\frac{(E+E')}{M}\sin^2\frac{\theta}{2} \right\} \qquad (5.5)$$

and from this point on we shall send $M_W \to \infty$ which has the effect of removing the term in the first parentheses above.

The similarity and difference with the electromagnetic case (2.9) is obvious. Further, in analogy with the electromagnetic case, we can define "W-absorption cross sections" for right, left-handed or scalar W as σ_R, σ_L σ_S. The calculation of the relations between these cross sections and the structure functions proceeds as in the electromagnetic case and we obtain

$$\begin{aligned} W_1 &= \frac{K}{\pi G\sqrt{2}}(\sigma_R+\sigma_L) \\ W_2 &= \frac{K}{\pi G\sqrt{2}}\frac{Q^2}{Q^2+\nu^2}(\sigma_R+\sigma_L+2\sigma_S) \\ W_3 &= \frac{K}{\pi G\sqrt{2}}\frac{2M}{\sqrt{\nu^2+Q^2}}(\sigma_R-\sigma_L) \end{aligned} \qquad (5.6)$$

In the electromagnetic interaction parity invariance forces $\sigma_R = \sigma_L$ and hence $W_3^{e.m.}$ was zero, and $\sigma_T = 1/2\ (\sigma_R + \sigma_L)$. The other important difference with the electromagnetic case is that $W_{1,2}$ contain now both vector-vector (VV) and axial-axial (AA) pieces in contrast to the electromagnetic $W_{1,2}$ which are purely VV. The vector-axial vector interference is given by W_3 and hence the sign change in eqn.(5.5) upon replacing a neutrino beam (V-A) by an anti-neutrino beam (V + A).

Questions to be answered experimentally include:

(i) do the weak interaction structure functions $W_{1,2}$ scale analogously to their electromagnetic counterparts $W_{1,2}$?

(ii) what are the magnitudes of the weak as compared to the electromagnetic structure functions?

Before we investigate these questions from the point of view of data let us return to the quark-parton model introduced in the chapter on electron scattering and see what it predicts for the neutrino interaction. First of all, what predictions does it make for the scaling of the W_i?

In the electromagnetic case we were able to understand the data by postulating that the electromagnetic current (photon) interacted with the partons in the nucleon whose electromagnetic currents were $\bar{u}\ \gamma_\mu\ \bar{u}$, i.e. like the muon's electromagnetic current, hence "pointlike". The one new assumption that is invoked in the weak interaction is that the parton's weak current has the familiar form of the neutrino $\bar{u}\ \gamma_\mu(1 - \gamma_5)\ u$, i.e. V - A, while the anti-parton is V + A. Hence it is almost obvious by inspection that the model predicts that W_1 and $\nu\ W_2$ will scale (compare the electron case) and that $|\ W_{1,2}^{VV}\ | = |\ W_{1,2}^{AA}\ |$. As an exercise the reader should calculate this explicitly using chapter 2 as a guide (see also ref. 24). In the process you will find that the prediction is that the W_i scale as $W_1(\nu, Q^2)$, $\nu\ W_2(\nu, Q^2)$, $\nu\ W_3(\nu, Q^2) \rightarrow F_{1,2,3}(\omega)$ and that F_3 is maximal and negative. (i.e. that the scattering is predicted to be all in the left-handed mode compare eqn.(5.6)). This is a consequence of the parton current being $\bar{u}\ \gamma_\mu(1 - \gamma_5)u$; for anti-partons with $\bar{u}\ \gamma_\mu(1 + \gamma_5)u$ then the scattering would be right-handed. Hence one has a potential test of the relative importance of partons and anti-partons in the data description. Stated another way, the parity violation is maximal if <u>only</u>

partons or only anti-partons are contributing, whereas if the partons and anti-partons are equally important then the parity violation is minimal.

Do the data support such a scaling behaviour of the W_i? This question is investigated as follows. Assuming that the W boson, if it exists, has $M_W^2 >> Q^2$ then we can drop the brackets involving M_W^2 in eqn.(5.5). Defining $x = Q^2/2M\nu \equiv 1/\omega$ and $y = \nu/E$ (y is therefore the ratio of the actual energy transferred to the maximum possible transferable) then eqn.(5.5) is rewritten as

$$\frac{d^2\sigma}{dxdy}\left(\equiv \frac{2M\nu E^2E'}{\pi}\frac{d^2\sigma}{d\Omega dE'}\right) = \frac{G^2ME}{\pi}\left\{ \nu W_2(x,y)\left[1 - y - \frac{Mxy}{2E}\right] + My^2x\right.$$
$$\left. W_1(x,y) \mp y(1 - \frac{y}{2})\ x\ \nu W_3(x,y)\right\} \qquad (5.7)$$

The parton model predicts that

$$M\ W_1(x,y) \to F_1(x); \quad \nu W_{2,3}(x,y) \to F_{2,3}(x) \qquad (5.8)$$

and on substituting into (5.7) we have

$$\frac{d\sigma}{dx} = \frac{G^2ME}{\pi}\int_0^1 dy\left\{F_2(x)\left[1 - y - \frac{Mxy}{2E}\right] + F_1(x)\ y^2x \mp y(1 - \frac{y}{2})x\ \ F_3(x)\right\}$$
$$= \frac{G^2ME}{\pi}\left\{F_2(x)\left[1/2 - \frac{Mx}{4E}\right] + 1/3\ \ F_1(x)x \mp 1/3\ x\ \ F_3(x)\right\} \qquad (5.9)$$

so that

$$\sigma(E) = \frac{G^2ME}{\pi}\int_0^1 dx\left\{1/2\ \ F_2(x) + \frac{x}{3}\ \ F_1(x) \mp \frac{x}{3}F_3(x)\right\} - \frac{G^2M^2}{4\pi}\int_0^1 dx\ x\ \ F_2(x) \qquad (5.10)$$

Thus for $4E > M$ we can neglect the final term and we see that the total cross section is predicted to grow linearly in E if the scaling (5.8) holds true in

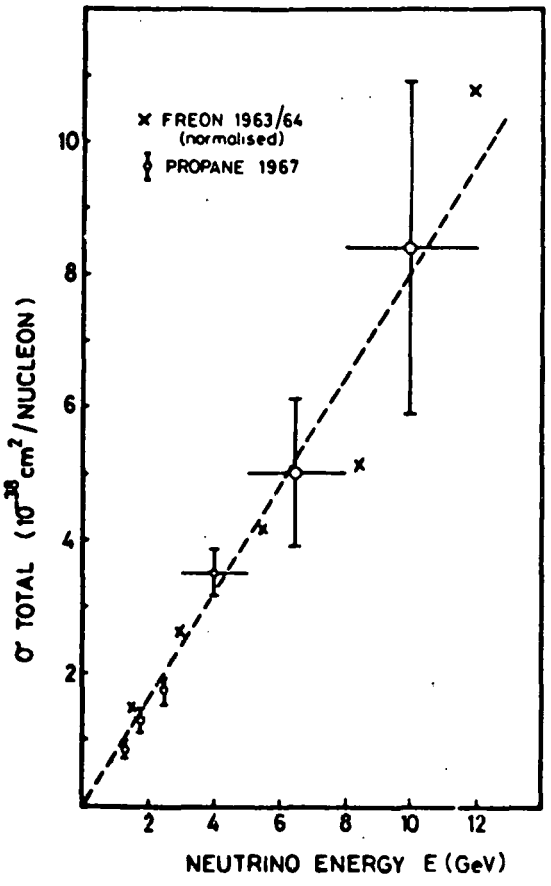

Fig. 17 Total cross section for neutrino scattering on nucleons. The data is consistent with a linear rise with neutrino energy.

nature. The data on propane (fig. 17) indeed suggest such linear behaviour

$$\sigma(E) = (0.51 \pm 0.13) \frac{G^2ME}{\pi} \text{ per nucleon} \qquad (5.11)$$

and hence it is probable that the structure functions do scale in the predicted fashion. More detailed analyses of the data have enabled a tentative extraction of the individual structure functions to be made and seem to confirm the scaling hypothesis at least in the small range of ω so far explored. This will be a fruitful field of study in the high energy experiments just beginning at NAL and later at CERN II.

The coefficient of G^2ME/π in (5.11) is directly related to an integrated combination of the weak structure functions (5.10). The next test of the parton model is to compare this magnitude with the prediction made in the previous chapter when we assumed that the partons were the quarks of Gell-Mann and Zweig.

We must first perform some preliminary algebra to formulate the problem more transparently.

Define

$$R,L = \sigma_{R,L}/\sigma_R + \sigma_L + 2\sigma_S \tag{5.12}$$

where $\sigma_{R,L,S}$ are the W-absorption cross sections of (5.6) and hence $0 \leq R, L \leq 1$. From (5.6) we see that

$$\begin{aligned} \frac{x F_1}{F_2} &= \frac{R+L}{2}\left(1 + \frac{Q^2}{\nu^2}\right) \\ \frac{x F_3}{F_2} &= (R-L)\left(1 + \frac{Q^2}{\nu^2}\right)^{1/2} \end{aligned} \tag{5.13}$$

where $\frac{Q^2}{\nu^2} \equiv \frac{2Mx}{Ey}$ and tends to zero for large E. We shall neglect this in the subsequent analysis (though this is not really a good approximation at present energies). Hence eqn.(5.10) becomes

$$\underset{E\to\infty}{\sigma(E)}\ \frac{\pi}{G^2ME} = \int_0^1 dx\ F_2(x)\left\{1/2 + \frac{R+L}{6} \pm \frac{L-R}{3}\right\} \tag{5.14}$$

which may be further simplified by assuming that $\sigma_S \simeq 0$ (as suggested in the electron data and hinted at in the neutrino data) in which event $R+L = 1$ and (5.14) simplifies to

$$\underset{E\to\infty}{\text{Lim}}\ \frac{\sigma(E)\,\pi}{G^2ME} = \int_0^1 dx\ F_2(x)\left\{2/3 \pm \frac{1-2R}{3}\right\} \tag{5.15}$$

Data with both ν and $\bar{\nu}$ beams are now available and hence the relative magnitudes of R and L can be determined since from eqn.(5.15) the ratio of cross sections for $\bar{\nu}$ to ν is formally

$$\underset{E\to\infty}{\text{Lim}}\ \frac{\sigma^{\bar{\nu}}}{\sigma^{\nu}} \simeq \frac{1+2R}{3-2R} \tag{5.16}$$

and hence lies between 1/3 (R = 0) and 3 (R = 1). Parity conservation (R = L = 1/2) would yield $\sigma^{\bar{\nu}} = \sigma^{\nu}$. Partons with V - A current would predict this

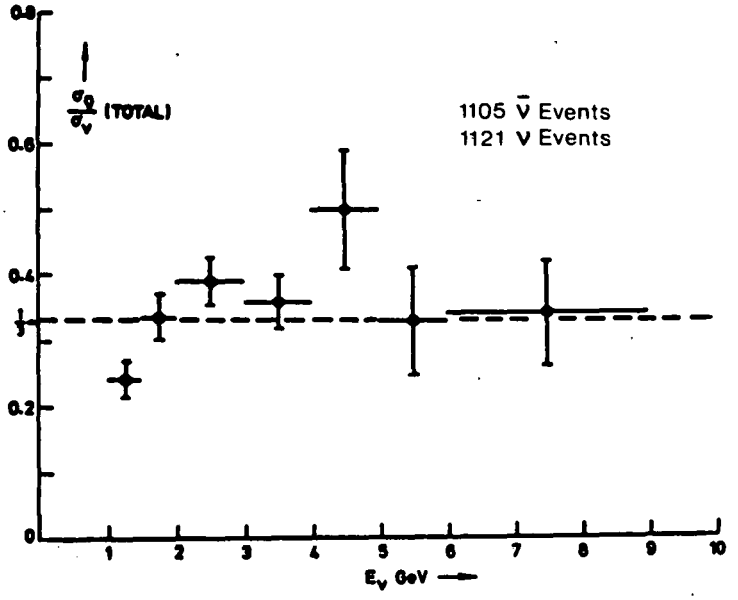

Fig. 18 Data on $\bar{\nu}$ compared to ν cross sections on nucleons (CERN Gargamelle).

ratio to be 1/3 while the presence of anti-partons would tend to raise this ratio towards unity. Experimentally this ratio appears to be 0.38 ± 0.02 suggesting that R = (5 ± 2)%, see fig. 18. The violation of the lower bound of 1/3 that we see at small E is probably a reflection of the large E assumption used in deriving our formulae. From the data we are therefore seeing that W_3 is maximal and negative which suggests that very few anti-partons are present in the kinematic region explored so far. Note that the form of the cross sections are weighted towards small ω (eqn.(5.15)) ($dx = d\omega/\omega^2$) and hence, combined with the fact that presently available neutrino energies are low and hence large q^2 means small ω, we expect that the present cross section data is very sensitive to only very small ω probably less than about 3 say. The conclusion that the anti-partons are unimportant is really to be interpreted therefore as a conclusion that the anti-partons are unimportant at small ω. This fits in with our understanding of the electromagnetic data from neutron and proton targets where the ratio F_2^{en}/F_2^{ep} at small ω suggested that the anti-partons were unimportant there.

Taking R = (5 ± 2)% together with the magnitude for the neutrino cross section (5.11) then we see that

$$1/2 \int \frac{d\omega}{\omega^2} \left(F_2^{\nu n} + F_2^{\nu p} \right) = 0.55 \pm 0.16 \qquad (5.17)$$

(where allowance has been taken of the fact that propane contains 26 protons and 18 neutrons). Since $\sigma^{\nu n} \neq \sigma^{\nu p}$ a correction must be applied before (5.17) can be extracted; we took $\sigma^{\nu n} = 3/2\ \sigma^{\nu p}$ which yielded a 4% effect which has been included in (5.17). Further discussion of this point can be found in ref. 13.

In order to compare this with the electromagnetic results we must extract the VV contribution from (5.17). The parton model predicts that VV = AA in magnitude; let us be more general and write AA = g^2 VV in which case

$$\int (F_2^{\nu n} + F_2^{\nu p})_{VV} \frac{d\omega}{\omega^2} = (0.55 \pm 0.16) \times \frac{2}{1+g^2} \overset{\text{Define}}{\equiv} \nu N \qquad (5.18)$$

to be compared with the electron data (where we have assumed naive Regge behaviour at large ω)

$$\int (F_2^{ep} + F_2^{en}) \frac{d\omega}{\omega^2} = 0.28 \pm 0.04 \overset{\text{Define}}{\equiv} eN \qquad (5.19)$$

and so for the integrated data

$$\frac{eN}{\nu N} = (0.51 \pm 0.15) \times \left(\frac{1+g^2}{2} \right) \qquad (5.20)$$

Without reference to partons or quarks one might ask what constraints are imposed by CVC for the weak structure functions. The weak current is solely isovector whereas both isovector and isoscalar pieces are present in the electromagnetic case. By looking at the sum of proton and neutron, then the isoscalar-isovector interference does not contribute and we may write

$$F^{ep} + F^{en} \equiv F(1) + F(0) \qquad (5.21)$$

$$\left[F^{\nu p} + F^{\nu n} \right]_{VV} \equiv F(1) \xrightarrow{CVC} 2F(1) \qquad (5.22)$$

and so

$$\frac{eN}{\nu N} = 0.5 + \frac{F(0)}{2F(1)} \geq 0.5 \qquad (5.23)$$

In general one would not expect the isoscalar contribution to be absent and it is interesting to compute the typically expected size of isoscalar to isovector content in the electron data. In SU(3) the photon transforms as the third and eighth components of an octet, "ρ, ω, ϕ" and the contribution to Compton scattering from each of these components follows by noting the SU(3) coupling ratios[26] for

$$g_{\gamma\rho} : g_{\gamma\omega} : g_{\gamma\phi} = 3 : 1 : \sqrt{2} \tag{5.24}$$

so that the Compton amplitudes mediated by ρ, ω, ϕ are in ratios 9 : 1 : 2. (Note that ρ, ω, ϕ here are used in the generic sense of SU(3) couplings and transformation properties. If there is a ρ' so there is an ω' and ϕ' with the above couplings, etc.) Therefore the I = 1 mode comes from ρ while the I = 0 comes from ω and ϕ with the result

$$\frac{F(0)}{F(1)} = \frac{1+2}{9} = 1/3 \tag{5.25}$$

yielding

$$\frac{eN}{\nu N} = 2/3 \tag{5.26}$$

While this is probably true for diffraction where $F^{en} = F^{ep}$, for non-diffraction things are different, in particular "ϕ"-nucleon cross sections are purely diffractive if we believe in the two component duality[19] and accept the absence of ϕ - N resonances in nature[27]. If we therefore hypothesise that for non-diffractive scattering only the ρ and ω pieces of the photon contribute then

$$\frac{F(0)}{F(1)} = 1/9 \tag{5.27}$$

and so

$$\frac{eN}{\nu N} = .5/9 \tag{5.28}$$

which is the result that we obtained previously when we allowed only non-strange quarks to contribute. Although we have not used quark-partons in the above

derivation the similarity between the two approaches is quite clear. The 5/9 (eqn.(5.28)) obtained when we removed the ϕ; in duality diagram language the ϕ does not contribute due to it being made from strange quarks (for a discussion of duality diagrams see, e.g. Storrow op cit). This removal of the ϕ ($\lambda\bar{\lambda}$) corresponds directly therefore with our earlier removal of strange quarks. In the quark-parton approach we saw that including strange quarks caused the electromagnetic structure functions to increase (because the strange quarks have charges and so couple to the photon) while the weak were unaltered (the $\lambda,\bar{\lambda}$ were isoscalar and the strangeness conserving weak current is isovector and so cannot be absorbed by the isoscalar quark) and so the inequality eqn.(4.22) resulted. In the approach of the present chapter the inclusion of the ϕ piece of the photon increases the isoscalar contribution to the electromagnetic structure functions whereas no contribution to the (isovector only) weak structure functions obtains. The one additional piece of information that we get from this SU(3) approach is knowledge of the relative amount of strange to non-strange quarks and hence instead of just an inequality we obtain an equality.

The empirical result eqn.(5.20) suggests that non-diffraction is dominant (unless $g^2 > 1$) which is consistent with the small value of R/L (eqn.(5.16) et seq.) (which in the parton model suggested that the anti-quarks - which are assumed relevant only to the diffractive scattering - are unimportant) and also with the fact that the cross section (eqn.(5.18)) is probing the small ω region where diffraction is believed negligible. We conclude that at small ω only non-strange quarks contribute to the electromagnetic and weak structure functions. It is encouraging that out of the a priori infinite range of possibilities for the eN/νN ratio, empirically it appears close to our theoretical prejudices. Much more data is required to be able to determine this ratio as a function of ω and see how much diffraction or non-diffraction is important. It might even be that the CVC constraint is being strained unless $g^2 > 1$.

Finally it is amusing to note that for diffraction $F^{en} = F^{ep}$ and $\frac{eN}{\nu N} = 2/3$ in which case (assuming $g^2 = 1$)

$$\left[F_2^{\nu n} + F_2^{\nu p} = 6\, F_2^{ep} \right]_D \qquad (5.29)$$

Similarly for non-diffraction one expects $F^{en} = 2/3\ F^{ep}$, and $\frac{eN}{\nu N} = 5/9$ and again

$$\left[F_2^{\nu n} + F_2^{\nu p} = 6\ F_2^{ep} \right]_{ND} \tag{5.30}$$

and so this relation should hold irrespective of the relative importance of diffraction to non-diffraction. However, since $F_2^{en} < 2/3\ F_2^{ep}$ as $\omega' \to 1$ it is probable that this relation (5.29, 5.30) is violated as $\omega' \to 1$. It will be interesting to see in what way it is violated (see also chapter 13 for further discussion of this topic).

6 FORWARD COMPTON SCATTERING

6.1 Kinematics and Amplitudes

The previous discussion has essentially been involved with the data on photoabsorption cross sections and hence the imaginary part of the forward Compton amplitude. We now discuss the full forward Compton amplitude as measured in the experiments $\gamma p \to \gamma p$ and see what the parton model predicts. In particular we shall concentrate on what is known as a $J = 0$ fixed pole in this data[28].

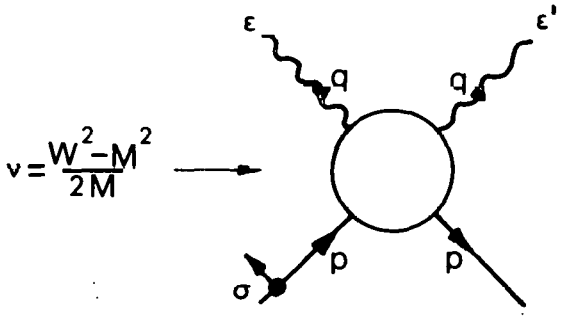

Fig. 19 Compton scattering on nucleons.

We concentrate first on the Compton scattering of real (on-shell) photons, fig. 19, for which the S-matrix element is written[29] as

$$S_{fi} = \delta_{fi} + (2\pi)^4\, i\, \delta^{(4)}(p_2 + k_2 - p_1 - k_1) \sqrt{\frac{M^2}{4k_{10}k_{20}E_1E_2}}\, \bar{u}(p_2)\, T\, u(p_1) \tag{6.1}$$

where $E_{1,2}$ are the energies of the nucleons, M the nucleon mass. The differential cross section in the centre-of-mass frame is

$$\left(\frac{d\sigma}{d\Omega} \right)_{c.m.} = |f_{c.m.}|^2$$

where

$$f^{c.m.} = \frac{M}{4\pi W} \bar{u}(p_2) T u(p_1) \tag{6.2}$$

with $W = (p_1 + k_1)^2$ the total centre-of-mass energy.

Specialising to forward scattering then only one variable remains upon which the scattering depends, viz (and compare eqn.(3.3))

$$\nu = \frac{W^2 - M^2}{2M} \tag{6.3}$$

In the laboratory frame $f(\nu) = \frac{W}{M} f^{c.m.}$. We write $f(\nu)$ as

$$f(\nu) = \chi_f^* T \chi_i$$

where $\chi_{f,i}$ are the nucleon Pauli (two component) spinors for the nucleon[29,30] at rest in the lab, and T is the most general scalar involving $\underset{\sim}{\varepsilon}_{f,i}$ - the polarisation vectors of the photons. What is the most general form that T can take?

In the lab. frame $p = (M, \underset{\sim}{0})$. We choose the photon to be moving the $\hat{z}$ direction with $k = (\nu, \underset{\sim}{0}, \nu)$. The photon polarisation vectors must satisfy $k.\varepsilon = k.\varepsilon' = 0$ and we write conventionally

$$\varepsilon, \varepsilon'(\pm) = \mp \frac{1}{\sqrt{2}} (0, 1, \pm i, 0) = (0, \underset{\sim}{\varepsilon}) \tag{6.4}$$

The possible ways that the two vectors $\underset{\sim}{\varepsilon}_{f,i}$ can contract are

(a) $\underset{\sim}{\varepsilon}'^* \cdot \underset{\sim}{\varepsilon}$ scalar

(b) $\underset{\sim}{\varepsilon}'^* \times \underset{\sim}{\varepsilon}$ axial vector

(c) $\underset{\sim}{\varepsilon}'^{*}\ \underset{\sim}{\varepsilon}$ tensor

(this corresponds to saying that two spin 1 can combine to form angular momentum 0, 1 or 2). Since (a) is a scalar already then it can contribute

$$f_{(a)}(\nu) \sim A\ \underset{\sim}{\varepsilon}'^{*} \cdot \underset{\sim}{\varepsilon}$$

while (b) needs to have a scalar product formed with an axial vector. Since the possible axial vectors $p \times p = k \times k = p \times k = 0$ then the only available axial vector is $\underset{\sim}{\sigma}$ the Pauli spin matrix, which operates on the nucleon spinors. Hence

$$f_{(b)}(\nu) \sim i B \underset{\sim}{\sigma} \cdot \underset{\sim}{\varepsilon}'^{*} \times \underset{\sim}{\varepsilon}$$

where the i is introduced to keep B real (since $\underset{\sim}{\varepsilon}'^{*} \times \underset{\sim}{\varepsilon}$ is imaginary). Finally (c) needs to be scalar produced with a tensor. Since $k.\varepsilon = k.\varepsilon' = 0$ and $p.\varepsilon = p.\varepsilon' = 0$ then the only available scalar product is

$$f_{(c)} \sim C\ \underset{\sim}{\sigma} \cdot \underset{\sim}{\varepsilon}'^{*}\ \underset{\sim}{\sigma} \cdot \underset{\sim}{\varepsilon}$$

Hence we have

$$f(\nu) = \chi_f^{*} \left[A\ \underset{\sim}{\varepsilon}'^{*} \cdot \underset{\sim}{\varepsilon} + i B \underset{\sim}{\sigma} \cdot \underset{\sim}{\varepsilon}'^{*} \times \underset{\sim}{\varepsilon} + C\ \underset{\sim}{\sigma} \cdot \underset{\sim}{\varepsilon}'^{*}\ \underset{\sim}{\sigma} \cdot \underset{\sim}{\varepsilon} \right] \chi_i$$

By using a familiar identity of Pauli matrices[30]

$$\underset{\sim}{\sigma} \cdot \underset{\sim}{a}\ \underset{\sim}{\sigma} \cdot \underset{\sim}{b} = \underset{\sim}{a} \cdot \underset{\sim}{b} + i \underset{\sim}{\sigma} \cdot \underset{\sim}{a} \times \underset{\sim}{b}$$

we can rewrite the final term in the above expression for $f(\nu)$ and obtain

$$f(\nu) = \chi_f^{*} \left[(A+C)\ \underset{\sim}{\varepsilon}'^{*} \cdot \underset{\sim}{\varepsilon} + i\ (B+C)\ \underset{\sim}{\sigma} \cdot \underset{\sim}{\varepsilon}'^{*} \times \underset{\sim}{\varepsilon} \right] \chi_i$$

or, as conventionally written[29,31]

$$f(\nu) = \chi_f^{*} \left[f_1(\nu)\ \underset{\sim}{\varepsilon}'^{*} \cdot \underset{\sim}{\varepsilon} + i\ f_2(\nu)\ \underset{\sim}{\sigma} \cdot \underset{\sim}{\varepsilon}'^{*} \times \underset{\sim}{\varepsilon} \right] \chi_i$$

The amplitudes $f_{1,2}(\nu)$ contain information about the proton dynamics and so if we can measure them we learn something about the proton.

If we average over the nucleon spins in the amplitude then clearly we are left with only $f_1(\nu)$ which is therefore called the "spin averaged" forward amplitude. To separate $f_{1,2}$ we must do experiments with polarised photons: $f_1(\nu)$ corresponding to parallel and $f_2(\nu)$ to perpendicular linear polarisations of the initial and final photons (this is because f_1 multiplies a scalar product, hence picks up the parallel polarisation vectors while f_2 multiplies the vector product). An alternative way of looking at these two amplitudes is to think in terms of helicity amplitudes for the forward Compton scattering. Imagine the photon to have helicity +1 and consider the two degrees of freedom: proton helicity $\pm$ 1/2 (parity relates these to the case of -1 with $\mp$ 1/2). Then for helicity +1 we see from (6.4) that

$$\underset{\sim}{\varepsilon}'^{*} \cdot \underset{\sim}{\varepsilon} = 1$$

$$i\, \underset{\sim}{\varepsilon}'^{*} \times \underset{\sim}{\varepsilon} = (-1)_z$$

and hence

$$f(\nu) = \chi_f^{*} \left[f_1(\nu) - f_2(\nu)\, \underset{\sim}{\sigma}_z \right] \chi_i$$

with the result that depending upon whether the proton spin is $\pm$ 1/2 we obtain $f(\nu) = f_1 \mp f_2$. If the photon and proton spins are parallel (i.e. photon helicity +1, nucleon helicity = - 1/2 in the centre-of-mass frame) then

$$f_p(\nu) = \frac{W}{M} f^{\text{c.m.}}_{1\text{-}1/2,1\text{-}1/2}(\nu) = f_1(\nu) - f_2(\nu)$$

(note than $J_z^{\text{nucleon}} = + 1/2$ since the photon is moving in the positive z direction and the nucleon in negative z with negative helicity) while if the spins are anti-parallel

$$f_a(\nu) = \frac{W}{M} f^{\text{c.m.}}_{1\ 1/2,\ 1\ 1/2}(\nu) = f_1(\nu) + f_2(\nu)$$

These amplitudes are related by the optical theorem to the total cross sections for $\gamma + N \to$ hadrons (working to order α in the amplitude) and we have

$$\text{Im}\, f_p(\nu) = \frac{\nu}{4\pi} \sigma_p(\nu)$$

$$\text{Im}\, f_a(\nu) = \frac{\nu}{4\pi} \sigma_a(\nu)$$

(where $\sigma_{P,A}$ are the total cross sections for photoabsorption when the photon and proton spins are parallel or anti-parallel), and hence

$$\text{Im } f_1(\nu) = \frac{\nu}{4\pi} \; 1/2 \left[\sigma_a(\nu) + \sigma_p(\nu) \right] = \frac{\nu}{4\pi} \; \sigma_T(\nu)$$

where $\sigma_T(\nu)$ is the spin averaged total cross section, and

$$\text{Im } f_2(\nu) = \frac{\nu}{4\pi} \; 1/2 \left[\sigma_a(\nu) - \sigma_p(\nu) \right]$$

In the absence of <u>both</u> a polarised proton target <u>and</u> a circularly polarised photon beam (i.e. a beam with well defined helicity ± 1) it is only the combination $\sigma_a(\nu) + \sigma_p(\nu)$, i.e $\sigma_T(\nu)$ and hence Im $f_1(\nu)$ which is measured up to now[25]. Although the amplitude $f_2(\nu)$ is not directly measured as yet, one can put an upper limit on its magnitude by performing measurements of the differential cross section for forward Compton scattering for which

$$\left(\frac{d\sigma}{d\Omega} \right)^{lab}_{\theta = 0} = |f(\nu)|^2 = |f_1(\nu)|^2 + |f_2(\nu)|^2$$

or

$$\left(\frac{d\sigma}{dt} \right)_{t = 0} = \frac{\pi}{\nu^2} |f(\nu)|^2 \equiv \frac{[\sigma_T(\nu)]^2}{16\pi} + \frac{\pi}{\nu^2} |\text{Re } f_1(\nu)|^2 + \frac{\pi}{\nu^2} |f_2(\nu)|^2$$

where t is minus the square of the four momentum transfer. From the data on $\sigma_T(\nu)$ one can calculate Re $f_1(\nu)$ by dispersion relations and one finds that $f_2(\nu)$ is less than 10% of $f_1(\nu)$ at comparable ν.

6.2 Dispersion Relations and the Drell-Hearn Sum Rule

The amplitude $f_1(\nu)$ is even and $f_2(\nu)$ odd under crossing ($\nu \to -\nu$). We write a dispersion relation for $f_2(\nu)$ and obtain[31]

$$\text{Re } f_2(\nu) = \frac{2\nu}{\pi} P \int_{\nu_0}^{\infty} \frac{d\nu'}{\nu'^2 - \nu^2} \text{ Im } f_2(\nu')$$

(where P denotes the principal value of the integral is to be taken) while a

once subtracted dispersion relation for $f_1(\nu)$ reads[31]

$$\text{Re } f_1(\nu) = f_1(0) + \frac{\nu^2}{\pi} P \int_{\nu_0}^{\infty} \frac{d\nu'^2}{\nu'^2 - \nu^2} \frac{\text{Im } f_1(\nu')}{\nu'^2}$$

where $\nu_0 = m_\pi + \frac{m_\pi^2}{2M_N}$ is the threshold for single pion production. Low energy theorems derived on very general grounds tell us that[32]

$$f_1(0) = -\alpha/M_N \text{ and } \lim_{\nu \to 0} \frac{f_2(\nu)}{\nu} = -\frac{\alpha \kappa^2}{2M_N^2}$$

where κ is the anomalous magnetic moment of the target nucleon. The $-\alpha/M_N$ is known as the Thomson limit magnitude - 3 μb GeV. The second result together with the dispersion relation yields the sum rule[33]

$$\kappa^2 = -\frac{4M_N^2}{\pi\alpha} \int_{\nu_0}^{\infty} \frac{d\nu'}{\nu'^2} \text{Im } f_2(\nu')$$

hence

$$\frac{2\pi^2\alpha}{M_N^2} \kappa^2 = \int_{\nu_0}^{\infty} \frac{d\nu'}{\nu'} \left[\sigma_p(\nu') - \sigma_A(\nu') \right]$$

which is known as the Drell- Hearn-Gerasimov Sum Rule. This appears to be satisfied when saturated with low lying resonances[34], see fig. 20, but direct experimental verification is still awaited. This sum rule is derived on general grounds, the only assumption being the validity of an unsubtracted dispersion relation. Is this justified? If there is an energy independent contribution to the difference of σ_p and σ_A then the assumption is violated. The Pomeron pole does not contribute since it has τP positive (for discussion on Regge theory see e.g. J.K. Storrow op. cit) whereas the contributions to $\sigma_p - \sigma_A$ have τP negative (since σ_p and σ_A differ by rotating the lines at one vertex in fig. 21). Pomeron-pomeron cuts can have τP negative and hence could contribute to the difference, if this gives rise to a constant energy dependence then the sum rule must be subtracted. Direct measurement of $\sigma_{p,A}(\nu)$ especially at large ν is required, both with regards to testing the sum rule and also for gaining information on τP negative Regge trajectory couplings.

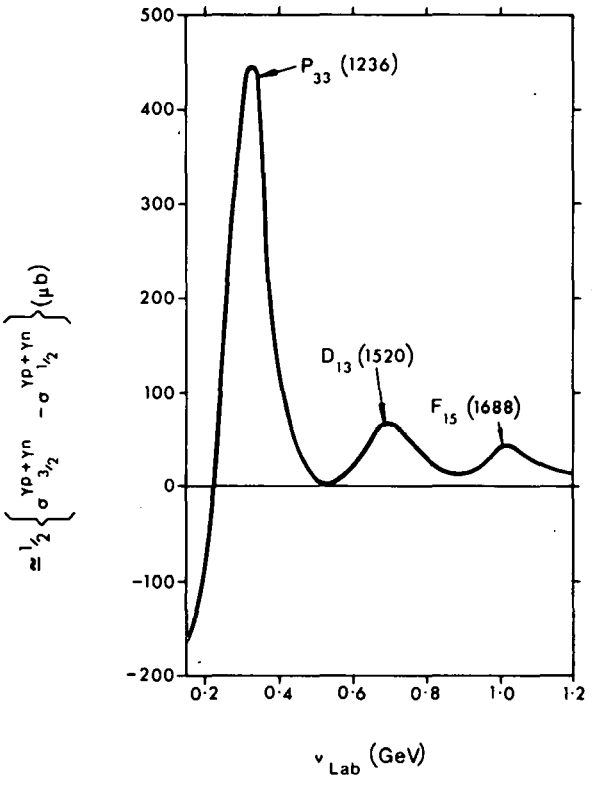

Fig. 20 Contribution to Drell-Hearn sum rule from the resonance region for half the sum of proton and neutron targets (after ref. 34).

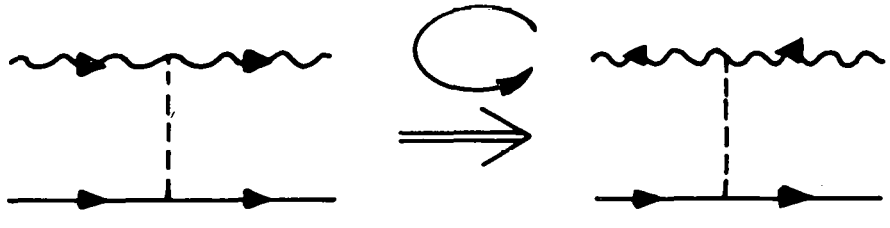

Fig. 21 The Compton helicity amplitudes f_P and f_A related by rotating the photon vertex.

7 COMPTON SCATTERING IN SIMPLE MODELS

Before discussing the analysis of the Compton amplitudes that was performed by Damashek and Gilman[29] and which suggested that there might be a $J = 0$ fixed pole present in $f_1(\nu)$ at high energies, it will be instructive to consider some simple models for Compton scattering. The reason for doing this is to highlight the differences between this fixed pole and the Thomson limit, there having been much confusion as to this point in the literature. We shall first give an example where the Thomson term and the fixed pole are the same, and then show a similar model where they are quite different. We shall then describe the nuclear physics analogue in order to motivate the parton model description of this fixed pole.

7.1 Compton Scattering from an Elementary "Pion"

Imagine a world where there existed only photons and an elementary scalar charged "pion" with mass m. The only contributions to the Compton scattering amplitude to order α would then be as shown in fig. 22. We shall refer to these diagrams as the s-channel, u-channel and "seagull" respectively. The s- and u-channel diagrams contain both real and imaginary parts (due to the propagator between the two photons) whereas the seagull diagram is real. The contribution to $f_1(\nu)$ from the seagull diagram is $-\alpha/m$.

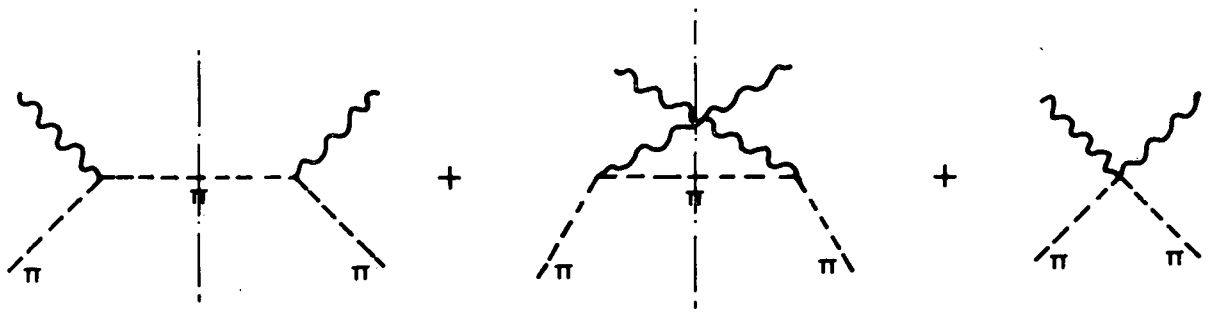

Fig. 22 Compton scattering in a world containing only photons and scalar "pions".

For scattering of real photons in the forward direction then the first two diagrams cannot contribute since the photons have helicity ± 1 and hence cannot be absorbed by a spinless particle if the intermediate state is also spinless. Therefore in this example only the seagull contributes and so we have, for all ν

$$f_1(\nu) = -\alpha/m \tag{7.1}$$

$$\text{Im } f(\nu) = 0 . \tag{7.2}$$

Therefore, as $\nu \to 0$ we have $f_1(0) = -\alpha/m$ and the Thomson limit is satisfied (as it must). Secondly we note that this example satisfies the dispersion relation

$$\text{Re } f_1(\nu) = -\frac{\alpha}{m} + \frac{2\nu^2}{\pi}\int_{\nu_{TH}}^{\infty} \frac{\text{Im } f_1(z)}{z(z^2 - \nu^2)} \tag{7.3}$$

trivially since $f_1(\nu) = -\frac{\alpha}{m}$ for all ν and the imaginary part is zero (eqn.(7.2)). Finally we see that as $\nu \to \infty$ then $f_1(\nu) = -\frac{\alpha}{m}$ which is a real constant (energy independent)which in the language of the complex J plane is the residue of a J =0 pole. Therefore in this example the Thomson limit and the J =0 fixed pole are generated by the same mechanism, viz the seagull term.

7.2 Compton Scattering from a "Physical" Pion

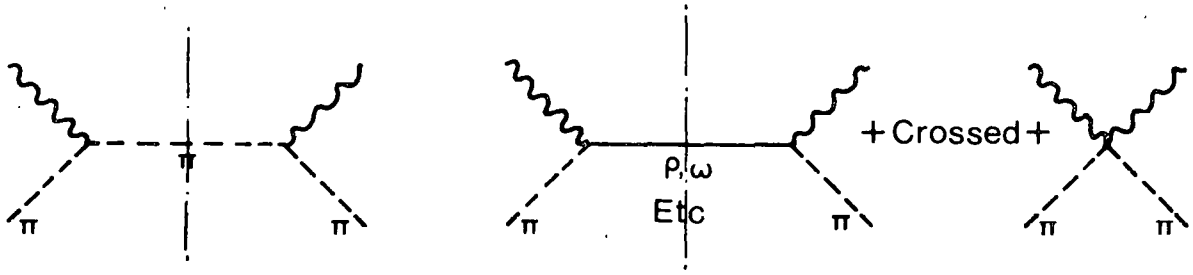

Fig. 23 As in fig. 22 but including excited states - e.g. vector-mesons "ρ, ω, ..".

This model is precisely the same as the previous one except that we now admit the existence of higher mass "resonance" states with non-zero spin to which the pion can be excited by the incident photon. The possible contributions are now represented by the fig. 23. The new diagrams involving the "rho" mesons can now contribute to both the imaginary part above threshold (total cross section for $\gamma\pi \to$ hadrons) and also to the real part. As $\nu \to 0$ one can show that

$$f_1(0) = -\alpha/m \tag{7.4}$$

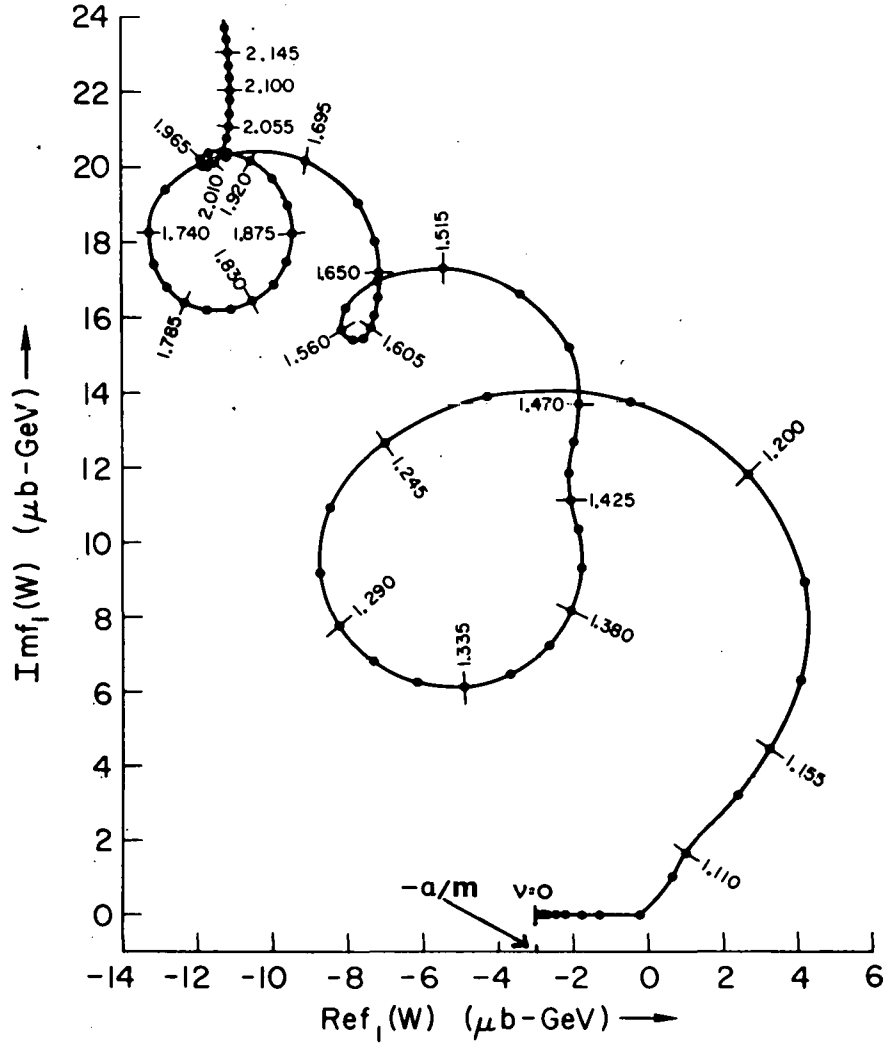

Fig. 24 Real and imaginary parts of the Compton amplitude f_1 as a function of W. At $\nu = 0$ the real part equals the Thomson limit. The imaginary part is only non zero above one pion threshold at which point the real part is nearly zero.

i.e. the Thomson limit. Due to the presence of the "rho" diagrams we have

$$\text{Im } f_1(\nu) = \frac{\nu}{4\pi} \sigma_{tot}(\gamma\pi \to \rho \ldots) \neq 0 \tag{7.5}$$

and hence from the dispersion relation

$$\text{Re } f_1(\nu) = -\frac{\alpha}{m} + \frac{2\nu^2}{\pi} \int_{\nu_{TH}}^{\infty} \frac{\text{Im } f_1(z)}{z(z^2 - \nu^2)}$$

we would expect that $f_1(\nu) \neq -\alpha/m$ when $\nu \neq 0$. The question to which we do not know the answer is whether the integral over the imaginary part generates contributions in the real part which "wash out the Thomson term" or whether the Thomson term survives at high energy as a $J = 0$ fixed pole.

To illustrate what we mean by "washing out" the Thomson term we show in fig. 24 the result of calculating the dispersion relation for the case of a proton target. Plotted are the real and imaginary parts of the amplitude $f_1(\nu)$ from $\nu = 0$ through the resonance region. At $\nu = 0$ we see that the real part is $-3\,\mu b$ GeV (which is the magnitude of $-\alpha/M$) while the imaginary part is zero. The imaginary part stays zero until the energy is at the one pion threshold at which point $f_1(\nu)$ develops an imaginary part. The interesting thing is that by the time we have reached threshold the $-3\,\mu b$ GeV that we started with has been almost washed out. The fact that this $-3\,\mu b$ GeV seems to reappear at high energies as a $J = 0$ fixed pole (as we shall show in the next chapter) is therefore non-trivial.

7.3 Compton Scattering from a Nucleus

We shall consider a nucleus made up of Z protons and N neutrons with $A = N + Z$. The mass of the nucleus is therefore approximately $A \times M$ (with M the nucleon mass) while its charge is Ze. The Thomson limit for a target of mass AM and charge Ze reads

$$f_1(0) = -\frac{Z^2\alpha}{AM} \tag{7.6}$$

and hence is the Thomson limit for this particular nucleus. The fact that the scattering amplitude at zero photon energy depends only upon the overall

properties of the nucleus and not upon its internal structure may be understood if one realises that low energy means long wavelength and in the limit of infinite wavelength then the light sees the nucleus as a whole and does not resolve its internal structure. At high energies the light's wavelength is short enough that the internal nucleons are seen and hence the scattering amplitude is the coherent sum of the scattering amplitudes from the constituent nucleons. If the nucleons were elementary, or if the wavelength of the light was not short enough to probe inside the nucleons (i.e. the photon energy is greater than the nuclear binding energy but below that for pion photoproduction) then the individual nucleon amplitudes would be the nucleon Thomson limits, viz - α/M for every proton and zero for every neutron. Hence the high energy behaviour of $f_1(\nu)$ for this nucleus will be[35]

$$f_1(\nu) = \sum_{n,p} f_1^{n,p}(\nu) \rightarrow - \sum_{p} \frac{\alpha}{M} = - \frac{Z\alpha}{M} \qquad (7.7)$$

which is constant (energy independent) and hence the residue of a $J = 0$ (fixed) pole in the J plane. Note that its magnitude is different from the magnitude of the Thomson term, this latter arises from the properties of the nucleus as a whole, the $J = 0$ pole at high energies arose from the scattering from the target's constituents.

7.4 From Nuclei to Nucleons

We now show how the parton model predicts that there will be a $J = 0$ fixed pole in the Compton amplitude for nucleon targets. The analogy with the previous nuclear example is clear - the NUCLEI are built from partons (the NUCLEONS!) - the NUCLEONS are built from partons (the QUARKS).

For the nucleus we saw that

$$f_1(0) = - \frac{Z^2\alpha}{M_{nucleus}} \qquad (7.8)$$

and if we assumed that the proton had no internal structure (or at least, if the photon did not probe that internal structure) then the high energy behaviour of the amplitude was

$$f(\nu \rightarrow \infty) = - \frac{Z\alpha}{M_{proton}} \qquad (7.9)$$

For the nucleon, in particular the proton, we have

$$f_1(0) = -\frac{\alpha}{M}$$

and if the proton is built from partons then the high energy behaviour in the model by direct analogy to the nuclear example will be generated by the scattering from the constituent quarks. Therefore the prediction is that[35] (m_i the parton mass, e_i its charge)

$$f_1(\nu \to \infty) = -\sum_i \frac{\alpha e_i^2}{m_i} \neq -\frac{\alpha}{M} \text{ in general} \qquad (7.10)$$

In the absence of Regge behaviour this would be the leading energy behaviour in $f_1(\nu)$. However, Regge behaviours with intercepts $\alpha(0) > 0$ exist in nature and so the fixed pole is overshadowed by them, but the model predicts that it is there all the same. In this naive parton example of analogy with nuclear physics we do not generate Regge behaviour with $\alpha(0) > 0$ in any obvious fashion; this was also apparent in the discussion of quasi elastic peaks (see section 3) where the presence of leading Regge behaviour gave a high energy tail to the quasi elastic peak. We shall return to the question of how to introduce Regge behaviour into the parton model when we discuss the non-perturbative parton model of Landshoff, Polkinghorne and Short[36]; suffice to say that even in the presence of leading Regge behaviour the parton model (by essentially the above picture) predicts that there will be a $J = 0$ fixed pole in the Compton amplitude[35,37] $f_1(\nu)$.

In the next section we shall examine the empirical evidence for such a fixed pole.

8 A J = 0 FIXED POLE IN COMPTON SCATTERING?

Having shown that parton models predict that there should be a $J = 0$ fixed pole in the Compton amplitude $f_1(\nu)$ we shall now review the empirical evidence as to the existence of such a term in the data. There are two, essentially equivalent, ways of tackling this question and we shall look at each of them in

turn. Both have as their starting point the dispersion relation for the amplitude $f_1(\nu)$

$$\text{Re } f_1(\nu) = -\frac{\alpha}{M} + \frac{\nu^2}{2\pi^2}\int \frac{d\nu' \, \sigma_{tot}(\nu')}{\nu'^2 - \nu^2} \qquad (8.1)$$

One approach is to form a finite energy sum rule from this dispersion relation and we shall describe that approach later. The approach that we look at first of all is the direct analysis of the dispersion relation[29]. We shall perform an uncritical analysis and show that a $J = 0$ fixed pole with magnitude consistent with the Thomson term may be present, and then we shall raise questions as to the correctness of this conclusion and look for possible sources of error in the analyses.

8.1 Dispersion Approach

In the direct approach one writes down the dispersion relation (eqn.(8.1)) and using the data for the magnitude of the total photoabsorption cross section $\sigma^{\gamma p}_{total}(\nu)$ one can compute the integral and hence determine the real part of $f_1(\nu)$ as a function of the photon energy ν. If data on $\sigma^{\gamma p}_{tot}(\nu)$ existed from threshold all the way to infinite photon energy then this would be a simple task. However, the data is only known at the present time for $\nu < 20$ GeV. In order to compute the integral we must make some hypothesis as to the behaviour of the cross section at energies above 20 GeV. The data on the cross section at energies up to 20 GeV are shown in figs. 25. Above about 2 GeV the cross section has a smooth slowly varying behaviour suggesting that a simple Regge exchange picture may be a good approximation to the data. Damashek and Gilman made such an assumption in their analysis (ref. 29) and parametrised the high energy behaviour by a constant (Pomeron) and a piece falling like the square root of energy (Pomeron prime and A_2), hence

$$\sigma^{\gamma p}_{tot}(\nu > 2 \text{ GeV}) \sim A + B/\sqrt{\nu} \qquad (8.2)$$

and $A \sim 100$ μb, $B \sim 60$ μb $\text{GeV}^{1/2}$. One then assumes that this is the behaviour of the total cross section not just for $\nu < 20$ GeV but for all high energies up to infinity. One can then compute the integral over the cross section in eqn.(8.1) and hence determine the real part of $f_1(\nu)$ at all energies.

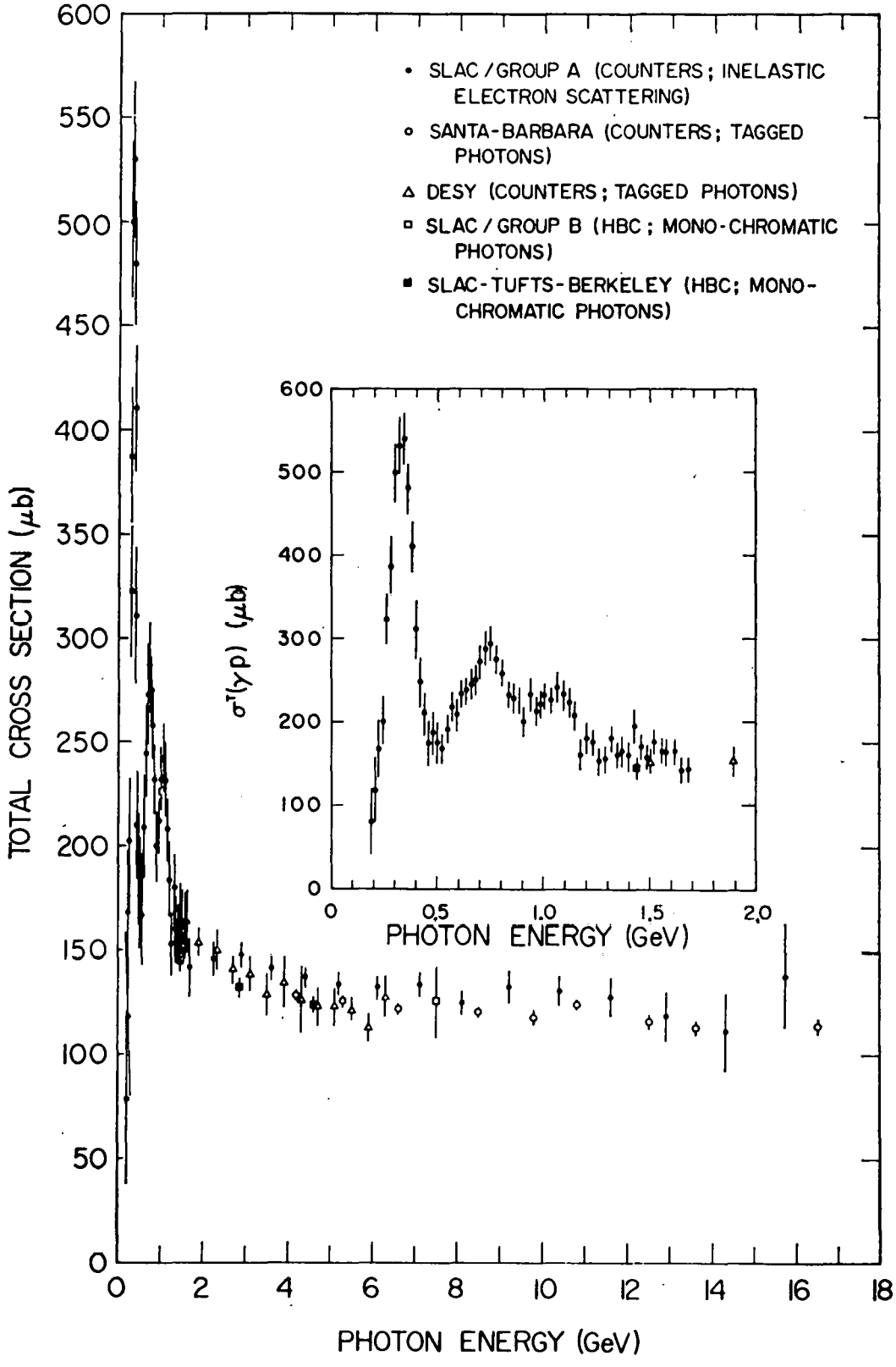

Fig. 25 Total photoabsorption cross section $\sigma_T(\nu)$ for $\gamma + p \rightarrow$ hadrons.

The result for the behaviour of $f_1(\nu)$ in the resonance region we have already seen in fig. 24. The behaviour at energies greater than 2 GeV is shown in the lower curve in fig. 26.

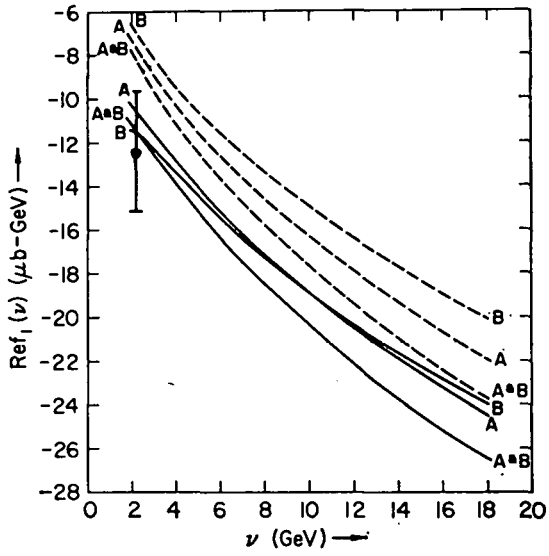

Fig. 26 Values of Re $f_1(\nu)$ at high energy calculated using the dispersion relation eqn.(8.1) are indicated by the solid lines for different fits (A, B, A and B) to the high energy total cross section. The real parts expected from Regge theory and observed behaviour of the imaginary part of the amplitude are indicated by the dashed lines for each of the three high energy fits. The measurement of the real part by Alvesleben et al. DESY 72/66 is shown at ν = 2.2 GeV and is consistent with the dispersion relation.

How do we determine whether or not there is a J = 0 term present? We assumed that the high energy cross section, which is essentially the imaginary part of the forward Compton amplitude, was described by Pomeron and Regge exchanges. The Pomeron had intercept 1 and hence is pure imaginary. The Regge with intercept $1/2$ has a real part which, by the phase energy relation, is equal in magnitude but opposite in sign to the imaginary part. In other words the high energy Compton amplitude has been parametrised as

$$f_1^R(\nu) = \frac{iA\nu}{4\pi} + \frac{B\sqrt{\nu}}{4\pi}(-1+i) + \{C?\} \qquad (8.3)$$

where

$$\sigma^{R}_{tot}(\nu) = \frac{4\pi}{\nu} \text{Im } f^{R}_{1}(\nu) = A + B/\sqrt{\nu} \qquad (8.4)$$

and hence $A \sim 100$ μb and $B \sim 60$ μb $GeV^{1/2}$. The question under contention is whether or not there is an energy independent term C present in the real part at high energies. The behaviour of Re $f^{R}_{1}(\nu) = -60\sqrt{\nu}/4\pi$ is shown in fig. 26 and is the upper curve. Note that it differs by a constant amount from the Re $f_1(\nu)$ that we calculated from the dispersion relation. Hence we deduce that there is indeed an energy independent piece in the real part of $f_1(\nu)$ and from the figure we see that its magnitude is about - 3 μb GeV (which is the magnitude of the Thomson term - α/M for a proton target).

Since we have only looked at <u>forward</u> Compton scattering we cannot deduce that this extra real part is a <u>fixed</u> pole. In the absence of any known Regge pole with $\alpha = 0$ (there are no zero mass hadrons in nature) we shall refer to this extra real part as a $J = 0$ fixed pole.

8.2 <u>Finite Energy Sum Rule (FESR) Approach</u>

We start by defining a function (for all ν)

$$f^{R}(\nu) = \sum_{\alpha_i > 0} \frac{-1 - e^{-i\pi\alpha_i(0)}}{\sin \pi\alpha_i(0)} \left(\frac{a_i}{4\pi} \right) \nu^{\alpha_i(0)} + C \qquad (8.5)$$

(note that for $\alpha_i(0) = 1$ and $1/2$ this is the function eqn.(8.3)). One can verify by direct calculation that this function satisfies the dispersion relation

$$f^{R}(\nu) = C + \frac{\nu^2}{\pi} \int \frac{d\nu'^2}{\nu'^2 - \nu^2 - i\varepsilon} \frac{\text{Im } f^{R}(\nu')}{\nu'^2} \qquad (8.6)$$

Contrast and compare this with the Compton amplitude $f_1(\nu)$ which satisfies the similar dispersion relation

$$f_1(\nu) = -\frac{\alpha}{M} + \frac{\nu^2}{\pi} \int \frac{d\nu'^2}{\nu'^2 - \nu^2 - i\varepsilon} \frac{\text{Im } f_1(\nu')}{\nu'^2} \qquad (8.7)$$

Finally we shall assume that the functions $f_1(\nu)$ and $f^R(\nu)$ are asymptotically equal

$$\lim_{\nu \to \infty} \left[f_1(\nu) - f^R(\nu) \right] \to 0 \qquad (8.8)$$

A diagrammatic representation of these functions is shown in fig. 27.

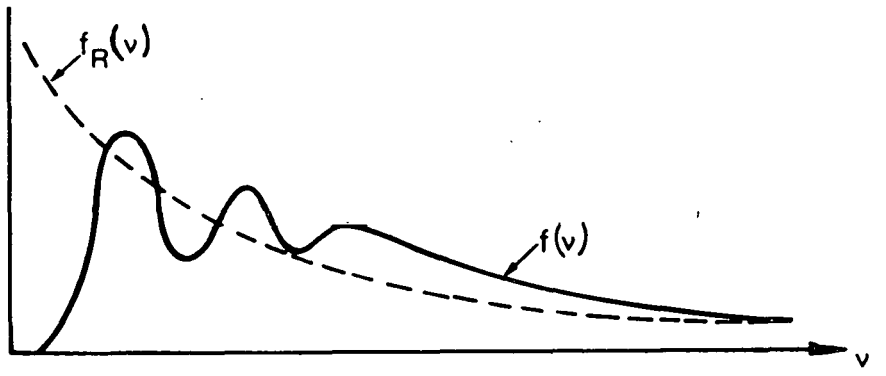

Fig. 27 Examples of the functions f_1 and f_1^R.

Setting $\nu = \infty$ in the integrals (assuming that taking the limit under the integral sign is a legitimate procedure) and subtracting eqn.(8.7) from eqn.(8.6) we obtain

$$C = -\frac{\alpha}{M} - \frac{1}{\pi} \int \frac{d\nu'^2}{\nu'^2} \left\{ \text{Im } f_1(\nu') - \text{Im } f^R(\nu') \right\} \qquad (8.9)$$

For $\nu' > N$ we have $f_1(\nu') - f^R(\nu') \to 0$ and so we can cut off the upper limit of the integral at N. Then, using the optical theorem, viz.

$$\sigma_{tot}(\nu') = \frac{4\pi}{\nu'} \text{ Im } f(\nu') \qquad (8.10)$$

and rewriting $d\nu'^2 = 2\nu' \, d\nu'$, the form of finite energy sum rule that we shall use is obtained

$$C = -\frac{\alpha}{M} - \frac{1}{2\pi^2} \int^N d\nu' \left\{ \sigma_{tot}(\nu') - \sigma_{tot}^R(\nu') \right\} \qquad (8.11)$$

The integral is then the difference of the areas under the wobbly curve and the smooth "Regge" curve in fig. 27. Hence the fixed pole is related to the difference of these areas. The analysis of Damashek and Gilman showed that the area under the data and under the Regge curves were almost equal and hence $C \sim -\alpha/M$.

8.3 Critique of Errors and Assumptions

An analysis of the errors and assumptions is most easily facilitated by examining the FESR calculation. We shall phrase the question in this fashion: in what way and by how much must we change the magnitude of the integral in eqn.(8.11) in order to reduce C to zero?

Since C is of order $-\alpha/M$, i.e. $-3\,\mu b$ GeV then we have to decrease the quantity in the integral by about 60 μb GeV. This could be done if the data was systematically wrong by about 30 μb throughout the range of 2 GeV that we are integrating over. A comparison of the SLAC and Daresbury data (fig. 28) show that this is quite unreasonable. The only course left is to change the Regge by a similar amount, i.e. increase the contribution of $\sigma^R(\nu')$. This one can do by changing the assumption on the magnitude of $\alpha(0)$ for the Regge trajectories contributing. A small change in $\alpha(0)$ can make a very dramatic effect upon the integrated $\sigma^R(\nu')$ at small ν'. This then is the only way in which we can destroy the conclusion that there is a $J = 0$ piece in the amplitude. The problem is that it is very easy to make good fits to the photoabsorption cross section data with $\alpha(0)$ anywhere between about 0.2 and 0.9. Hence unless one is convinced that $\alpha(0) = 1/2$ then one cannot conclude that there is a $J = 0$ term with magnitude similar to the Thomson term. If one compares with hadronic processes or draws lines through the meson resonances of the Regge trajectories then one can constrain $\alpha(0)$ to lie between 0.4 and 0.6 and the resulting magnitude of C then lies between -1.5 and -4.5 μb GeV, i.e. $C = -(3 \pm 1.5)\,\mu b$ GeV.

This is the conclusion stated by Damashek and Gilman[29] and examined more quantitatively by Tait and White[38]. The reader who wishes to learn more about this fascinating topic is advised to read the references cited[29,38,39-43].

In summary, the only possible source of uncertainty in the analysis is the assumption made for the high energy Regge behaviour. Unfortunately this assumption plays a very sensitive role in the analysis and the conclusions vary

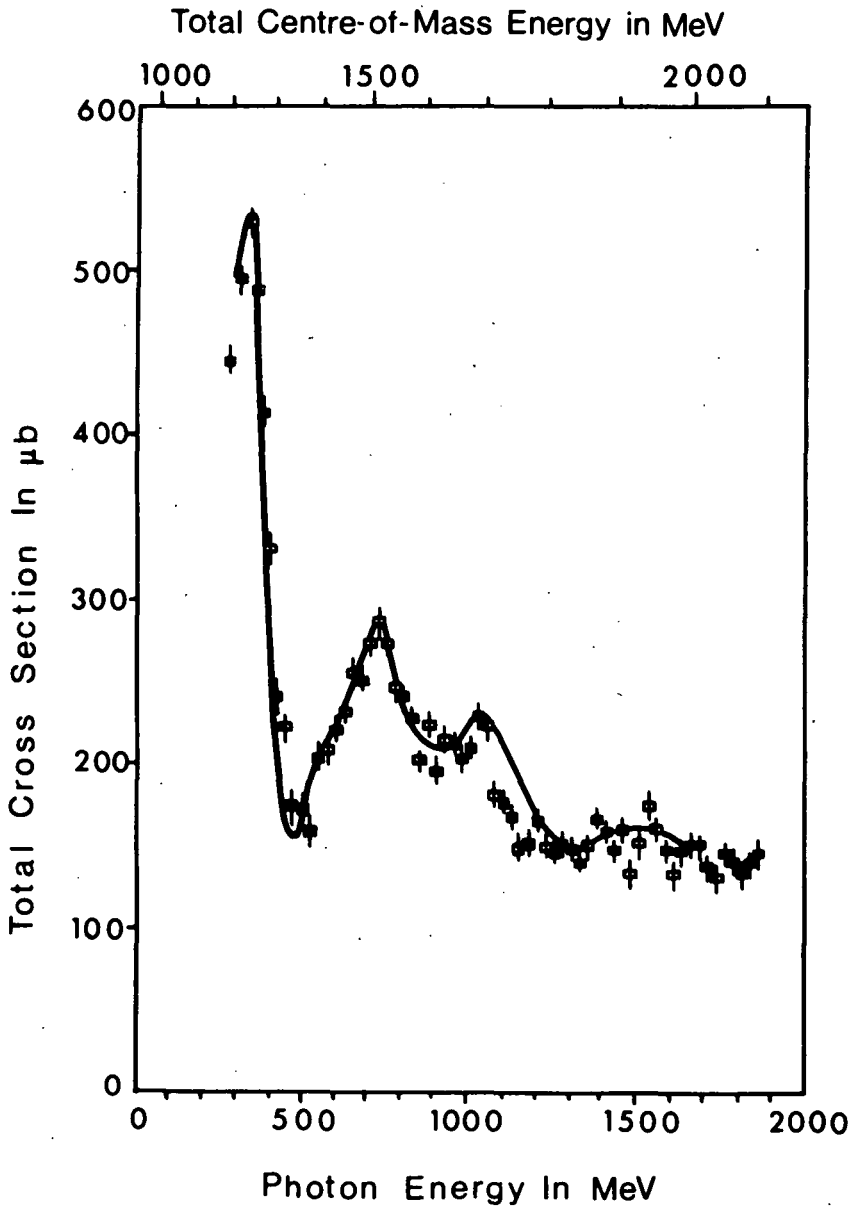

Fig. 28 Comparison of low energy $\sigma_T(\gamma p)$ data from SLAC and Daresbury (see also G. Wolf, Int. Symp. on Electron and Photon Interactions at High Energies, Cornell, op. cit., p.189).

widely under even small changes in the Regge assumptions. This question will not be resolved until very high energy data is available from NAL and CERN II.

8.4 A J = 0 Fixed Pole in Off-Shell Compton Scattering?
(Can one turn off the strong interactions?)

The finite energy sum rule that we used in the preceding analysis of the

fixed pole question in on-shell Compton scattering was

$$-\frac{\alpha}{M} - \frac{1}{2\pi^2}\int_0^N \left[\sigma(\nu) - \sigma^R(\nu)\right] d\nu = C \qquad (8.12)$$

If the strength of the electromagnetic interaction was completely independent of the strong interaction strength then one could perform the gedanken experiment of turning off the strong interactions while leaving the electromagnetic interactions untouched[39]. The turning off the strong interactions is taken to mean the setting of the pion nucleon coupling to zero (and similarly for the couplings of all mesons to the nucleon). If we did this then the cross section to produce hadrons would vanish in eqn.(8.12). The Thomson term depends only on the charge of the target and was derived on general grounds having nothing to do with strong interaction physics so is unaltered in the "turning off" process. The sum rule eqn.(8.12) will then only remain consistent if there is a term C with magnitude $-\alpha/M$! It is not at all clear that such a mysterious procedure is possible or has any relevance to nature but it is amusing that empirically C is consistent with the Thomson term and we shall assume that it is indeed equal to it. What further consequences of the switching off argument would ensue? The most obvious is that we would expect there to be no fixed pole for a neutron target since its charge, and hence Thomson term, is zero. The analysis of this question is riddled with nuclear physics uncertainties in addition to the sorts of troubles that we met in the analysis of the proton data, but brave people have performed such an analysis and claim that C is consistent with zero[40]. More interesting is to consider the impact upon the off-shell scattering (recall that the imaginary part of the virtual forward Compton amplitude is related to our old friend νW_2).

Writing the sum rule for the virtual Compton amplitude whose imaginary part is νW_2 then we obtain[41]

$$\frac{Q^2}{2M}\,\frac{G_E^2(Q^2) + Q^2/4M^2\; G_M^2(Q^2)}{1 + Q^2/4M^2} + \int_0^N d\nu \left[\nu W_2(\nu, Q^2) - \nu W_2^R(\nu, Q^2)\right] = R(Q^2) \qquad (8.13)$$

The analogy with the on-shell sum rule eqn.(8.11) is clear; the Born term (elastic) contribution to νW_2 is seen (compare eqn.(2.12)) and we have written $\nu \equiv Q^2/2M$ for elastic scattering. On the right hand side we see that we have allowed for the possibility of a fixed pole with residue $R(Q^2)$. Multiplying both sides by $-\frac{2\alpha}{Q^2}$ the sum rule becomes

$$-\frac{\alpha}{M}\,\frac{G_E^2 + Q^2/4M^2\, G_M^2}{1 + Q^2/4M^2} - \frac{2\alpha}{Q^2}\int_0^N d\nu \left[\nu W_2 - \nu W_2^R\right] = -\frac{2\alpha}{Q^2} R(Q^2) \qquad (8.14)$$

We shall consider this sum rule in the two limits (i) $q^2 \to 0$ (ii) $q^2 \to \infty$.

In the limit $q^2 \to 0$ the sum rule becomes

$$-\frac{\alpha}{M} - \frac{1}{2\pi^2}\int_0^N d\nu \left[\sigma_T(\nu) - \sigma_T^R(\nu)\right] = \lim_{Q^2 \to 0} \frac{-2\alpha\, R(Q^2)}{Q^2} \equiv C \qquad (8.15)$$

(where we have used eqn.(2.17) to relate νW_2 as $q^2 \to 0$ to the photoabsorption cross section). This is exactly our on-shell sum rule (8.12) where from the conclusion $C \sim -\frac{\alpha}{M}$

$$\lim_{Q^2 \to 0} R(Q^2) = +\frac{Q^2}{2M} \qquad (8.16)$$

In the limit $q^2 \to \infty$ then $\nu W_2(\nu, Q^2) \to F_2(\omega)$ where $\omega = 2M\nu/q^2$, the elastic form factors $G_{E,M}$ vanish, and so the sum rule becomes

$$\int_0^N d\omega \left[F_2(\omega) - F_2^R(\omega)\right] = \lim_{Q^2 \to \infty} \frac{2MR(Q^2)}{Q^2} \qquad (8.17)$$

Thus for any q^2 large enough that νW_2 is scaling, i.e. $\to F_2(\omega)$ this form of the sum rule obtains and since the left hand side is independent of q^2 then so must be the right hand side. Therefore we have that for $q^2 \gtrsim 1$ (GeV/c)^2 that

$$\lim_{Q^2 \to \infty} R(Q^2) = AQ^2 \qquad (8.18)$$

with A some unknown constant.

A question which immediately comes to mind is whether $A = 1/2\,M$ so that

$$R(Q^2) = \frac{Q^2}{2M} \tag{8.19}$$

for <u>all</u> q^2 (i.e. does the fixed pole have a residue that is a polynomial in q^2?) This need not be the case since a perfectly possible form could be

$$R(Q^2) = Q^2 \left(\frac{1 + 237\ Q^2}{2M + Q^2} \right) \tag{8.20}$$

which satisfies the two limiting conditions. If we play the game of turning off the strong interactions then $G_E = G_m = 1$, the integral vanishes as before and we deduce that

$$R(Q^2) = \frac{Q^2}{2M} \quad \text{for all } Q^2$$

i.e. a polynomial residue[42]! If this is the case empirically then we can substitute this behaviour for $R(Q^2)$ into the relation 8.16 and we obtain the sum rule[41]

$$\int_0^N d\omega \left[F_2(\omega) - F_2^R(\omega) \right] = 1. \tag{8.21}$$

Why are we pursuing the idea of turning off the strong interactions? If the strong and electromagnetic interactions are uncoupled in nature then such an exercise may have meaning. Our example would be correct if the electromagnetic and strong interactions were incoupled at the nucleon level. The parton model, which motivated our examination of the fixed pole question in the first instance, is a theory where the electromagnetic and strong interactions are uncoupled not at the nucleon level but at the quark level. That is why the quark-parton model predicted a fixed pole whose magnitude is the sum of Thomson terms of the partons (quarks) (eqn.(7.8)). In the present example we have been uncoupling the strong and electromagnetic interactions at the nucleon level and

hence the resulting fixed pole had the Thomson limit of the nucleon. Why nature seems to like the nucleon to be a parton in on-shell scattering whereas the quarks are the partons in off-shell (scaling, sum rules eqn(3.14)) is a mystery - perhaps the whole picture is crazy after all. Whether the correct place to turn off the strong interactions is at the nucleon level or at the quark level the result that the fixed pole has a polynomial residue, i.e. is linear in Q^2 obtains (the reader who wants more details of this should read refs.[35,41,43]. Hence we are pursuing this question of polynomial residues because our theory predicts such a behaviour.

If the fixed pole has a polynomial residue, as suggested by the theories, then the sum rule (8.21) obtains. Do the data on $\bar{F}_2(\omega)$ satisfy this sum rule? The data are shown in fig. 9. It is clear that one cannot hope to make a meaningful "fit" to this data at present ω values (though this has not prevented people from trying!) Ones first guess is that the behaviour of $F_2(\omega)$ at large ω will have similar behaviour to the behaviour of the total cross section at $q^2 = 0$, viz something like $0.30 + 0.18/\sqrt{\omega}$ so that the Pomeron to Regge has the same relative magnitude in the two cases (100/60 = 30/18). Such a behaviour is shown in fig. 29 and would not satisfy the sum rule eqn(8.21) since the area under the Regge is greater than that under the data and so the difference in eqn.(8.21) would yield a negative quantity. In order to obtain the desired

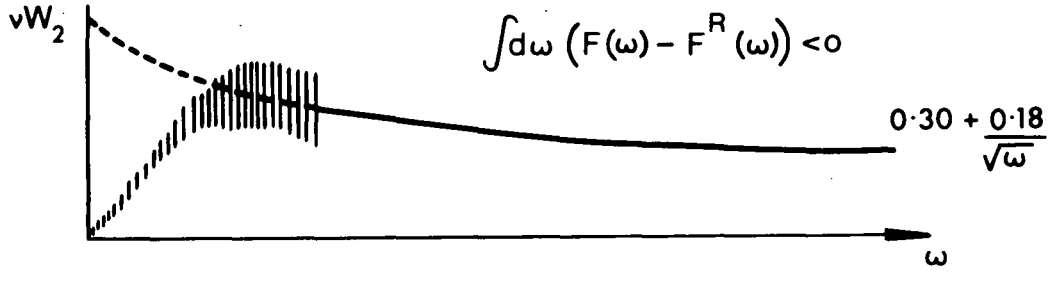

Fig. 29 $F^R(\omega) = 0.30 + 0.18/\sqrt{\omega}$ yields $\int d\omega\ (F(\omega) - F^R(\omega)) < 0$.

positive quantity then the data must approach the Regge behaviour from above. This would mean the the Regge region is at values of ω which are higher than the present data have attained. A typical behaviour that the data would need in order to satisfy the sum rule is shown in fig. 30. No theoretical significance is to be attached to the third term $4/\omega^{3/2}$, this is merely a way of

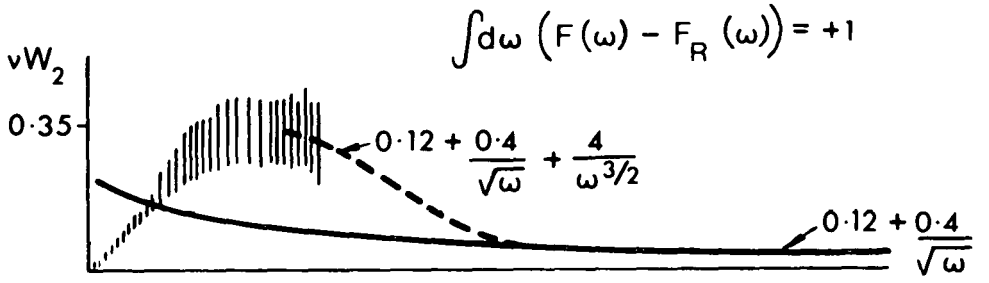

Fig. 30 For $\omega > 12$, a typical behaviour required if the sum rule is to be satisfied.

parametrising the sort of behaviour that the data must have. The Regge is approached from above and hence the area under the data is greater than that under the Regge curve with the result that the sum rule is satisfied.

Therefore if the fixed pole does have a polynomial residue in q^2, as required if the parton model is correct, then the data must have this dramatic behaviour. Whether it does or does not have this behaviour we shall soon know from NAL. Note that if the quark model is correct then the fixed pole residue is very probably larger than the Thomson term of the nucleon in which case the right hand side of the sum rule (8.21) will be larger than 1 and the data will have to have quite remarkable behaviour if the sum rule is to be satisfied.

How is it possible for the large q^2 data to have this sort of behaviour when the on-shell data do not appear to exhibit this sort of shape? Is it possible to have a smooth connection between the photo- and electroproduction data? The answer is that you can and an example is shown in detail in ref. 42. The essential feature to notice is that the ν which appears in the on-shell has dimensions of GeV whereas the ω is dimensionless. To make a comparison of the two cases we must introduce an energy scale into the problem at some point. Stated another way it is like asking what value of ν in photoproduction corresponds to a given value of ω in electroproduction. The Pomeron and Regge contributions to the deep inelastic data are equal in magnitude when ω is about 16. In the on-shell data they are equal when ν is about 300 MeV (!) Stated in a more comprehensible fashion, 2 GeV in photoproduction is like $\omega \sim 100$. This amazing statement is perhaps more easily understood by referring to the curves

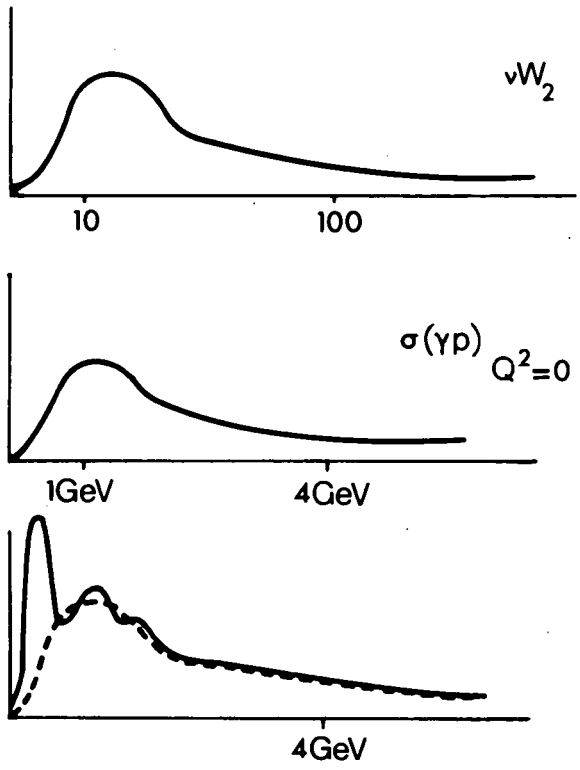

Fig. 31 Diagrammatic representation of the way that the deep inelastic νW_2 with shape shown in fig. 30 and the shape of photoproduction total cross section could be the same due to the change of scale. The bump around 1 GeV is obscured due to the presence of resonances (bottom figure).

in fig. 31. The curves are the same, the scales are different. It is the presence of the resonances in the on-shell data which prevents us seeing the bump in the curve. In fig. 32 we show the total cross section for the sum of $\sigma_T(pp)$ and $\sigma_T(\bar{p}p)$. This combination receives the same t channel contributions as do photoabsorption cross sections. The absence of prominent resonances in this process enables one to see the bump quite clearly. The curve which agrees beautifully with the data is approximately $77 + \frac{41}{\sqrt{\nu}} + \frac{121}{\nu^{3/2}}$ (note the $\nu - 3/2$ term!)

If this picture is realised in nature then it may provide an understanding[43] as to why the shadowing observed in photoabsorption on nuclei at $q^2 = 0$ for $\nu \sim 20$ GeV seems to have vanished by $q^2 \sim 0.5$ (GeV/c)^2. $q^2 \sim 0.5$ (GeV/c)^2 at $\nu \sim 20$ GeV would correspond to $\nu \sim 2$ GeV when $q^2 = 0$ in which region we know

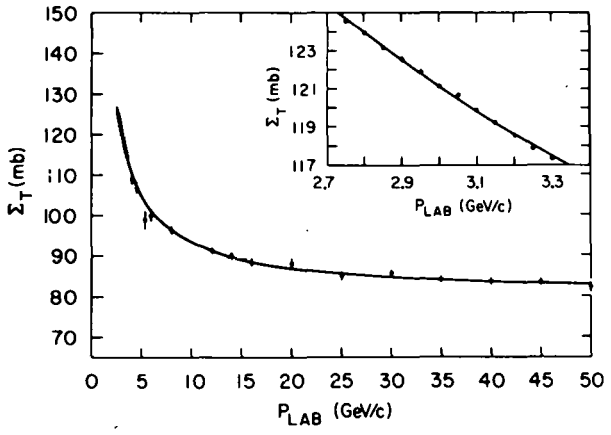

Fig. 32 $\sigma_{tot}(pp) + \sigma_{tot}(\bar{p}p)$ from 2.75 GeV/c to 50 GeV/c incident laboratory momentum. The solid curve is a best fit to the data given by $77 + 41\ \nu^{-1/2} + 121\ \nu^{-3/2}$. The insert is an enlarged version of the region $2.75 \lesssim P_{lab} \lesssim 3.5$ GeV/c.

there is no shadowing. Conversely, we would expect the shadowing to be present when $q^2 \sim 0.5$ but ν near 500 GeV!

9 THE NON-PERTURBATIVE PARTON MODEL WITHOUT TEARS

In section 3 we saw that if inelastic electron-proton scattering was viewed as elastic electron-parton scattering then the structure function $\nu W_2(\nu, Q^2) \to F_2(\omega = 2M\nu/Q^2)$. The virtual photoabsorption cross section, fig. 33

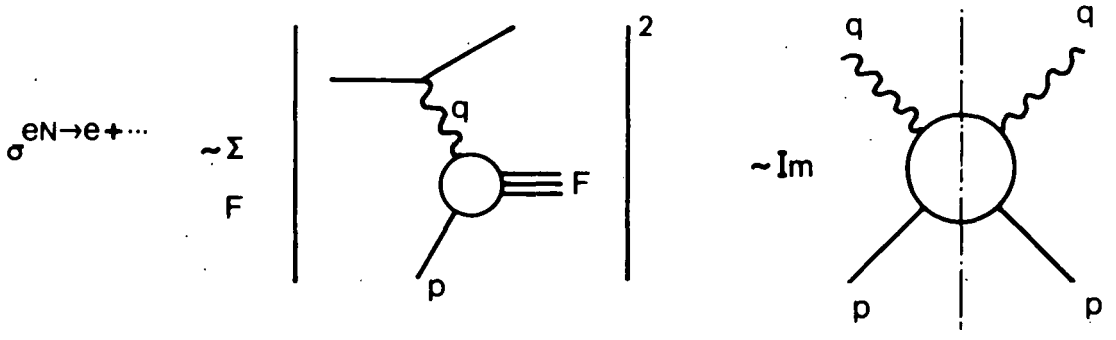

Fig. 33 Photoabsorption cross section and imaginary part of the forward Compton amplitude.

may be viewed as the imaginary part of the forward Compton scattering amplitude. In the parton model we draw this as in fig. 34 where the scaling behaviour of the structure function arises because of the presence of the "free" parton

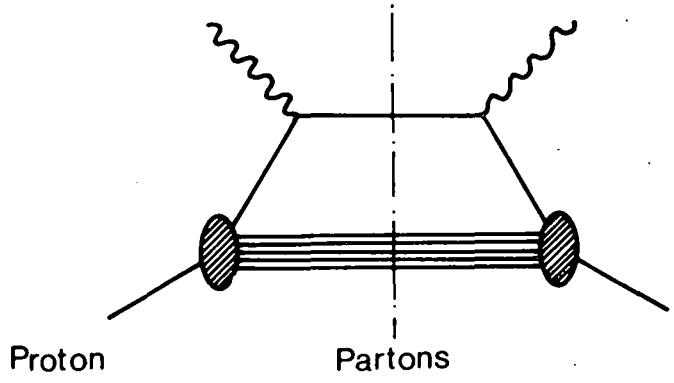

Fig. 34 A contribution to forward Compton scattering in the parton model.

propagator between the photons. If the four-momenta are labelled as in fig. 35 then the propagator of the parton is (apart from spin dependent parts which are

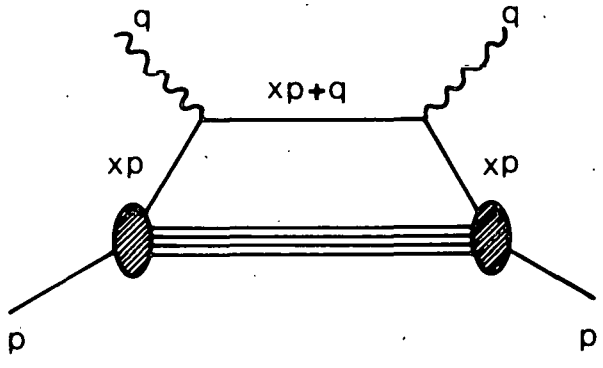

Fig. 35 Momentum routing with neglect of transverse momenta.

not material here, and neglecting any momenta transverse to the proton-photon axis)

$$\left[(xp + q)^2 - m^2 - i\varepsilon \right]^{-1} \qquad (9.1)$$

where m is the parton's mass. The imaginary part of the amplitude includes the delta function

$$\delta(x^2M^2 + q^2 + 2xp.q - m^2) \qquad (9.2)$$

arising from the imaginary part of the parton propagator (9.1). At very large ν, q^2 we may neglect the x^2M^2 and m^2 with the result that the amplitude contains the delta function constraint

$$\delta\left(\frac{2M\nu}{q^2} - x\right) \tag{9.3}$$

and the structure function is dependent only on the ratio ν/q^2 due to this delta function.

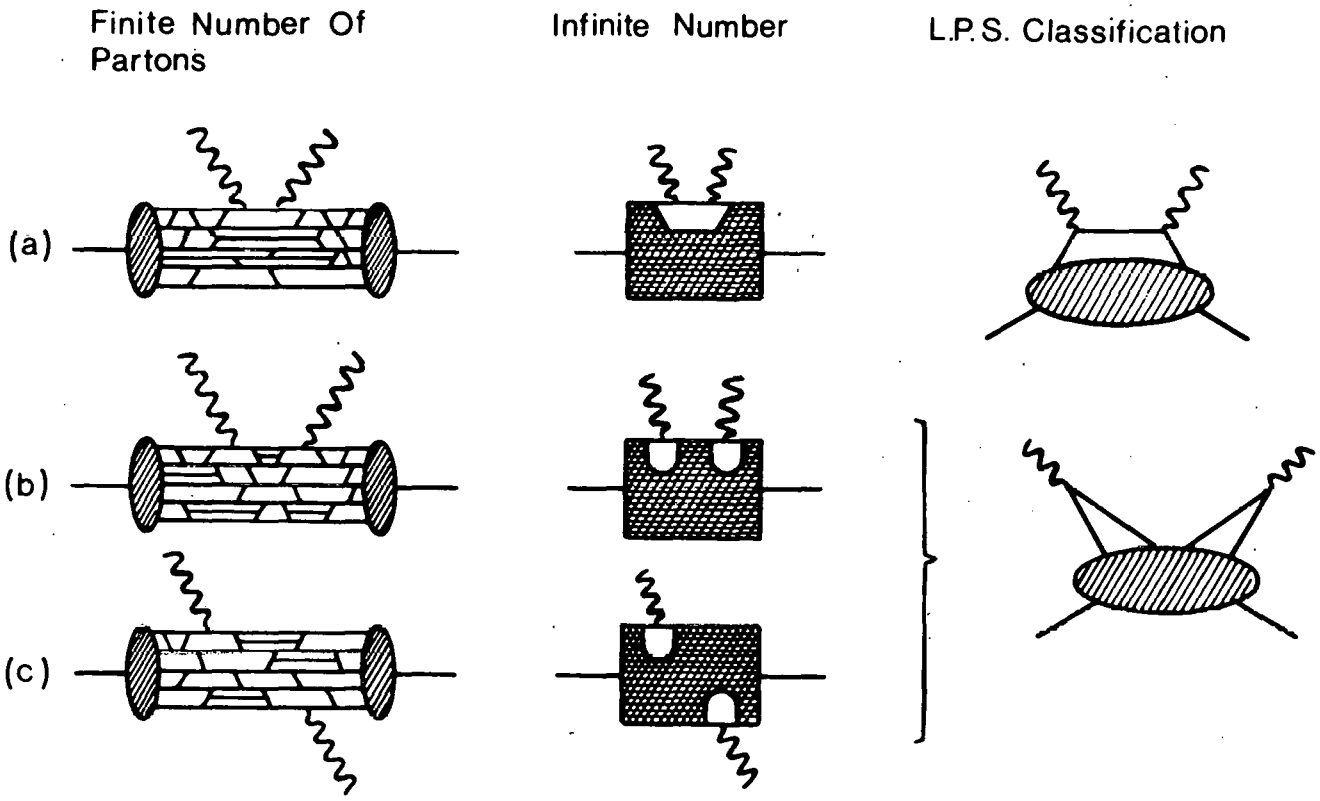

Fig. 36 Topological classification of Compton scattering diagrams in the parton model. (a) is distinguished by the absence of interactions on the parton line between the times of its interacting with the photons. (b) contains interactions and (c) the photons interact with different partons. The LPS classification refers to ref. 36.

If the diagram 35 (or 36c) was the only diagram that one could draw for Compton scattering in the parton model then the structure functions would scale. However one can draw diagrams where the photons couple to different partons or where the photons couple to the same parton but that parton interacts with other partons between the interactions with the two photons (figs. 36b,c). Only if these diagrams are negligible compared to the "incoherent impulse" diagrams (fig. 36a) will the scaling automatically obtain.

In the parton model one removes these diagrams by heuristic arguments (e.g. "when a heavy photon lands on a parton it will knock it out of the proton unless that same parton throws off the photon immediately so that the parton can bind together with its fellows to reform the proton, hence only fig. 36a survives").

The contributions to the amplitude arising from configurations with a finite number of partons always die away as the photon energy increases (cf. the quasi-elastic peak where the area under the peak was proportional to the summed charges squared of the constituents. A finite number of constituents yielded a finite area under the peak); in other words leading Regge behaviour is not obtained. To generate Regge behaviour, configurations with an infinite number of partons are required (compare field theories where Regge behaviour obtains only after summing up ladder graphs with an infinite number of rungs[44]). For a diagram with an arbitrary number of partons (or even infinite number) the crucial property that yields the scaling is the existence of the "free" parton propagator (9.1), i.e. diagrams of the type in figs. 34, 35 and 36a. The idea of the "non-perturbative" parton model of Landshoff-Polkinghorne and Short[36] is to throw all of the N - 1 partons into a black box and concentrate on the parton(s) that interact with the external photons. The diagrams come in two types, fig. 36, the first (36a) we shall refer to as the "box diagram" and the others (36b,c) as the "cats ears". The classification into these two classes will be described later. The blobs contain arbitrary numbers of interacting partons and are treated as parton-proton scattering amplitudes with Regge behaviour (think of the infinite number of partons having formed the ladders that generate the Regge behaviour, Eden et al. op.cit).

When calculating the Compton amplitude in this model the diagram (amplitude) contains the parton-proton scattering sub-amplitude which is parametrised with Regge behaviour. This Regge sub-amplitude causes the whole Compton amplitude to have Regge behaviour. The important physics, in which we are really interested, comes from the coupling of the photons to the partons and yields the scaling property, which we shall discuss after explaining the classification of the diagrams into "box" or "cats ears" categories.

For a configuration with any arbitrary number of partons, then if and only if the diagram contains a freely propagating parton between the two photons is

it classified in the box. Thus the defining feature of this diagram is the freely propagating parton and hence the scale invariance of the structure functions arises from this box diagram. All other diagrams with interactions on the parton which was hit by or emitted the photon are classified in the cats ears, thus the defining feature here is that after the parton has interacted with the photon, the next interaction that that parton undertakes is NOT with the second photon. If this is not clear, the examples in the fig. 36 should clarify the scheme.

As stated above, only the box diagram contains the freely propagating parton required for the scaling of νW_2. Therefore we must invent a rule that will cause this diagram to dominate over the cats ears in the kinematic realm where this scaling is observed ($q^2 \gtrsim 1$ GeV^2, W^2 > Resonance masses). The dynamical assumption of this model[36] is that for a parton off its mass shell, then the parton-proton scattering amplitude goes rapidly to zero. If a heavy photon hits a parton then the parton has to transport this mass through the maze until the final photon can take it away. The only way this mass can flow through to the final photon without entering a parton-proton scattering blob is if it flows across the top of fig. 36a. For all other diagrams (36b,c) a heavy parton enters the blob and the amplitude vanishes. Hence the required diagram dominates.

To show the scaling behaviour we label the momenta as in figs. 37.

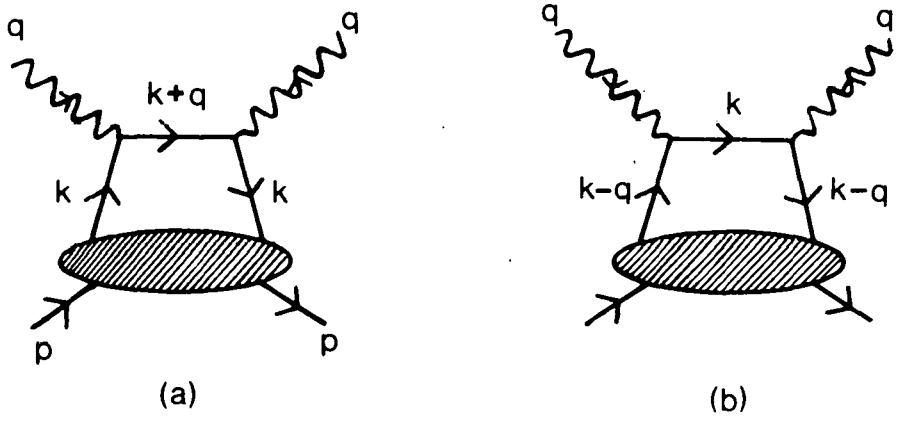

Fig. 37 Two extreme routings of the momentum q through the diagram 36a. Only routing (a) survives at large q^2 since q enters the lower vertex in (b) causing this latter to vanish.

The routing of momenta as in (b) means that a large q enters the blob and the diagram is killed. Only the routing (a) survives (the general approach of Landshoff, Polkinghorne and Short utilises Sudakhov variables. This enables one

CATS EARS

(a)

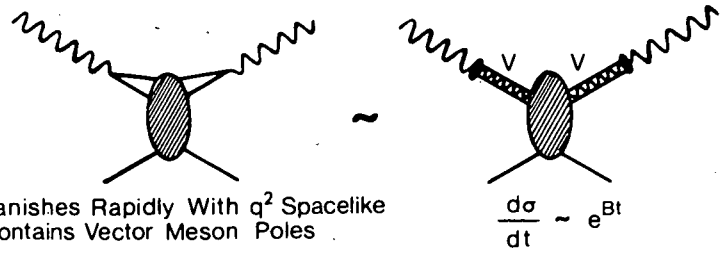

Vanishes Rapidly With q^2 Spacelike
Contains Vector Meson Poles

$\frac{d\sigma}{dt} \sim e^{Bt}$

BOX DIAGRAM

(b)

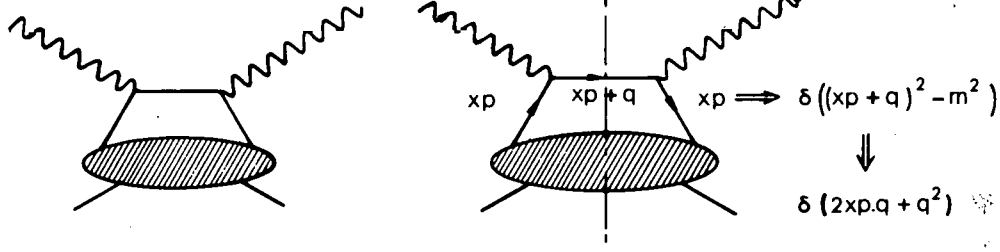

Imaginary Part Scales If We Can Neglect
Transverse Momenta

Always Present In Compton
Dominated By Cats Ears At $q^2 = 0$
q^2 Spacelike: Cats Ears Killed: Box Dominates → Scaling
No Vector Meson Poles In Photon Channel
Hence Contribution To Compton Additional To VMD Models

SEAGULL

(c)

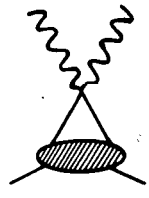

Real Part Contribution Only
$J = 0$ Fixed Pole: Residue Polynomial In q^2
t Dependence Like G(t) Since Like Elastic Form Factor

Fig. 38 Summary of non-perturbative parton model for Compton scattering and vector-meson photoproduction.

to look and see where the momenta is flowing. They show that the routing (i) is dominant for what amounts to the reasons we have outlined). The parton propagator is then essentially of form (9.1) and the resulting delta function (9.2) yields the scaling behaviour of νW_2.

Note that the box diagram only dominates at large q^2. At small q^2 the cats ears diagrams can contribute because the partons can stay near their mass shell and so the parton-proton amplitude need not vanish. Thus the scaling does not obtain at small q^2 due to the presence of the cats ears diagrams. The box diagrams are still present in the data but swamped by the cats ears. A summary of this and subsequent discussion is given in the fig. 38.

The advantage of this model is that not only does it show how to incorporate Regge behaviour in the parton picture but also enables us to extend our discussion of Compton scattering in the parton model to include on-shell Compton and also photoproduction[35]. We have seen that the parton model predicts the existence of $J = 0$ fixed poles. We shall now see how the non-perturbative parton model, in particular the existence of the box diagrams, enables us to understand the inter-relation of the old parton model and the vector dominance model, in particular the failure of the vector dominance model in Compton scattering.

10 THE PARTON MODEL AND VECTOR-MESON DOMINANCE-RIVALS OR PARTNERS?

Imagine a world made up of photons and quarks (partons) where the hadrons are bound states of the quarks and hence are never elementary objects. Then the contribution to Compton scattering from the box diagrams, which contain the freely propagating partons, do not have vector meson poles in the photon channel. This is equivalent to saying that these diagrams cannot be vector-meson dominated[35]. Vector-meson poles are only present if the quark and anti-quark bind together to form a meson (fig. 39) and hence are present only in the cats ears diagrams. Consequently one would expect that while vector-meson dominance (VMD) is satisfactory in comparing $\gamma p \to \rho p$ with $\rho p \to \rho p$ (where only the cats ears diagrams contribute) the comparison with $\gamma p \to \gamma p$ is more complicated

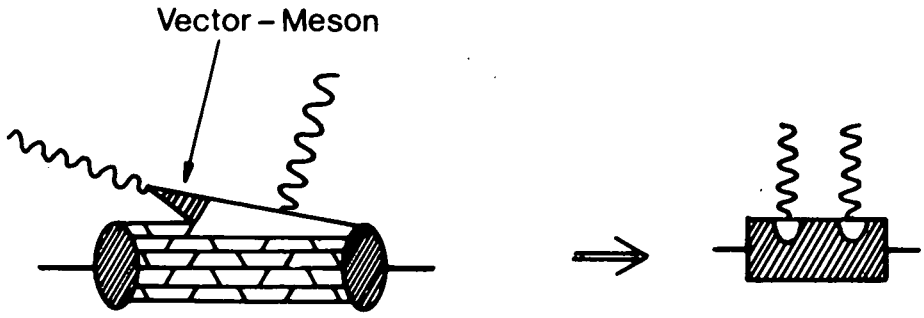

Fig. 39 Vector-mesons in the photon channel arise only in the cats ears diagram due to binding of the quarks being required to form the meson; compare figs. 36.

since these two photon processes contain not only the (vector dominated) cats ears diagrams but also the box diagram which has nothing to do with vector dominance*.

To decide whether or not the cats ears diagrams are really vector-meson dominated we compare $\gamma p \to \rho p$ with $\rho p \to \rho p$. Only the cats ears diagram contributes to these processes as interactions between the partons is necessary in order to bind them together.

Experimentally a value for the rho-photon[47,48] coupling of $\gamma_\rho^2/4\pi$ = 0.65 ± 0.01 is required for the vector dominance to work in relating these two processes (fig. 40). This is in agreement with the value 0.64 ± 0.06 measured directly by the Orsay experiment $e^+e^- \to \pi^+\pi^-$. We thus adopt as a working hypothesis vector dominance for the cats ears diagrams. The solid curve[49] is $\rho p \to \rho p$ "data" obtained from $\pi^\pm p$ differential cross sections and use of the quark model relation

$$\frac{d\sigma}{dt}(\rho p \to \rho p) = \left[1/2 \sqrt{\frac{d\sigma}{dt}(\pi^+ p)} + 1/2 \sqrt{\frac{d\sigma}{dt}(\pi^- p)} \right]^2$$

*We do not venture into discussions of generalised vector dominance (GVMD) see for example J. Sakurai, ref. 45 (1972 lectures). It seems probable that the high mass continuum states present in that model are in some sense dual or equivalent to the box diagrams, see J. Pestieau, ref. 46.

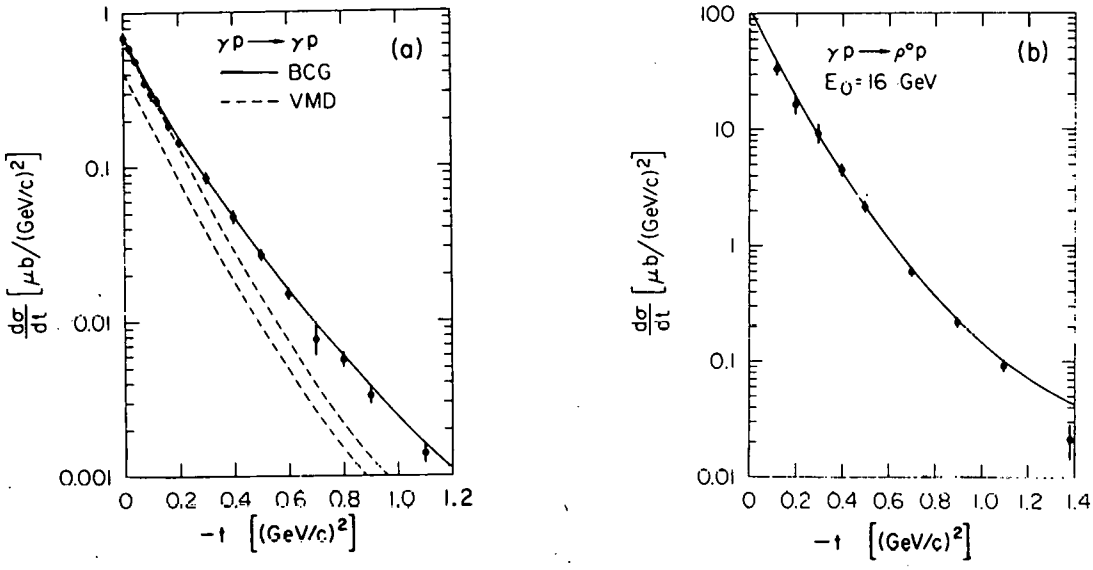

Fig. 40 Compton scattering at 16.6 GeV/c (data from ref. 51). The lower of the curves marked VMD is the result of taking the vector-meson photoproduction data of ref. 49 and using $\gamma_\rho^2/4\pi = 0.65$ (see text). (This of course is the Orsay value and is also that which works well in predicting γV from VV data; see fig. 40(b) where is shown a sample comparison between this latter VMD prediction and the γV data). Renormalising this curve so as to agree at small t yields the upper VMD curve (corresponding to $\gamma_\rho^2/4\pi = 0.35$). The curve labelled BCG is described in detail in ref. 35 (second paper) and discussed in the text.

The quark model also predicts that

$$\sigma(\rho N) = 1/2 \left[\sigma(\pi^+ N) + \sigma(\pi^- N) \right]$$

with N either neutron or proton, and this is very well satisfied by the direct measurement of σ(ρN) performed by Ritson et al., ref. 50. This latter experiment measured σ(ρN) directly by looking at γD → ρD and at large momentum transfers this process is dominated by the two step process $\gamma N_1 \to \rho N_1 \ldots \rho N_2 \to \rho N_2$ and so the first nucleon is acting as a "source" of a "beam" of ρ-mesons with

which one performs ρN elastic scattering. The value of $\gamma_\rho^2/4\pi$ obtained in this experiment directly is ~ 0.65 again in agreement with the above.

In fig. 40(b) we see the data for Compton scattering at 16 GeV. The lower curve is the VMD prediction for $\gamma p \to \gamma p$ using the data on $\gamma p \to Vp$ ($V = \rho, \omega, \phi$), $\gamma_\rho^2/4\pi = 0.65$ and the canonical SU(3) $1/9 : 1 : 1/2$ ratios for $\gamma_\rho^2 : \gamma_\omega^2 : \gamma_\phi^2$ with the actual data. The agreement is poor, at $t = 0$ there is a ratio of 35/65 mismatch between the data and the prediction. Not only is this forward normalisation incorrect but the shapes of the two are different at large t. We take this to be a consequence of the box diagrams and the seagull (fixed pole) contributions. The fixed pole is small in magnitude and contributes only a few percent to the forward cross section, but the box diagrams can yield important contributions. Indeed the comparision seems to be saying that these give about 25% contribution to the amplitudes at $q^2 = 0$. As t increases, all Regge contributions can be expected to fall off rapidly, perhaps exponentially, in t. The fixed pole will then dominate due to its slower fall off (assumed[35] to be like the elastic electromagnetic form factors due to the similarity of the seagull and elastic form factor diagrams). The change in shape of the $\gamma p \to \gamma p$ (relative to $\gamma p \to \rho p$) is thus a reflection of the transition from Regge to fixed pole dominance occurring in that region of t. A complete discussion of the shape and energy dependence of $\gamma p \to \gamma p$ include several important details which are discussed at length in ref. 35 (second paper).

The presence of the box diagrams also explains why VMD was unable[47,48] to agree with $\sigma_{tot}(\gamma p)$ where, using $\gamma_{\rho N}^2/4\pi \sim 0.65$, the predicted magnitude for $\sigma_{tot}(\gamma p)$ was only some 75% of the actual data. The reason for the failure is clear in the light of the above discussion of the Compton scattering data. $\sigma_{tot}(\gamma p)$ is related to the imaginary part of $\frac{d\sigma}{dt}(\gamma p \to \gamma p)$ at $t = 0$. Then

$$\frac{\sigma^{DATA}(\gamma p)}{\sigma^{VMD}(\gamma p)} = \sqrt{\frac{d\sigma^{DATA}(\gamma p \to \gamma p)}{d\sigma^{VMD}(\gamma p \to \gamma p)}} = \sqrt{\frac{65}{35}} \sim 4/3$$

(assuming the same real to imaginary part ratio in the cats ears and the box diagrams - this is probably reasonable since the agreement with $\gamma p \to \gamma p$ over all energies obtains in this parton model with the cats ears and box having the same

energy dependence). The fact that

$$\sigma_{tot}(\gamma p) \sim 1/4\ \sigma^{BOX}(\gamma p) + 3/4\ \sigma^{VMD}(\gamma p)$$

is very interesting since we can test it directly by looking at photoabsorption on nuclei where the cross section will be

$$\sigma(\gamma A) \sim 1/4\ \sigma^{BOX}(\gamma A) + 3/4\ \sigma^{VMD}(\gamma A)$$

The former is $A * \sigma^{BOX}(\gamma p)$ (since partons never escape from the nucleon then this contribution is unshadowed). The latter VMD piece can be, and is, shadowed, VMD predicting that*

$$\frac{\sigma^{VMD}(\gamma A)}{\sigma(\gamma N)} \sim A^{0.89}$$

It is well known that the data exhibit less shadowing than predicted by VMD. $A^{eff} \equiv \frac{\sigma(\gamma A)}{A\,\sigma(\gamma N)}$ is shown for deuterium, carbon, copper and lead targets at high energies in fig. 41. The lower curve is the prediction of naive VMD, viz. $A^{0.89}$; the top curve is for no shadowing. The data lie between these two extremes and the curve passing through them is

$$A^{eff} = 1/4\ A + 3/4\ A^{0.89}$$

i.e. the non vector dominated piece is non-shadowed and the parton model has given us a natural explanation of this phenomenon. This is not to say that

---

*If the ρN cross section were infinite then the photon having turned to a rho would be absorbed on the surface of the nucleus. Hence it would only see the surface nucleons and the cross section would go as $A^{2/3}$ since the surface to volume behaves as the 2/3 power. The fact that $\sigma(\rho N) \sim 26$ mb means that the shadowing is not that dramatic. Detailed calculation gives $A^{0.89}$, see D. Yennie, ref. 52.

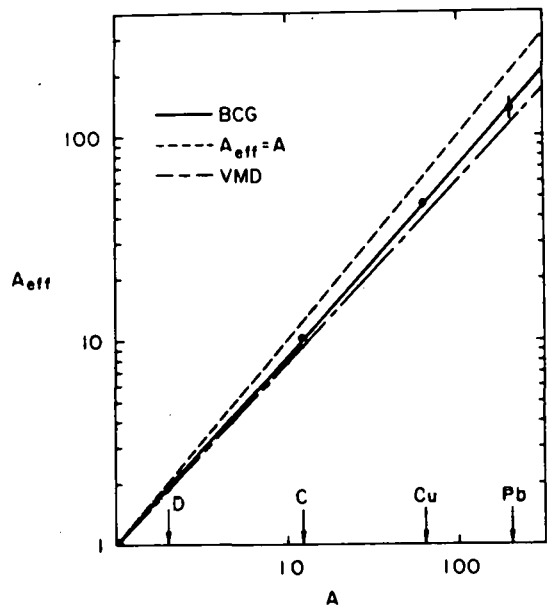

Fig. 41 Shadowing in 14.4 - 18.3 GeV on-shell nuclear photoabsorption. $A^{eff} = \sigma(\gamma A)/\sigma(\gamma N)$ for a nucleus containing A nucleons. "No shadowing" would predict $A^{eff} \sim A$ (the upper curve) while the VMD model with $\sigma(\rho N) \sim 26$ mb and a ratio of 20% for the real part of the $\gamma \to \rho$ amplitude to its imaginary part yields the lower curve. The curve labelled BCG is given by $0.22A + 0.78A^{0.89}$ (see ref. 35 and text) corresponding to the 22% point-like portion expected on the basis of the model of the text.

other models, e.g. generalised vector-meson dominance cannot give an equally adequate explanation. A place where they have some difficulty is when we scatter electrons off the nuclei, as we now show.

Empirically scaling sets in extremely rapidly with q^2. In the parton model this corresponds to rapid suppression of the cats ears diagrams so that the box diagrams dominate. This would in turn predict that the shadowing disappears very rapidly since these box diagrams are unshadowed. Experimentally[53] this shadowing seems to have vanished by $q^2 \sim 0.5$ $(GeV/c)^2$. This is much too fast for naive VMD and estimates suggest that it is also difficult to understand within the framework of GVMD. Better knowledge on the behaviour of the shadowing dependence upon energy and q^2 will be very useful in distinguishing among these theories (this picture is somewhat different than that mentioned at the end of

chapter 8 where the shadowing would be present at $q^2 \neq 0$ if one goes to very high ν).

It seems therefore that the parton model is able to give us an understanding of a wide range of phenomena and it is therefore worth pursuing its consequences further. A list of consequences of the parton model, some of which we have discussed and some of which we have not is given below.

1. The Compton amplitude will be predominantly real at high t.
2. s-channel helicity conservation will be violated in Compton scattering at high t. The sign of the asymmetry is predicted.
3. A slower fall off in the momentum transfer in Compton scattering cross sections as compared to rho photoproduction is predicted.
4. The cross section for $\gamma(q^2)p \to \gamma p$ compared to $\gamma p \to \gamma p$ will broaden as q^2 becomes more virtual space-like.
5. Amplitudes for two photon processes will fall off slowly as a function of the invariant masses of the photons. This will have dramatic implications for Bethe-Heitler wide angle bremsstrahlung and colliding beam experiments.
6. An increasing lack of shadowing in the A dependence of the total (off-shell) photoabsorption measurements on nuclei at high q^2.
7. Despite the breakdown of vector-meson dominance in comparing $\gamma \to \rho$ with $\gamma \to \gamma$ processes, the relations between $\gamma \to \rho$ and $\rho \to \rho$ processes are not necessarily affected, and VMD results could be in good agreement here.

Amplification upon the above implications of "extended" parton models are given in the paper "Phenomenology of photon processes, vector dominance and crucial tests for parton models" upon which the material in this chapter was drawn. Further discussion of many of the points in this chapter can be found in that paper (ref. 35).

11 DO RESONANCES SCALE?

In chapters 2 and 3 we looked at the process ep → e + anything and showed that the observed scale invariance

$$\nu W_2(\nu, q^2) \to F_2(\omega)$$

at large q^2, W^2 where

$$W^2 = M^2 + 2M\nu + q^2$$

obtained if one hypothesised that there were partons inside the proton with which the electromagnetic field interacted. Diagrammatically this was represented by fig. 34 which has the unfortunate consequence that it is predicting that partons will be seen in the final hadronic system. Empirically the final hadron system consists of π, N etc. rather than quarks. This is a central problem to all parton models and although we do not know of a satisfactory way of brushing this problem under the carpet we shall examine a possible clue in the data.

Let us look at the data for

$$ep \to eX$$

where we hold the missing mass X fixed = W^2. We then measure the cross section and extract νW_2 (q^2, W^2 = fixed). For fixed W^2 = 4, 9, 16 $(GeV)^2$ the resulting behaviour of νW_2 is seen in fig. 42 plotted against Q^2/W^2. Note that as $Q^2 \to \infty$ at any fixed W^2 then νW_2 is vanishing, just like the case of the elastic form factors. Note also that the data seem to lie on a single curve. In fact for <u>any</u> fixed $W^2 \gtrsim 4$ $(GeV)^2$ the data lie on the curve, fig. 43. Hence νW_2 $(Q^2/W^2, W^2) \to \nu W_2$ (Q^2/W^2) for each and every $W^2 \gtrsim 4$ $(GeV)^2$. Thus we have obtained the familiar result that for $W^2 > 4$, $Q^2 > 1$ νW_2 exhibits the phenomenon of scale invariance. When plotted against W^2/Q^2 the curve becomes fig. 44 which is the more familiar way of presenting the data (compare fig. 9). However we will continue to use the plot in terms of Q^2/W^2. Note that it is this phenomenon of scale invariance which inspired the parton model with incoherent impulse (figs. 34, 47(a)).

How does this "universal" Q^2 dependence of νW_2 at large values of W^2 compare with that at small W^2 where resonance excitation is present? A typical

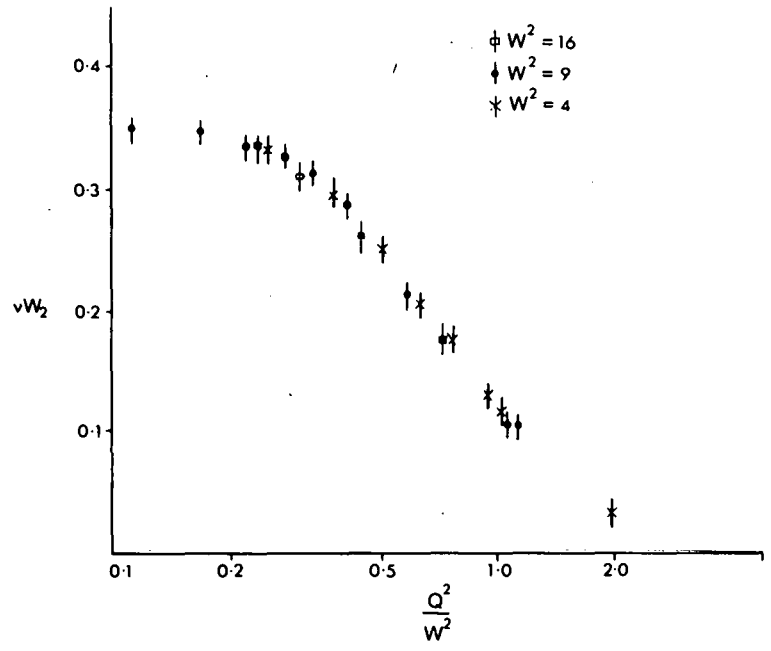

Fig. 42 νW_2 as a function of Q^2 at fixed W^2 = 4, 9, 16 $(GeV)^2$ data from M. Briedenbach et al., Phys. Rev. Letts. 23 (1969) 935, E.D. Bloom et al., ibid 930, M. Briedenbach, Ph.D. Thesis MIT (1970), G. Miller, SLAC-PUB-815 (1970).

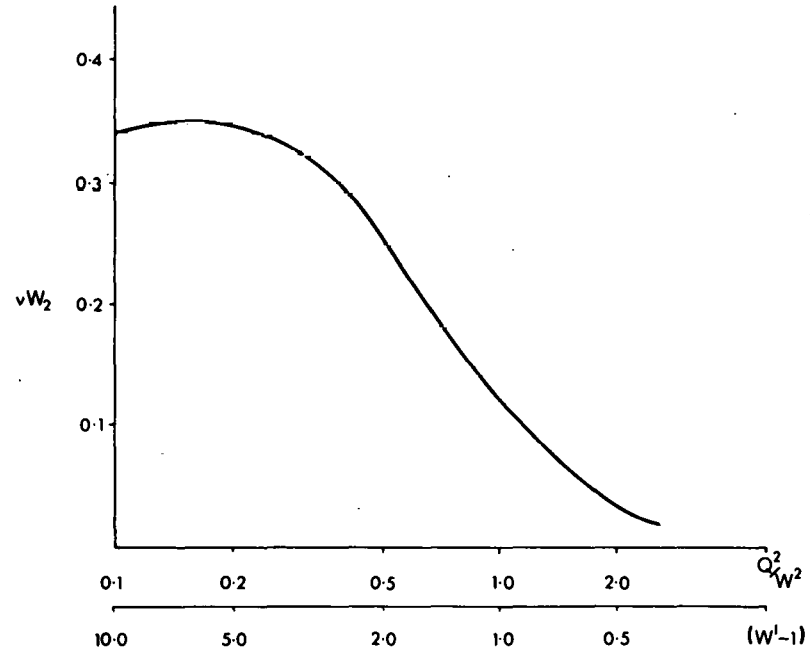

Fig. 43 Best fit to νW_2 (Q^2, W^2) for any $W^2 \geq 4$ $(GeV)^2$ plotted against Q^2/W^2.

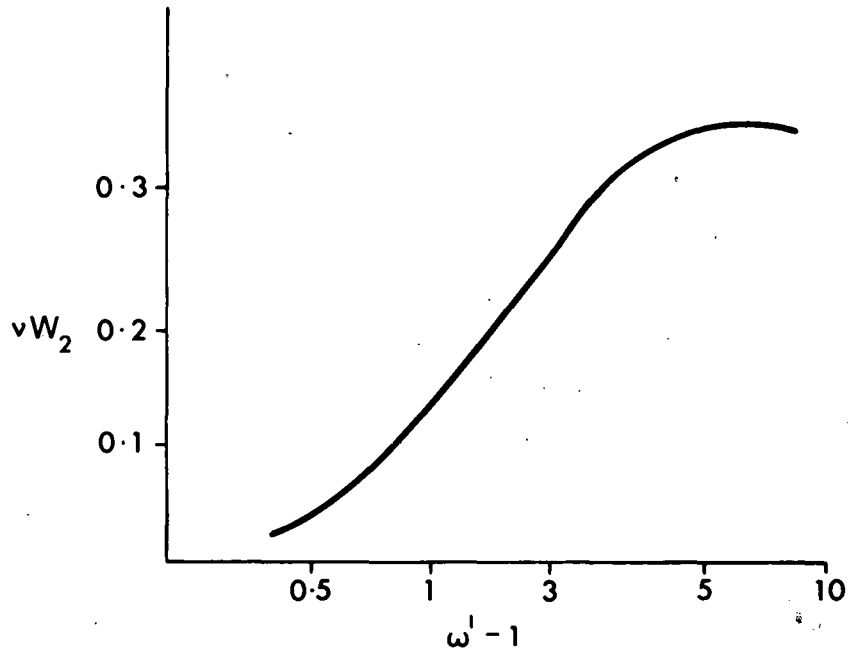

Fig. 44 As fig. 43 but against $\omega' - 1 = W^2/Q^2$.

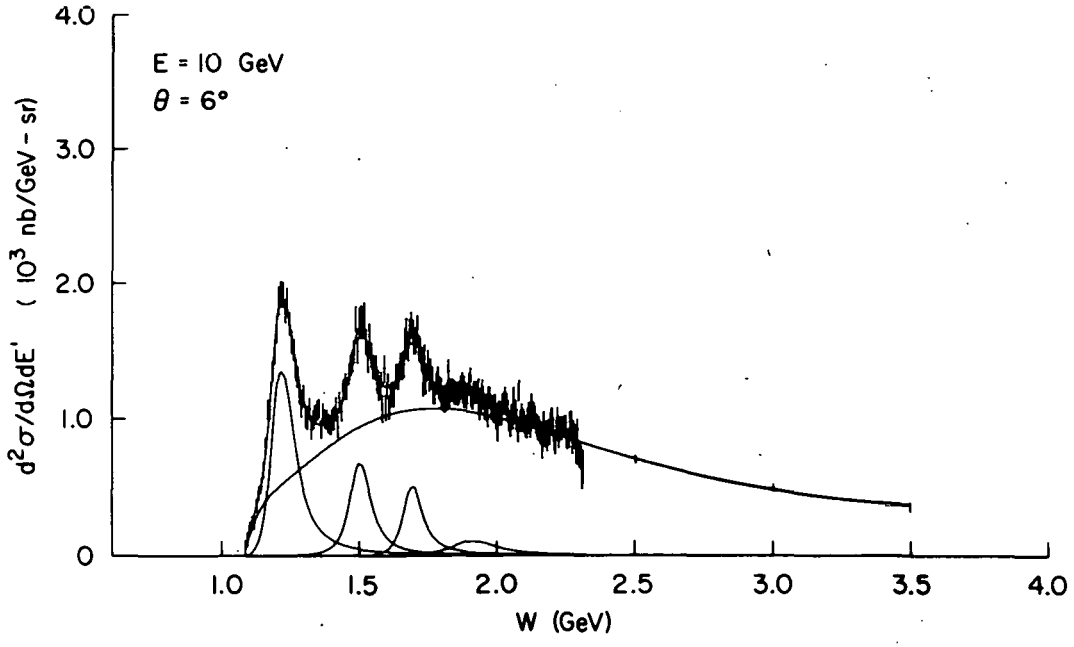

Fig. 45 Resolution of 10 GeV, 6° electron scattering spectrum into four modified Breit-Wigners and a smoothly varying background, after M. Briedenbach.

excitation data set is shown in fig. 45 where bumps corresponding to the 1st, 2nd, 3rd and possibly even 4th resonance regions can be seen. Combining data at various angles one can interpolate to obtain fixed q^2 cross sections and we can then extract νW_2 (W^2, Q^2) through the resonance region. For the moment we shall make no attempt to separate resonance from background and in fig. 46

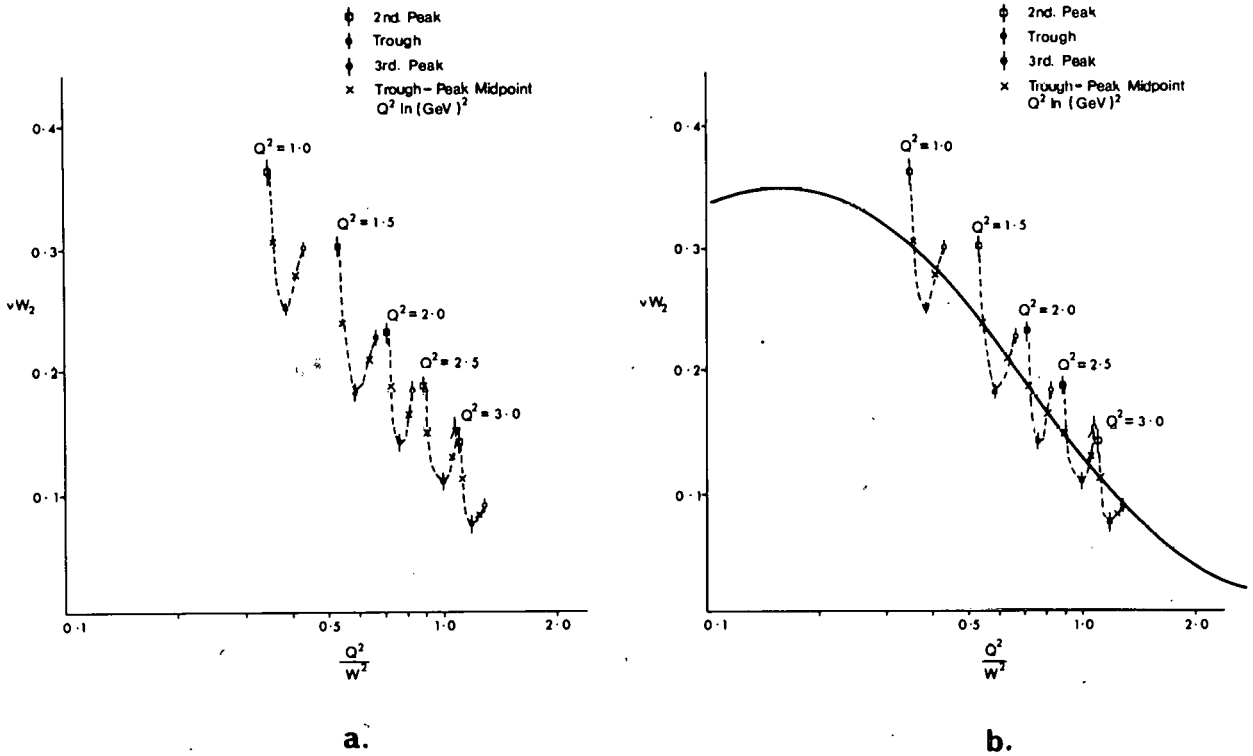

Fig. 46(a) Contribution to $\nu W_2(Q^2)$ from the second and third resonance regions plotted against Q^2/W^2.

(b) and compared with $\nu W_2(Q^2)$ for $W^2 \geq 4$ $(GeV)^2$.

we show the νW_2 contribution from the peak of the second resonance, the peak of the third and also the trough between them plotted against Q^2/W^2 for Q^2 = 1, 1.5, 2, 2.5 and 3 GeV^2. The crosses which fall midway between crest and trough follow almost exactly the universal behaviour found at large W^2 (fig. 43). Thus were it not for modulations caused by the resonating partial waves it would appear that the universal behaviour at large W would also obtain at small W[54].

At this point it is interesting to make a remark about parton models. The universal curve for the large W, large Q^2 behaviour is generated in such models by the incoherent impulse diagrams, fig. 47(a). Resonance excitation on the other hand is coherent excitation of the whole nucleon and may be represented

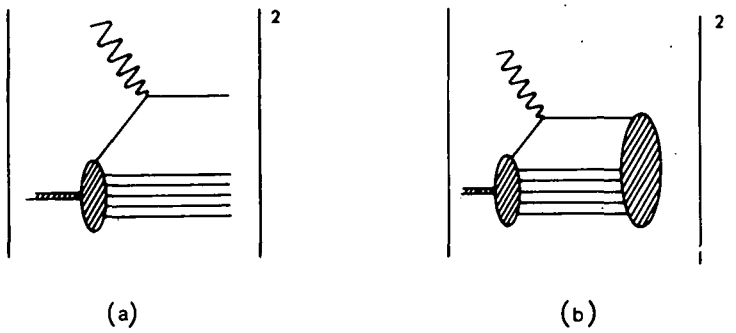

Fig. 47(a) Incoherent scattering from partons.

(b) Coherent excitation of nucleon in the parton picture.

by fig. 47(b). Since we know nothing about the blob ("final state interactions") there is no a priori reason for this diagram to exhibit scaling behaviour (nor, for that matter, for it not to). However, the scaling seems to persist empirically even into the small W region where N* excitation (and hence this latter diagram) is present.

Two possibilities emerge:

(a) This diagram does not scale - the "apparent" scaling of the data is due to the non-scaling N* excitation being small and superimposed upon a very large scaling background (fig. 47(a)).

(b) This diagram does scale - the N* themselves have "universal form factors", i.e. are functions of Q^2/W^2.

To attempt to settle which of these is realised in nature requires a separation of N* from background in the small W^2 data.

In fig. 48 we show $(d\sigma)^{N^*}/(d\sigma)^{ELASTIC}$ obtained from Briedenbach's fit to the small W data as four Breit-Wigner's plus a smooth background. That this behaviour is possibly consistent with being a function of Q^2/W^2 rather than Q^2 is shown in fig. 53 where universal behaviour in Q^2/W^2 would lead to $\sigma(N^*)/\sigma(ELASTIC)$ rising with Q^2 as against being constant if the excitation were universal in Q^2.

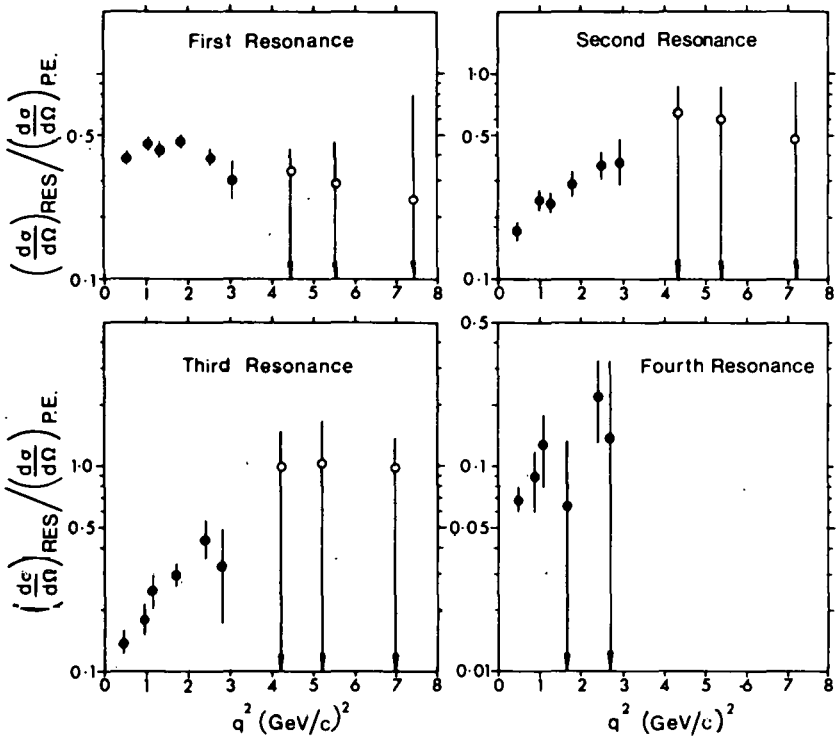

Fig. 48 Ratio of resonance excitation cross section to elastic cross section in electron proton scattering versus Q^2 (from SLAC-PUB-796 (1970)).

Encouraged by this qualitative suggestion we take Briedenbach's fits and plotting the 2nd and 3rd resonances against Q^2/W^2 we find they appear to be consistent with universal behaviour in Q^2/W^2 (fig. 49). The first resonance, however, appears to fall more rapidly. The fact that the second and third resonance form factors are functions of Q^2/W^2 means that they are a constant fraction of the universal curve (fig. 43) (which was the data for $W^2 > 4$ GeV)^2) as Q^2 varies. The ratio of the first resonance to the scaling curve falls as Q^2 increases as can be seen by comparing the resonance behaviour with the large W^2 "scaling curve" in fig. 50. This conclusion coincides with fig. 51 taken from Bloom and Gilman (ref. 54) supplemented by $Q^2 < 1$ (GeV)^2 data, where the resonant fraction in νW_2 at a given ω' is compared with the universal behaviour of νW_2 (fig. 50) at the same ω' as Q^2 varies. The second and third resonances appear to be a constant ratio of the νW_2 scaling curve (fig. 50) as Q^2 varies and hence themselves scale.

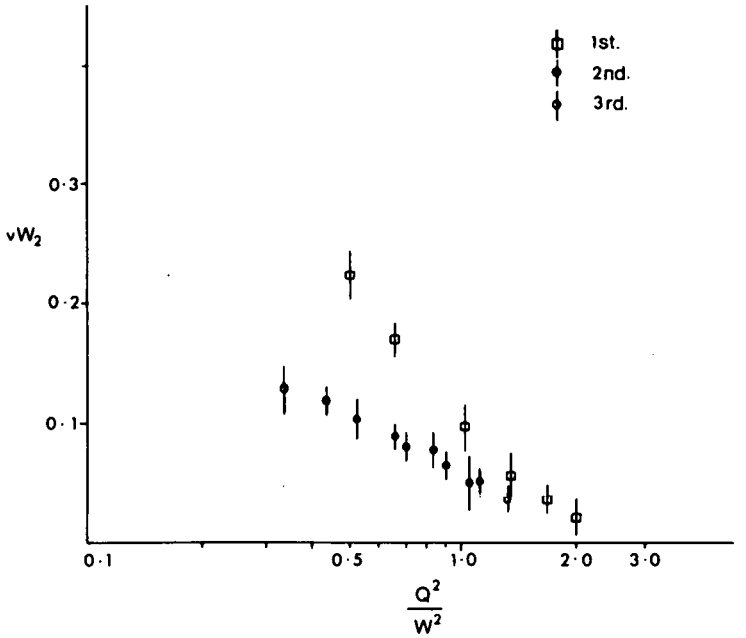

Fig. 49 νW_2^{Res} against Q^2/W^2 for first, second and third resonances.

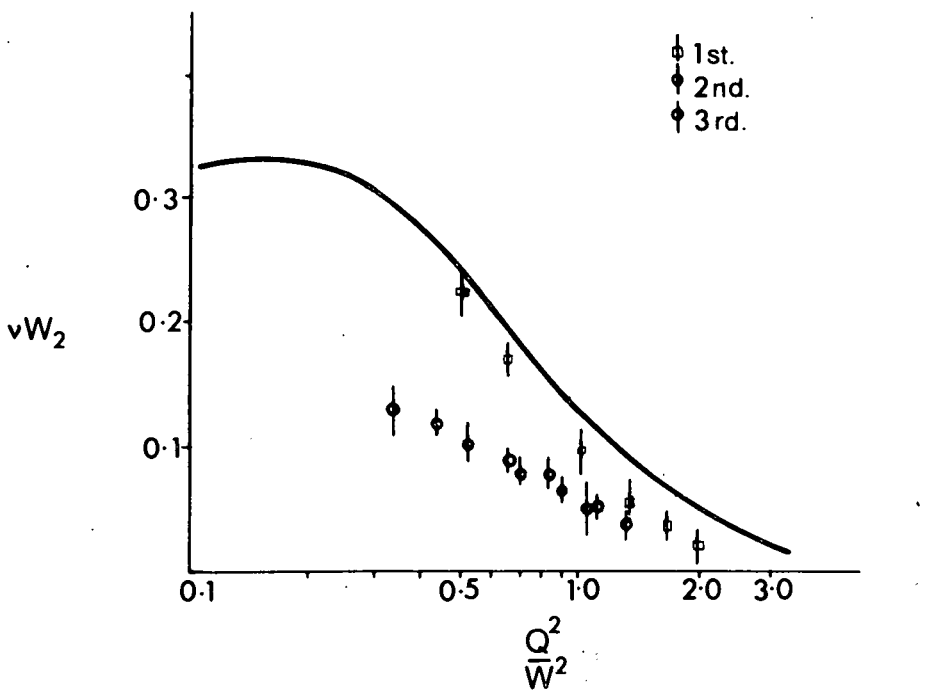

Fig. 50 As fig. 49 but compared with $\nu W_2(Q^2)$ and $W^2 > 4$ (GeV)^2.

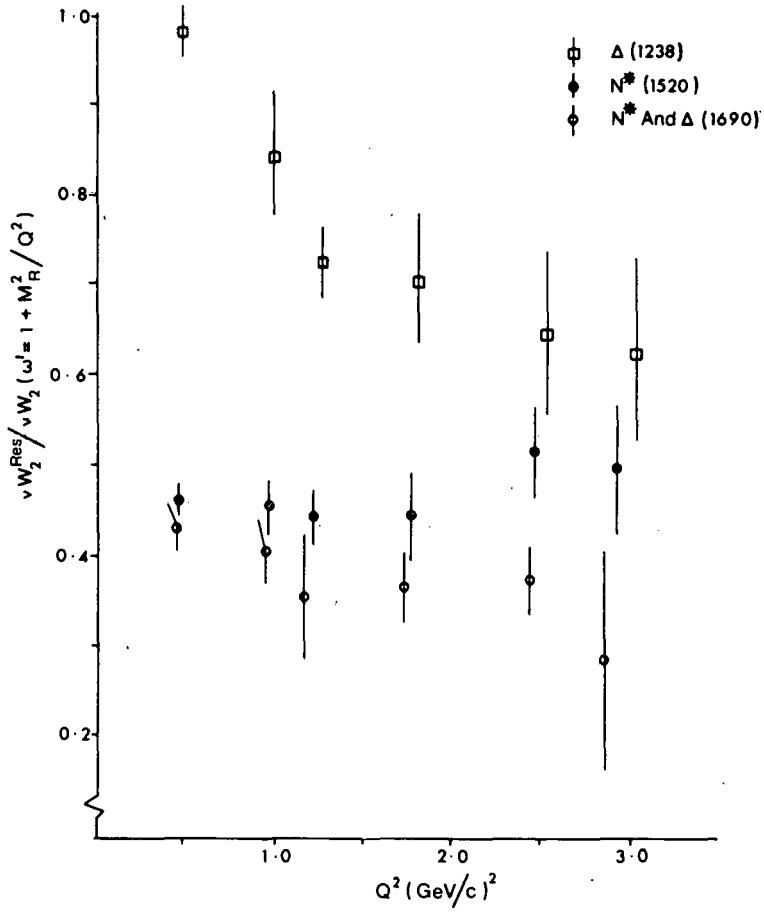

Fig. 51 The ratio of the heights of the resonance bumps in νW_2 to the value of the scaling limit curve $\nu W_2(\omega')$ at the corresponding value of $\omega' = 1 + M_N^2/Q^2$ (from ref. 54 supplemented by $Q^2 < 1$ (GeV)^2 points - F.J. Gilman unpublished). Values for the height of the resonance bump are taken from M. Briedenbach (fig. 45), the $\nu W_2(\omega')$ from G. Miller (fig. 43).

The possibility that the first resonance sinks into a scaling background as Q^2 increases while the second becomes more prominent (?) with the third staying roughly constant is also suggested by the DESY data[55] (fig. 52) where as Q^2 increases the prominence of the second bump becomes marked while the first bump is becoming less noticeable above the background. Could it be that the I = 3/2 states are becoming less important than the I = 1/2 as Q^2 gets large ($\omega' \to 1$)? This at least is a possibility although further study is needed to confirm this.

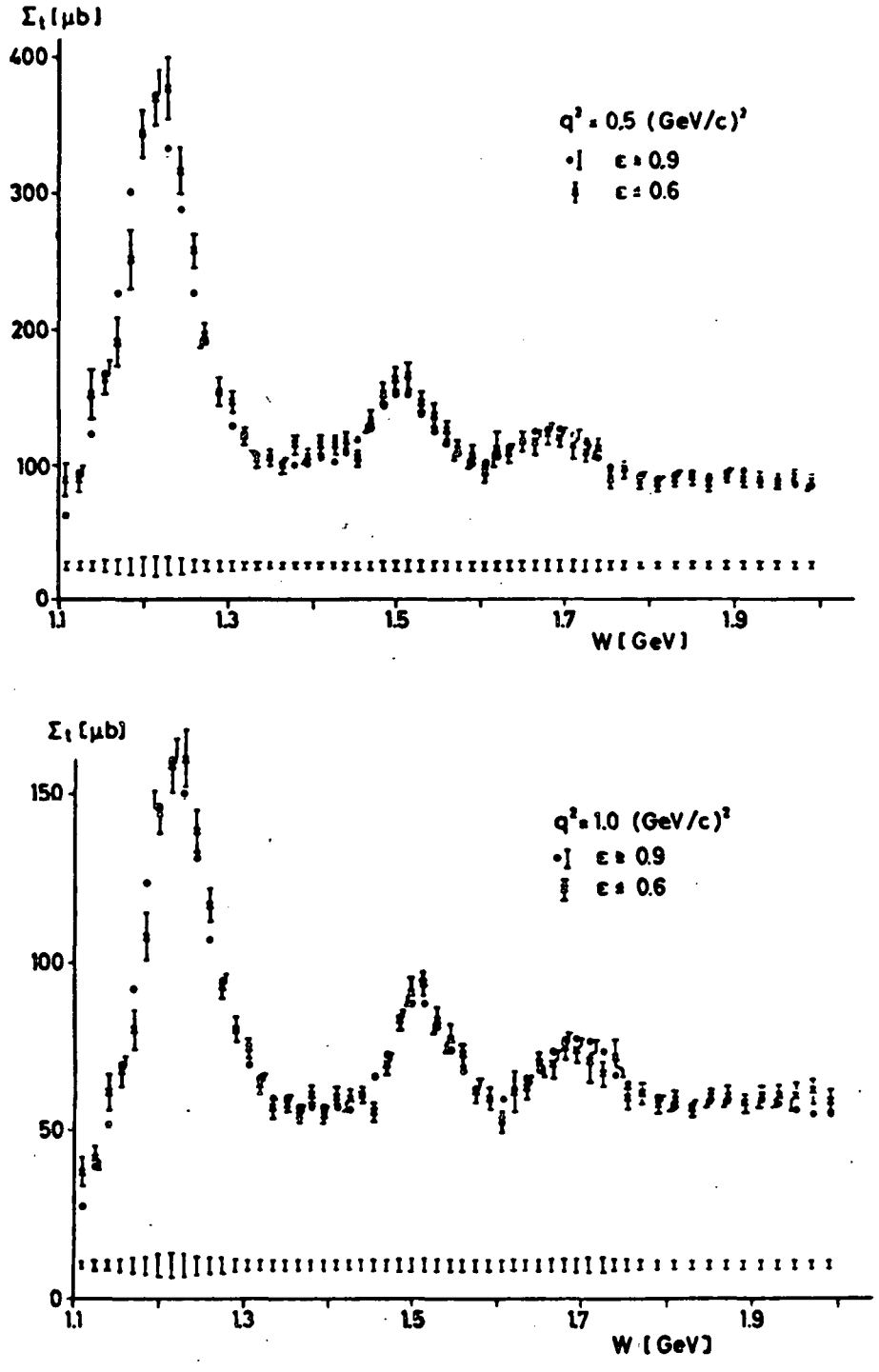
Σ_t (μb)
400
300
200
100
0
q^2 = 0.5 (GeV/c)^2
ε = 0.9
ε = 0.6
1.1
1.3
1.5
1.7
1.9
W [GeV]
Σ_t (μb)
150
100
50
0
q^2 = 1.0 (GeV/c)^2
ε = 0.9
ε = 0.6
1.1
1.3
1.5
1.7
1.9
W [GeV]

Fig.52

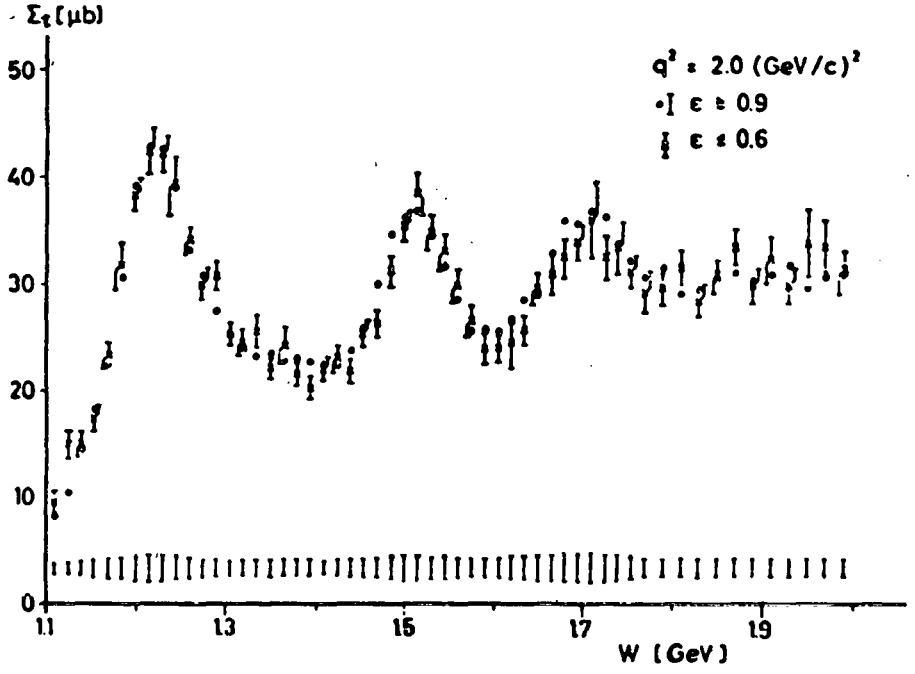
Σ_t (μb)
q^2 = 2.0 (GeV/c)^2
ε = 0.9
ε = 0.6
50
40
30
20
10
0
1.1
1.3
1.5
1.7
1.9
W (GeV)

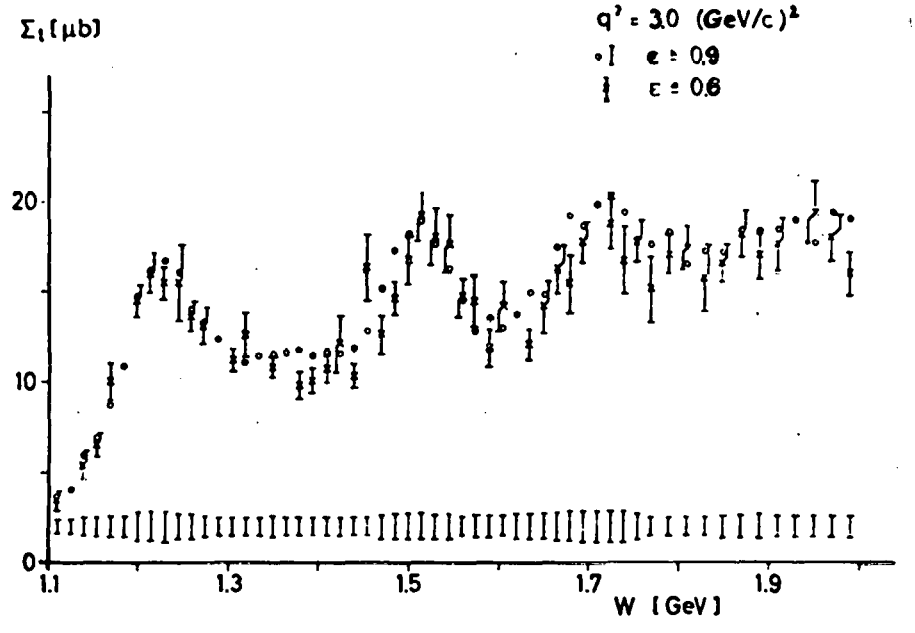
Σ_t (μb)
q^2 = 3.0 (GeV/c)^2
ε = 0.9
ε = 0.6
20
10
0
1.1
1.3
1.5
1.7
1.9
W (GeV)

Fig.52

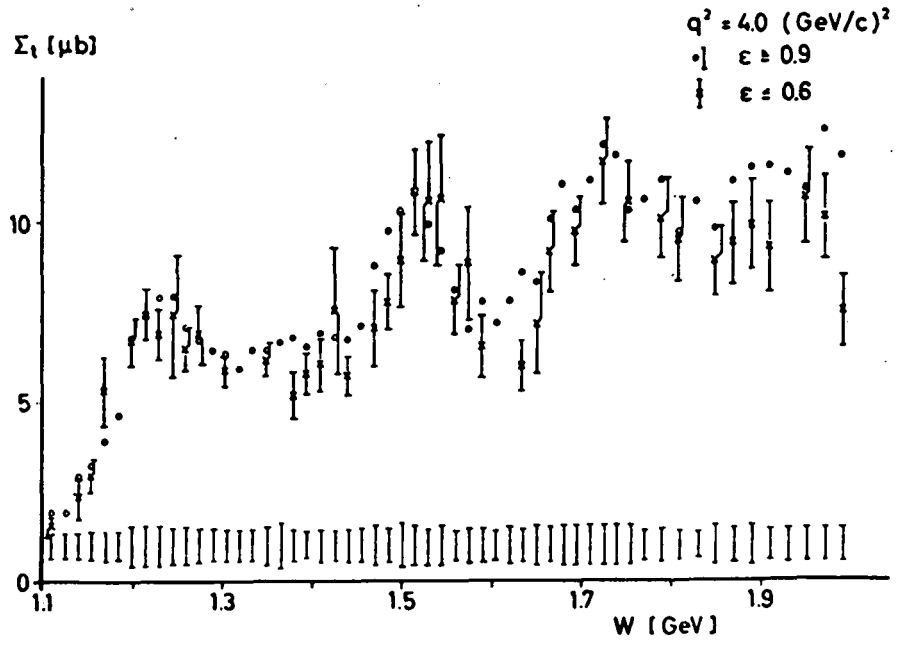

Fig. 52 Data for $\Gamma(\sigma_T + \varepsilon\sigma_S)$ (eqn.(2.19)) from ref. 55 for Q^2 = 0.5, 1.0, 2.0, 3.0 and 4.0 (GeV)^2.

Two comments are called for. In fig. 48 one notes that the $\sigma(N^*)/\sigma$(elastic) gets progressively steeper as one proceeds to the higher mass N^* and as shown in fig. 53 this is what one would expect if the data were a function only of Q^2/W^2. However, the higher the resonance mass then the higher its spin and so the steepening of the slope in $\sigma(N^*)/\sigma$(elastic) could be in part not so much a scaling effect as a kinematic effect arising from the higher angular momentum barriers that need to be overcome in exciting the higher spin resonances. One could then ask oneself at even larger W^2, into the deep inelastic region, whether the ever higher partial waves present means that the "scaling" of νW_2 has an origin, in part, in the higher angular momentum barriers[56].

Alternatively one may accept that the scaling is real, over and above angular momentum barrier effects, even down into the resonance region. As mentioned briefly earlier, in the deep inelastic (large W) region the scaling arises in the parton model from the incoherent impulse diagrams (fig. 47(a)). The resonance excitation is coherent excitation of the whole nucleon (fig. 47(b)) and empirically also exhibits scaling behaviour. Thus, in some sense, the

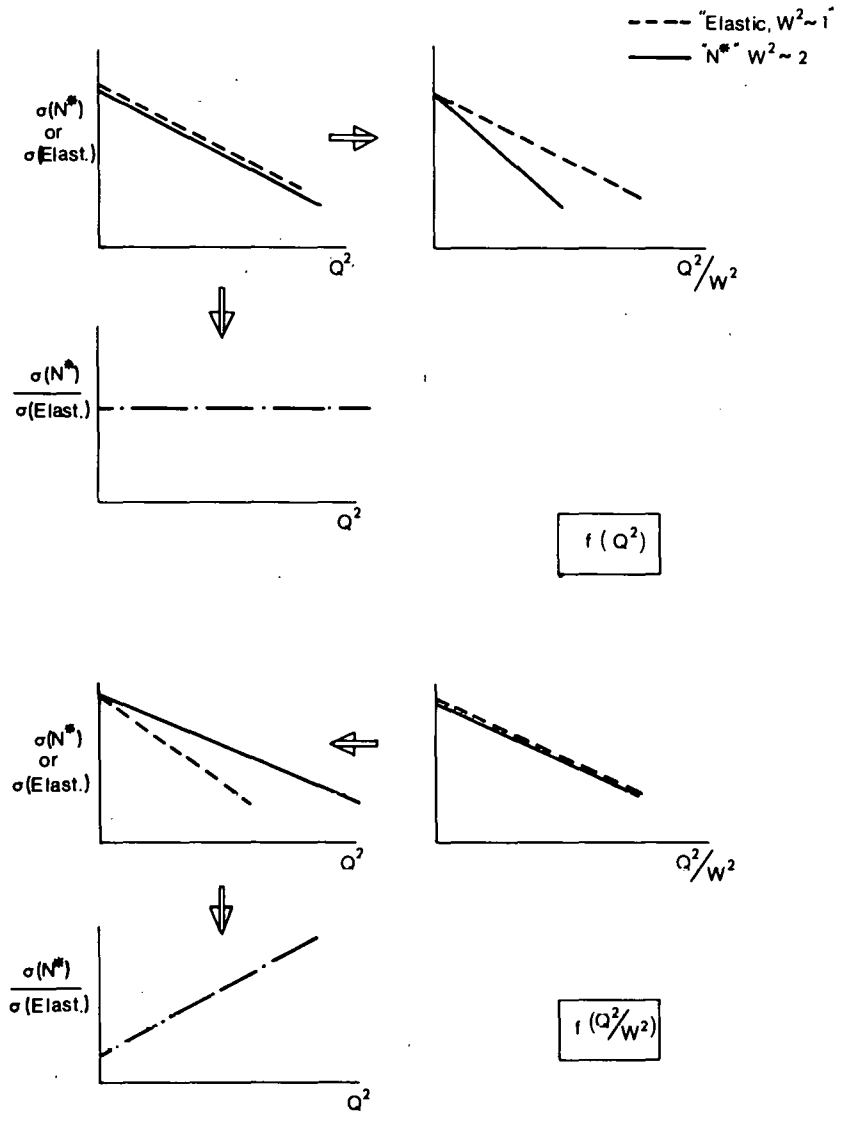

Fig. 53 Indication that data of fig. 48, in particular the steepening ratio as resonance mass increases, is consistent with resonance excitation being a function of Q^2/W^2 i.e. scales. For a function of Q^2 the resonance to elastic ratio is a constant (upper figures) while for Q^2/W^2 the ratio increases due to the higher the mass of the resonance then the slope increases as W^2 increases (lower figures).

diagram 47(a) is dual to 47(b). Hence one might summarise this by concluding that the final state interactions do not change things much from the incoherent situation (47(a)). Thus numerical predictions and sum rules derived in the incoherent quark parton model (47(a)) may well work but no partons are seen due to the final state interaction which does not affect the scaling nor the

essential underlying quark quantum numbers. The final state then consists of the decay products of hadrons (for a derivation of quark-parton model results by summing over s-channel hadrons states - fig. 47 (b) - see the next chapter).

Why it is that this diagram should scale is unknown, and it would be nice to have some theoretical understanding on this point. Accepting that resonance excitation does scale we now attempt to derive the relations between the electromagnetic and weak structure functions (chapter 4) by summing over the s-channel hadron states in this latter diagram as a first step in attempting to understand further the relation between these two types of diagrams.

12 RESONANCES, SU(6) AND THE QUARK PARTON MODEL

By assuming that the partons were quarks we derived in section 4 various relations among the structure functions of the weak and electromagnetic interactions with proton and neutron targets. A prime motivation of the quark model of hadrons has previously been its relevance for classifying resonances[57 - 59] and predicting their excitations[57-61], i.e. concerned with the coherent aspects of a nucleon containing three quarks. Having seen in chapter 11 that the scale invariance of νW_2 seems to obtain even for low W^2, and for the resonance region, it is of interest to see if the results of the quark-parton model (eqns. 4.8, 4.16, 4.19, 4.23), which emphasised the incoherent aspect of the electron-nucleon interaction, can be obtained from a quark model of resonance excitation and so provide some feeling for the inter-relation between the incoherent and coherent phenomena[62].

The structure functions are essentially the imaginary part of the forward Compton amplitude, fig. 33. We shall look at the non-diffractive part of the Compton amplitude by considering the couplings of the various baryon states that can be excited from the target nucleon. The Compton amplitude's non-diffractive part is then obtained after summing over all the hadron states that can be excited.

The computation of electromagnetic[59,60] and weak[61] nucleon resonance excitation in the quark model is discussed in detail in the cited references and is not reproduced here. We simply note that in SU(6) the nucleon belongs to a $\underset{\sim}{56}$ plet representation which is totally symmetric under interchange of any pair of quarks and as we only excite one quark at a time then only totally symmetric or mixed symmetry final states can be excited corresponding to the $\underset{\sim}{56}$ and $\underset{\sim}{70}$ dimensional representations of SU(6) respectively. (To excite the totally antisymmetric $\underset{\sim}{20}$ requires excitation of two quarks).

An example of a $\underset{\sim}{56}$ plet is the nucleon octet with spin 1/2 and the decuplet containing $\Delta(1236)$ with spin 3/2. Then, with spectroscopic notation for the spin states

$$^2 8 + {}^4 10 \rightarrow 16 + 40 = 56 \qquad (12.1)$$

We shall assume in our calculation that SU(6) is an exact symmetry of nature. This clearly is not true since the nucleon mass is only about 75% of that of the $\Delta(1236)$, so SU(6) is broken by 25% or so (a model incorporating SU(6) breaking is considered in the next chapter). An example of a 70 plet is the set of negative parity resonances in the 1500 - 1700 MeV mass range. For more details see R.H. Dalitz, ref. 57.

In exciting any member of a 56 plet there will be in the matrix element a known Clebsch-Gordan coefficient, which depends only upon its quantum number assignment in the SU(6) multiplet, multiplied by an unknown quantity which includes phase space, propagators and in general all the unknown dynamics of the universe over and above SU(6). We shall call this unknown function A for any 56 plet. Hence the form of the 56 plets contribution to the structure functions will be, for any N^*

$$\text{Clebsch - Gordan} * A \qquad (12.2)$$

and similarly for 70 plets

$$\text{Clebsch - Gordan} * B \qquad (12.3)$$

In a quark model picture A and B correspond to the dynamical factors related to the O(3) structure of the multiplets wave function, e.g. if the quarks sit in a harmonic oscillator well as against a Coulomb potential say, then the Clebsch-Gordans of SU(6) are always the same but A and B differ.

If we replaced the electron probe by a neutrino then the quantum numbers of the current probe are altered and so the Clebsch-Gordan coefficients are changed, but the A and B are clearly unaffected. A similar conclusion obtains if we replace neutron by proton. The resulting contributions to the structure functions are listed in the Table.

	en	ep	νn	νp
$\underset{\sim}{56}$	12A	17A	33A	24A
$\underset{\sim\sim}{70}$	6B	10B	21B	3B

This Table is the same for <u>any</u> 56 and for <u>any</u> 70 and so has the same form after summing over <u>all</u> 56 or <u>all</u> 70. Letting A, B now be interpreted as referring to the sum over all 56 or all 70 then

$$\begin{aligned} en &= 12A + 6B \\ ep &= 17A + 10B \\ \nu n &= 33A + 21B \\ \nu p &= 24A + 3B \end{aligned} \qquad (12.4)$$

Note that neither 56 alone nor 70 alone would give the quark parton model result of 2/3 for en/ep. We note that 2/3 lies between the results for 56 or 70 alone and so we could fit A/B in order to give this ratio and then, with the one unknown now determined, proceed to see if the other relations of the quark-parton model (chapter 4) obtain.

However, we still have one card left to play. If we demand that no exotic exchanges are allowed in the t-channel (i.e. only $\underset{\sim}{1}$ and $\underset{\sim\sim}{35}$ are exchanged) then this constrains the relative weights of $\underset{\sim}{56}$ and $\underset{\sim\sim}{70}$ in the s-channel. The result of this constraint may be computed by means of the crossing matrix and is that

$$A = B \qquad (12.5)$$

in the normalisation of our table. As a result we now obtain from eqns.(12.4)

$$\begin{aligned} en &= 18A \\ ep &= 27A \\ \nu n &= 54A \\ \nu p &= 27A \end{aligned} \qquad (12.6)$$

Therefore the following relations obtain

$$\frac{en}{ep} = 2/3 \qquad (12.7) \text{ or } (4.8)$$

$$\frac{\nu n}{\nu p} = 2 \qquad (12.8) \text{ or } (4.16)$$

$$ep - en = 1/3\ (\nu n - \nu p) \qquad (12.9) \text{ or } (4.19)$$

$$ep + en \doteq 5/9\ (\nu n + \nu p) \qquad (12.10) \text{ or } (4.23)$$

i.e. exactly the results derived previously in the quark-parton model.

Therefore we see that the results derived in the quark-parton model implicitly assume

(i) SU(6) is exact.

(ii) No t-channel exotics.

We know however that SU(6) is not exact (e.g. it is broken by 25% in the masses alone) and so we might therefore tolerate a violation of these relations eqns.(12.7 - 10) by up to 25% (cf. the sum rule eqn.(4.28) which only seems good to around 15% - chapter 3). Secondly, since these relations are supposedly q^2 independent then they require SU(6) to be exact for <u>all</u> q^2 and this is only possible if all N^* within a multiplet have the same q^2 dependences at high q^2. We shall see in the next chapter that the $\Delta(1236)$ excitation form factor has quite a different q^2 dependence from the proton's elastic magnetic form factor and so this manifestly breaks SU(6) symmetry.

So the conclusion is that the quark parton model relations eqns.(12.7-12.10) implicitly assume SU(6) symmetry. This symmetry is not exact in nature, so results obtained assuming it to be an exact symmetry are not to be expected to be satisfied. In what way will they be violated? This brings us to the stage of constructing dynamical quark (parton) models, which we discuss in the final chapter.

13 TOWARDS A DYNAMICAL PARTON MODEL

Let us briefly recapitulate some of the successes and problems in the parton-quark model that we have studied in these lectures. The scaling invariance of νW_2 (W^2, q^2) in the "deep inelastic region", i.e. large W^2 and large q^2, suggested that incoherent scattering of the photon from the constituent "partons" was being observed. Assuming that these partons were quarks we derived several relations among the structure functions of electromagnetic and weak interactions. Empirically the relation

$$F_2^{ep}(\omega) + F_2^{en}(\omega) \geq 5/9\ (F_2^{\nu n}(\omega) + F_2^{\nu p}(\omega)) \tag{13.1}$$

is beautifully satisfied, giving support to our hypothesis; on the other hand the relations between the proton and neutron electromagnetic structure functions $F_2^{en}(\omega)/F_2^{ep}(\omega) = 1$ for diffraction and $= 2/3$ for non-diffraction are fairly well satisfied but there is something odd happening near $\omega \sim 1$ which suggests that we have over-simplified at some point. The model is not violated in principle since we saw that the ratio was bounded from below by $1/4$ which is in agreement with the data.

Secondly we saw that the resonance region also exhibited scale invariance and that this was not understandable in the framework of the incoherent impulse parton model since this model contained no resonance enhancements in the final state. We concluded that for some reason the diagrams 47(b) also scaled. We then showed that the results of the quark-parton model

$$F_2^{ep} - F_2^{en} = 1/3\ (F_2^{\nu n} - F_2^{\nu p}) \tag{13.2}$$

$$F_2^{ep} + F_2^{en} = 5/9\ (F_2^{\nu n} + F_2^{\nu p}) \tag{13.3}$$

$$F_2^{en}/F_2^{ep} = 2/3 \tag{13.4}$$

$$F_2^{\nu n}/F_2^{\nu p} = 2 \tag{13.5}$$

corresponded to the assumption that SU(6) was exact and moreover that it was exact at each and every value of q^2 if these relations are to be q^2 independent. We will show that it is this assumption of exact SU(6) that is responsible for the violation of the ratio $F_2^{en}/F_2^{ep} = 2/3$. The relations (13.2) and (13.3) however derive from weaker (SU(3)) assumptions[63]. We shall therefore set up a version of the quark parton model which allows the SU(6) to be broken in a particular manner[64]. By imposing just one constraint on our new model we shall see that it collapses to the old model and hence we shall see that the old model implicitly assumed this constraint to be valid. However, we shall show that resonance excitation form factors show that this constraint is violated in nature (its violation corresponds to a particular form of SU(6) breaking) and hence results will be incorrect if derived in the quark-parton model assuming this constraint. At any point in the calculation we can impose the constraint and see how our model collapses to the old model; conversely we can relax the constraint and derive less restrictive results than the quark parton model and then impose nature's constraint (by empiricism) and see what results one obtains.

In our model the proton is made up of quarks and anti-quarks etc. As we shall be interested in the region $\omega \lesssim 3$ where it seems that strange quarks and also anti-quarks are unimportant (cf. section 4) we shall hypothesise that only the non-strange quarks interact with the external field. The remaining constituents in the proton we shall call the "core" and we do not care how many particles are contained in it, we shall treat it as a quasi-particle.

The quark that interacts with the external field can therefore be a p quark (charge $2/3$, $I = 1/2$, $I_3 = 1/2$) or an n quark (charge $-1/3$, $I = 1/2$, $I_3 = -1/2$). The core can then have only $I = 0$ or 1 since the original proton had $I = 1/2$ and the quarks also have $I = 1/2$. Then $1/2 \otimes 0$ can give $1/2$ as can also $1/2 \otimes 1$ but $1/2 \otimes 2$ and higher cannot; hence only isoscalar or isovector cores can exist. Therefore the wave function for the proton in isospin space

will be the sum of two terms

$$\psi = \psi_0 + \psi_1 \tag{13.6}$$

ψ_0 when there is an isoscalar core and ψ_1 for the isovector core.

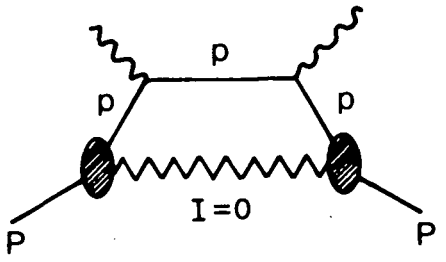

Fig. 54 Proton built of quark plus core, configurations with isoscalar core.

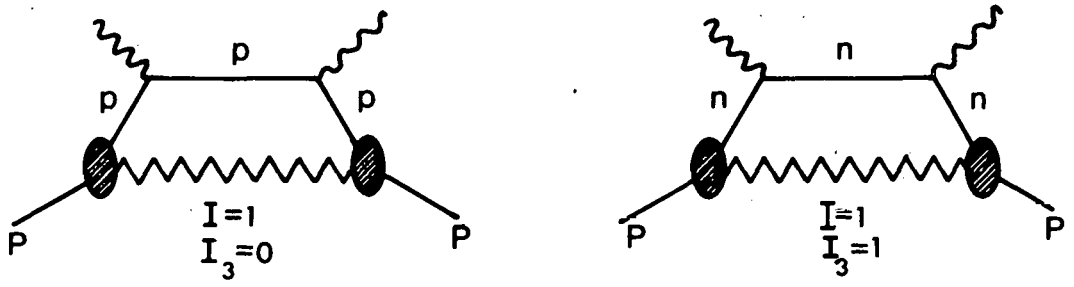

Fig. 55 Proton built of quark plus core, configurations with isovector core.

What are the possible configurations? Let us look first at the case of the isoscalar core. The proton has $I_3 = +1/2$, the core is isoscalar so clearly only the quark with $I_3 = +1/2$ can contribute, viz the p quark. So the configuration is as shown in fig. 54, and the wave function may be written

$$\psi_0 = p \mid 00\rangle \tag{13.7}$$

where $\mid II_3\rangle$ is the core's isospin.

The other possibility is that the core is isovector and in this case there are two configurations, (fig. 55). The first configuration is where there is a p quark and the I = 1 core has $I_3 = 0$, the second is when there is a n quark

and the core has $I_3 = +1$. The amplitude for the first of these is

$$\psi_1^{(p)} = p\,|\,10\rangle\,(1/2\ 1/2\,|\,1/2\ 1/2;\ 10) = -\sqrt{1/3}\ p\,|\,10\rangle \qquad (13.8)$$

where we have included the Clebsch-Gordan coefficient for the proton $(I, I_3 = 1/2, 1/2)$ to break up into the p quark $(1/2, 1/2)$ and the core $(1, 0)$. Similarly the configuration with the n quark is written

$$\psi_1^{(n)} = n\,|\,11\rangle\,(1/2\ 1/2\,|\,1/2\ -1/2;\ 11) = \sqrt{2/3}\ n\,|\,11\rangle \qquad (13.9)$$

so that finally

$$\psi_1 = \sqrt{2/3}\ n\,|\,11\rangle - \sqrt{1/3}\ p\,|\,10\rangle \qquad (13.10)$$

Similarly we can construct wave functions in spin space since the proton has spin $1/2$ as does the quark, then ignoring angular momentum the core can have spin 0 or 1. The resulting spin wave functions constructed in direct analogy to the isospin case above then read ($\uparrow$ denotes $S_3 = 1/2$, $\downarrow$ $S_3 = -1/2$)

$$\chi_0(x') = \uparrow\,|\,00\rangle\, f_0(x') \qquad (13.11)$$

$$\chi_1(x') = \left\{\sqrt{2/3}\downarrow\,|\,11\rangle - \sqrt{1/3}\uparrow\,|\,10\rangle\right\} f_1(x') \qquad (13.12)$$

where $f_{0,1}(x')$ are the amplitudes that the quark carries fraction x' of the proton's four momentum with scalar, vector core.

Exercise: derive this spin space wave function by following the isospin example.

The full wave function in spin and isospin space is postulated to be symmetric under interchange of any two quarks (since the proton is a member of a symmetric representation ($\underset{\sim}{56}$) of SU(6) - see for example R.H. Dalitz, ref. 57). Hence we write $\Phi(x') = \psi_0\chi_0(x') + \psi_1\chi_1(x')$. As it turns out we shall only need the isospin part of the wave function in our following example.

We will now calculate F_2^{ep} and F_2^{en} by taking the matrix element of the charge-squared operator between proton or neutron wave functions. Diagrammatically this is shown in fig. 54, the charge squared operator arising because the electromagnetic current acts twice on the same quark. Writing

$$\langle \Phi \mid \hat{e}^2 \mid \Phi \rangle \tag{13.13}$$

then we find for this matrix element

$$e_p^2 \, |f_0(x')|^2 + |f_1(x')|^2 \left\{ e_n^2 \, 2/3 + 1/3 \, e_p^2 \right\} \tag{13.14}$$

There are no cross terms because the quantum numbers of the core do not change, since in fig. 54 if the core is created in isospin $I = I_3 = 1$ for instance then it stays in this state.

Defining $\phi_{0,1} \equiv |f_{0,1}|^2$ then

$$F_2^{ep}(x') \sim e_p^2 \, \phi_0(x') + \phi_1(x') \left\{ 2/3 \, e_n^2 + 1/3 \, e_p^2 \right\} = 4/9 \, \phi_0(x') + 2/9 \, \phi_1(x') \tag{13.15}$$

and similarly for a neutron target we just replace p by n (and vice versa) and find that

$$F_2^{en}(x') \sim e_n^2 \, \phi_0(x') + \phi_1(x') \left\{ 2/3 \, e_p^2 + 1/3 \, e_n^2 \right\} = 1/9 \, \phi_0(x') + 3/9 \, \phi_1(x') \tag{13.16}$$

Taking the ratio of neutron to proton structure functions we find

$$\frac{F_2^{en}(x')}{F_2^{ep}(x')} = \frac{\phi_0(x') + 3 \, \phi_1(x')}{4\phi_0(x') + 2\phi_1(x')} \tag{13.17}$$

If, and only if, $\phi_0(x') = \phi_1(x')$ does the ratio 2/3 obtain. It is not a mystery that this happens since we have taken the old quark-parton model and described it in an isospin basis. We have introduced an extra degree of

freedom, viz that $\phi_0(x') \neq \phi_1(x')$ or that the probability of finding a spin 1 core does not equal that for finding a scalar core. The old model implicitly assumed that these probabilities were equal (as they would be if SU(6) were exact). It would be most surprising if this was realised in nature, and we shall see that in fact it is not.

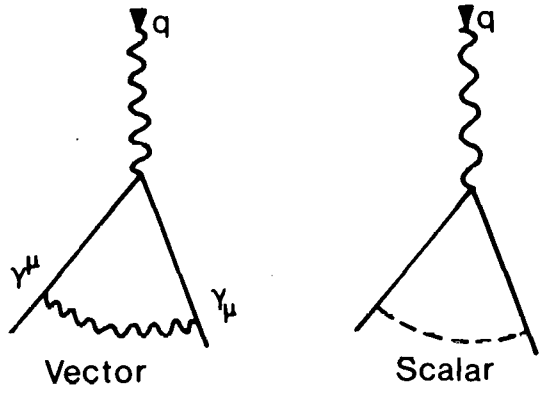

Fig. 56 Electromagnetic vertex corrections due to vector or scalar particle exchange. The q^2 dependence of these diagrams differs in general due to the presence of γ matrices in the first case.

A simple model will first show why one might expect the two spin states to have different probabilities in general. We might draw the diagrams in fig. 56 to represent the contributions to the elastic form factor of a spin 1/2 particle where the vertex contains either a scalar or vector particle. One could calculate the q^2 dependence of such a diagram and due to the presence of γ_μ factors in the case involving the vector particle as against the scalar particle then the q^2 dependences of these two configurations might be expected to differ (see for example Brodsky, Blankenbecler and Gunion, ref. 65). Hence this simple model has $\phi_0 \neq \phi_1$. Thus it is possible that <u>within</u> S = 1 (or S = 0) the symmetry is good but not <u>between S = 0 and S = 1</u>. Hence we allow for this particular, and expected (?), form of SU(6) symmetry breaking by allowing for ϕ_0 and ϕ_1 to be separate degrees of freedom.

Not only does the simple model suggest that $\phi_0 \neq \phi_1$ but nature also shows it. Exact SU(6) would predict that[59-61]

$$G_M^n(q^2)/G_M^p(q^2) = -2/3 \qquad (13.18)$$

and

$$G_M^{\Delta}(q^2)/G_M^{p}(q^2) = 2\sqrt{2/3} \tag{13.19}$$

for all q^2, where $G^{p,n}$ and G^{Δ} are the magnetic form factors of the proton (neutron) and for the transition to the $\Delta(1236)$. The data on the neutron are not good, but the G^p and G^{Δ} data exist and show that this ratio is wrong by about 20% at $q^2 = 0$ and moreover that this ratio is q^2 dependent, in particular the G_M^{Δ} is falling faster[66,67] with q^2 than is G_M^p (at least over the limited range of q^2 where data so far exist). Our programme will be to look at the data for this ratio and from it deduce $\phi_1(x')/\phi_0(x')$. Having done this we shall use the information as input in eqn.(13.17) for the ratio $F_2^{en}(x')/F_2^{ep}(x')$.

In our model the expressions for $G_M^{n,p,\Delta}$ look like

$$G_M^{\Delta}(q^2/m_{\Delta}^2) \sim 2\sqrt{2}\,\phi_1(x') \tag{13.20}$$

$$G_M^{n}(q^2/m_N^2) \sim -1/2(3\phi_0(x') + \phi_1(x')) \tag{13.21}$$

$$G_M^{p}(q^2/m_p^2) \sim 3\phi_0(x') + 0\,\phi_1(x') \tag{13.22}$$

That the excitation of the Δ involves only ϕ_1 is obvious since the Δ has spin and isospin $3/2$ and so only the $S = 1$, $I = 1$ core can contribute to its formation. The neutron and proton, with $S = I = 1/2$, can be "excited" with both ϕ_0 and ϕ_1 in principle (cf. eqn.(13.21)); it is interesting, therefore, that the elastic form factor of the proton only involves ϕ_0. The reason for this is that placing the charge operator between proton wave functions with an isovector core yields

$$2/3\, e_n + 1/3\, e_p = 0 \tag{13.23}$$

Hence the measurement of $G_M^p(q^2)$ tells one nothing about $\phi_1(x')$, only $\phi_0(x')$ is probed here! Therefore the $G_M^p(q^2)$ and $G_M^{\Delta}(q^2)$ are a priori <u>independent</u> quantities. In fig. 57 we show[66] the data for $G_M^{\Delta}(q^2)$ compared to $F_2^V(q^2)$ (the isovector <u>Pauli</u> form factor of the nucleon). It seems that $G_M^{\Delta}(q^2)$ is more similar to this than to the magnetic form factor of the proton $G_M^{\Delta}(q^2)$ (solid curve). Thus we

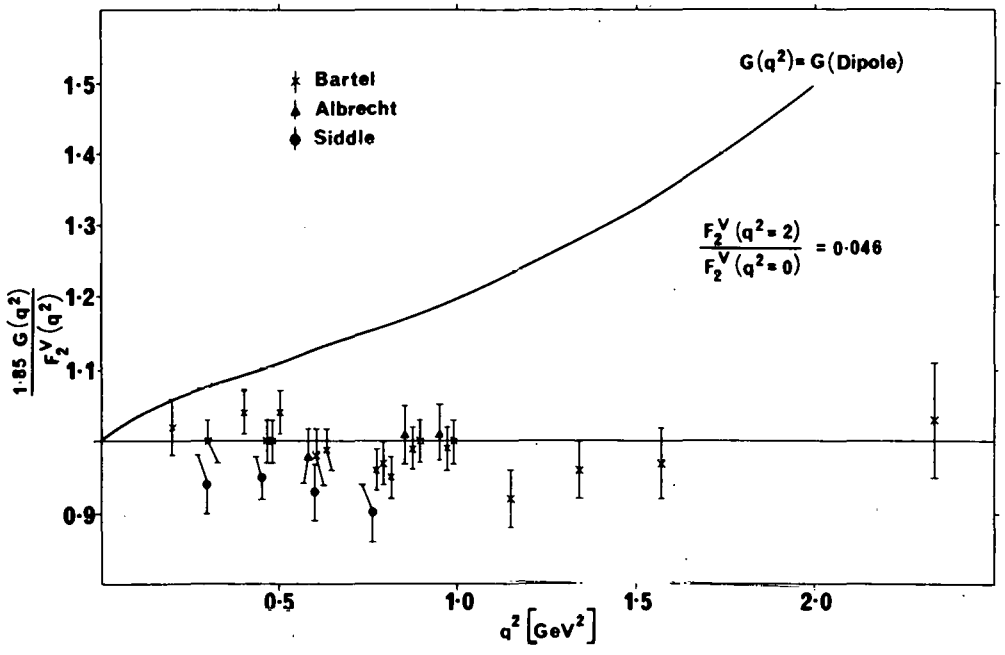

Fig. 57 Comparison of data on magnetic dipole transition form factor of the $\Delta^+(1236)$ resonance with the nucleon isovector form factor F_2^V. The dipole is also shown for comparison (after G. Shaw, ref. 66).

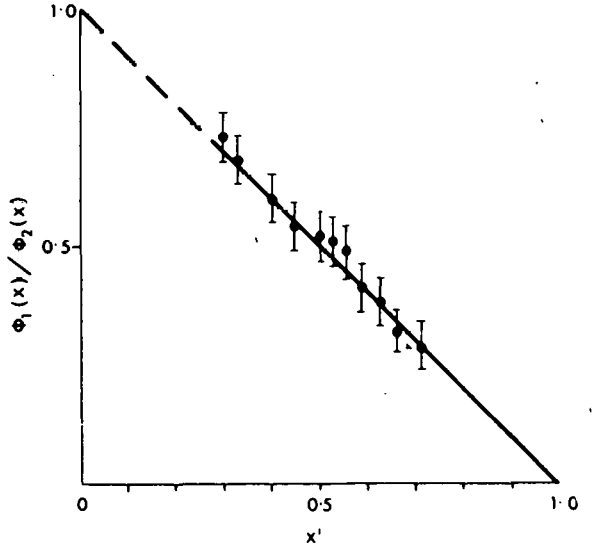

Fig. 58 Ratio of Δ^+ transition magnetic form factor to proton magnetic elastic form factor plotted against x' ($\equiv(S/Q^2 + 1)^{-1}$) to yield $\phi_1(x')/\phi_0(x')$ (see text). The solid line $1 - x'$ is shown for comparison.

conclude, from this limited range of q^2, that $G_M^{\Delta}(q^2)$ is falling faster with increasing q^2 than is $G_M^p(q^2)$. This enables us to determine $\phi_1(x')/\phi_0(x')$ which is shown in fig. 58 and seems to approximate $1 - x'$ (this is equivalent to saying that $G^{\Delta}/G^p \sim 1/q^2$ as $q^2 \to \infty$ since $1/q^2 \sim 1 - x'$ as $x' \to 1$).

This behaviour tells us that SU(6) is indeed broken in nature as well as in the simple model discussed earlier. Hence we should no longer be surprised that the quark-parton model prediction

$$\frac{F^{en}(x')}{F^{ep}(x')} = 2/3$$

which assumed SU(6) to be satisfied, is violated as $x' \to 1$. Using the suggestion that

$$\frac{\phi_1(x')}{\phi_0(x')} \simeq 1 - x' \qquad (13.24)$$

instead of the SU(6) prediction

$$\frac{\phi_1(x')}{\phi_0(x')} = 1 \qquad (13.25)$$

then

$$\frac{F_2^{en}(x')}{F_2^{ep}(x')} \to \frac{4 - 3x'}{6 - 2x'} \xrightarrow{x' \to 1} 1/4 \qquad (13.26)$$

This behaviour (13.26) is compared with the data in fig. 59 and indeed it does appear that the SU(6) breaking that caused the G_M^{Δ} to have different q^2 behaviour from G_M^p is also responsible for the behaviour of the F^{en}/F^{ep} ratio as $x' \to 1$. (The fact that we disagree as $x' \to 0$ is to be expected since strange quarks and anti-quarks - diffraction - contribute in general in that region of x').

Of course we must also check that the model agrees with other data since we have determined the behaviour of $\phi_1(x')/\phi_0(x')$ once and for all (13.24).

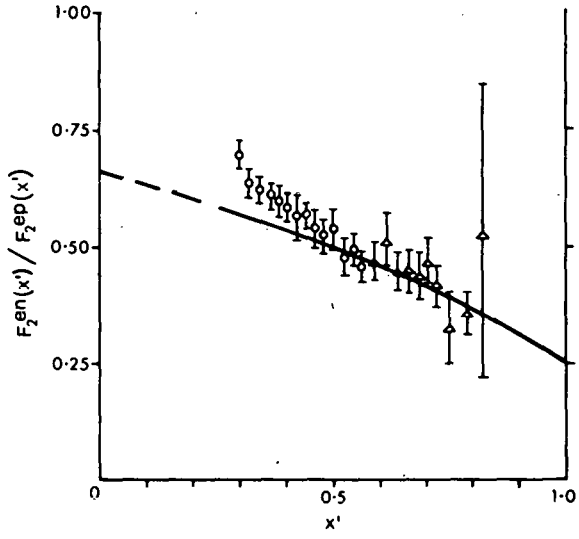

Fig. 59 Comparison of model and data for F_2^{en}/F_2^{ep} as $x' \to 1$. Details in ref. 64 (first paper) and text.

From (13.21) and (13.22) we find that the prediction is

$$\frac{G_M^n(q^2)}{G_M^p(q^2)} \xrightarrow{q^2 \to \infty} -1/2 \tag{13.27}$$

Present data are not in disagreement with this, but much more work is required here.

We should also check whether the "nice" result (chapters, 4, 5)

$$F^{ep} + F^{en} = 5/9\ (F^{\nu p} + F^{\nu n}) \tag{13.28}$$

is violated in this new model. Upon calculating the neutrino structure functions one finds

$$F_2^{\nu p}(x') \sim 6\,\phi_1(x') \tag{13.29}$$

$$F_2^{\nu n}(x') \sim 9\,\phi_0(x') + 3\,\phi_1(x') \tag{13.30}$$

Taken in conjunction with the results for the $F^{ep}(x')$ and $F^{en}(x')$ (13.15 and 13.16) we see that the relation (13.28) obtains for ϕ_0 and ϕ_1 separately and therefore is not affected by the SU(6) breaking. Empirical verification of this relation is therefore evidence that SU(6) is, to good approximation, unbroken within the S = 1 or S = 0 (see also ref. 63). The further tests of this breaking mechanism are discussed in detail in ref. 64. The most direct test involving neutrinos is by looking at

$$(F_2^{\nu n} + F_2^{\nu p})/3F_2^{ep} \tag{13.31}$$

which = 1 for all x' in SU(6) (diffractive or non-diffractive*)

---

*Exercise: Prove this using eqn.(5.26) with $F^{en} = F^{ep}$ for diffraction, and eqn.(5.28) with $F^{en} = 2/3\ F^{ep}$ for non-diffraction in exact SU(6).

---

whereas the SU(6) breaking model predicts that as $x' \to 1$ this ratio falls to 3/4.

The conclusion seems to be that the quark-parton model gives a remarkably good description of the deep inelastic structure functions with electron or neutrino beams. The assumption of SU(6) symmetry is too strong; including SU(6) breaking yields a significant improvement. Is nature really quark-partons with the specific form of broken SU(6) symmetry discussed above? Is this related to the broken $SU(6)_W$ models[68] of Rosner et al., or the approach of Melosh which seems in some ways to resemble those models? How are resonance models and quark-parton models related? Where do generalised vector dominance models[69] fit in with the discussion of chapter 10? How far do we have to go to a complete theory?

These we leave as the final exercises for the reader!

14 POSTSCRIPT

We have not ventured into the realms of polarised electroproduction nor made speculations as to the nature of the hadrons produced in the final state. Information on these topics is only now becoming known. For those readers who are interested in learning what quark-parton models say about these processes the cited literature is recommended. The bibliography quoted will also be found useful both as supplementary material to this lecture series and also in order that the reader should not be unnecessarily influenced by the biassed viewpoint and presentation of one author.

BIBLIOGRAPHY AND REFERENCES

B.1 S. Gasiorowicz. 'Elementary Particle Physics' (N.Y., London, Wiley, 1966).

B.2 J.D. Bjorken and S.D. Drell. 'Relativistic Quantum Mechanics' (N.Y., McGraw-Hill, 1964).

B.3 International Symposium on Electron and Photon Interactions at High Energies. Liverpool, 1969. Ed. D.W. Braben and R.E. Rand (Daresbury Nuclear Physics Laboratory, 1969).

B.4 International Symposium on Electron and Photon Interactions at High Energies. Cornell 1971. Ed. N.B. Mistry (Ithaca, N.Y., Cornell Univ. Pr., 1972).

B.5 S.D. Drell in Subnuclear Phenomena: 1969 Int. School of Physics 'Ettore Majorana', Erice. Ed. A. Zichichi (N.Y. Academic Pr., 1970).

B.6 R.H. Dalitz in Proc. 2nd Hawaii Topical Conf. in Particle Physics, eds. S. Pakvasa and S.F. Tuan (Honolulu, Univ. of Hawaii Press, 1968) p.325.

B.7 J.K. Storrow. 'Regge Theory for Experimentalists'. Daresbury Lecture Note Series No. 6, Daresbury Laboratory Report, DNPL/R17 (1971).

B.8 R.P. Feynman. 'Photon-Hadron Interactions'. (N.Y., W.A. Benjamin, 1972).

REFERENCES

1. See Gasiorowicz or Bjorken and Drell, op. cit.
   More details of this calculation can be found in Bjorken and Drell, p.100 et. seq.
2. Gasiorowicz, p.434 et. seq.
   Bjorken and Drell, p. 242 et. seq.
3. For discussion and data on these form factors see J. Rutherglen, Int. Symp. on Electron and Photon Interactions at High Energies, Liverpool (1969) op. cit. p.163.
4. See F.J. Gilman and also R. Taylor, Int. Symp. on Electron and Photon Interactions at High Energies, Liverpool (1969) op. cit, p.177 and 251 and H. Kendall, Int. Symp. on Electron and Photon Interactions at High Energies, Cornell, op. cit. p.247.
5. S.D. Drell and J.D. Walecka, Ann. Phys. (N.Y.) 28 (1964) 18.
6. See Gasiorowicz, op. cit.
7. S.D. Drell and J.D. Walecka, Ann. Phys. (N.Y.) 28 (1964) 18;
   J.D. Bjorken and J.D. Walecka, Ann. Phys. 88 (1966) 35.
8. F.J. Gilman, Phys. Rev. 167 (1968) 1365.
9. L.N. Hand, Phys. Rev. 129 (1963) 1834;
   See also S.D. Drell, op. cit.
10. J.D. Bjorken, Phys. Rev. 179 (1969) 1547.
11. R.P. Feynman, Phys. Rev. Letts. 23 (1969) 1415;
    J.D. Bjorken and E.A. Paschos, Phys. Rev. 185 (1969) 1975.
12. See also S.D. Drell, op. cit.
13. See C.H. Llewellyn-Smith, Phys. Repts. 3C (1972) 264.
14. M. Gell-Mann, Phys. Letts. 8 (1964) 214;
    G. Zweig, CERN Report CERN TH.401, 412 (unpublished) (1964).
15. K. Gottfried, Phys. Rev. Letts. 18 (1967) 1174.
16. J. Kuti and V. Weisskopf, Phys. Rev. D4 (1971) 3418;
    P.V. Landshoff and J.C. Polkinghorne, Nucl. Phys. B28 (1971) 240.

17. See also F.J. Gilman, Phys. Repts. 4C (1972) 95.

18. H. Harari in 'Hadronic Interactions of Electrons and Photons': Proc. 11th Scottish Universities Summer School in Physics, 1970. Eds. J. Cumming and H. Osborn (London, Academic Pr., 1971) p.560.

19. See for example J.K. Storrow, op. cit.

20. R.P. Feynman op. cit.

21. For the current (1973) situation see C.H. Llewellyn-Smith, Proc. 4th Int. Conf. on High Energy Collisions, Oxford, April 1972 (Chilton, Rutherford High Energy Laboratory, 1972) vol. 1, p.87.

22. S. Adler, Phys. Rev. 143 (1966) 1144.

23. J.D. Bjorken and S.F. Tuan, SLAC-PUB-1049 (1972); J.J. Sakurai, H.B. Thacker and S.F. Tuan, UCLA Preprint TEP/58 (1973).

24. D. Gross and C.H. Llewellyn-Smith, Nucl. Phys. B14 (1969) 337.

25. For a review of polarised photo-and electroproduction see for example F.E. Close,Daresbury Laboratory Preprint, DNPL/P154 and references therein.

26. See for example D.W.G.S. Leith in ref. 18.

27. Particle Data Group, Rev. Mod. Phys. Vol. 45, No. 2 Part II (1973).

28. M. Creutz, S.D. Drell and E.A. Paschos, Phys. Rev. 178 (1969) 2300.

29. M. Damashek and F.J. Gilman, Phys. Rev. D1 (1970) 1319, where a detailed discussion of kinematics and data analysis may be found.

30. See Gasiorowicz or Bjorken and Drell, op. cit.

31. M. Gell-Mann, M.L. Goldberger and W. Thirring, Phys. Rev. 95 (1954) 1612.

32. M. Gell-Mann and M.L. Goldberger, Phys. Rev. 96 (1954) 1433; F.E. Low, Phys. Rev. 96 (1954) 1428.

33. S.D. Drell and A.C. Hearn, Phys. Rev. Letts. 16 (1966) 908; S.B. Gerasimov, Sov. J. Nucl. Phys. 2 (1966) 430.

34. I. Karliner, SLAC-PUB-1179 (1973).

35. S.J. Brodsky, F.E. Close and J.F. Gunion, Phys. Rev. D5 (1972) 1384, and Phys. Rev. D6 (1972) 177.

36. P.V. Landshoff, J.C. Polkinghorne and R.D. Short, Nucl. Phys. B28 (1971) 225.

37. P.V. Landshoff and J.C. Polkinghorne, Phys. Rev. D5 (1972) 2056.

38. See for example N.R.S. Tait and J.N.J. White, Nucl . Phys. B43 (1972) 27.

39. H. Harari in ref. 18.

40. C. Dominguez, J.F. Gunion and R. Suaya, Phys. Rev. D6 (1972) 1404.

41. F.E. Close and J.F. Gunion, Phys. Rev. D4 (1971) 742, Phys. Rev. D4 (1971) 1576;
R. Rajaraman and G. Rajasekran, Phys. Rev. D3 (1971) 266;
M. Elitzur, Phys. Rev. D3 (1971) 2166;
J. Cornwall, D. Corrigan and R. Norton, Phys. Rev. Letts. 24 (1970) 1141 and Phys. Rev. D3 (1971) 536.

42. T.P. Cheng and Wu-Ki Tung, Phys. Rev. Letts. 24 (1970) 851;
F.E. Close and J.F. Gunion, ref. 41.

43. H. Harari, Int. Symp. on Electron and Photon Interactions at High Energies, Cornell, op. cit., p.299.

44. R. Eden, P.V. Landshoff, D.I. Olive and J.C. Polkinghorne, 'The Analytic S-Matrix' (London, Cambridge Univ. Pr., 1966).

45. J.J. Sakurai, 'Generalised Vector-Meson Dominance', Lectures at Canadian Summer School (1972) UCLA preprint (1972).

46. J. Pestieau, Univ. of Louvain Preprint (1973).

47. D.W.G.S. Leith in ref. 18.

48. G. Wolf and also K. Gottfried in Int. Symp. on Electron and Photon Interactions at High Energies, Cornell, op. cit. p.189 and p.221.

49. R. Anderson et al., Phys. Rev. D1 (1970) 27. See also G. Wolf, Int. Symp. on Electron and Photon Interactions at High Energies, Cornell, op. cit., p.189.

50. R. Anderson et al., Phys. Rev. D4 (1971) 3245.

51. R.L. Anderson et al., Phys. Rev. Letts. 25 (1970) 1218;
A.M. Boyarski et al., Phys. Rev. Letts. 26 (1971) 1600.

52. D. Yennie in ref. 18.

53. See H. Kendall in Int. Symp. on Electron and Photon Interactions at High Energies, Cornell, op. cit., p.247.

54. Compare E.D. Bloom and F.J. Gilman, Phys. Rev. D4 (1971) 2901.

55. F.W. Brasse et al., DESY Report DESY 71/2 (1971).

56. See also F.E. Close, ref. 25.

57. See for example R.H. Dalitz, op. cit.

58. D. Faiman and A. Hendry, Phys. Rev. 173 (1968) 1720, Phys. Rev. 180 (1969) 1609.

59. R.P. Feynman, M. Kislinger and F. Ravndal, Phys. Rev. D3 (1971) 2706.

60. L. Copley, G. Karl and E. Obryk, Nucl. Phys. B13 (1969) 303, and Phys. Rev. D4 (1971) 2844;
F. Ravndal, Phys. Rev. D4 (1971) 1466;
R. Lipes, Phys. Rev. D5 (1972) 2849.

61. T. Abdullah and F.E. Close, Phys. Rev. D5 (1972) 2332;
F. Ravndal, Lett. Nuovo Cim. 3 (1972) 631.

62. F.E. Close and F.J. Gilman, Phys. Rev. D7 (1973) 2258.

63. H.J. Lipkin and E.A. Paschos, Phys. Rev. D6 (1972) 817.

64. F.E. Close, Phys. Letts. 43B (1973) 422;
See also R.P. Feynman op. cit., and M. Chaichian and S. Kitakado, CERN Report CERN TH.1640 (1973).

65. J.F. Gunion, S.J. Brodsky and R. Blankenbecler, Phys. Letts. 39B (1972) 649.

66. See for example G. Shaw, Phys. Letts. 39B (1972) 255.

67. W. Bartel, et al., Phys. Letts. 28B (1968) 148;
W. Albrecht et al., Nucl. Phys. B27 (1971) 615;
R. Siddle et al., Nucl. Phys. B35 (1971) 93.

68. J. Rosner, Phys. Rev. D6 (1972) 1781;
H.J. Melosh, California Institute of Technology, Ph.D. Thesis (unpublished).

69. J.J. Sakurai and D. Schildknecht, SLAC-PUB-1094 (1972) and ref. 45.